UNIVERSITÉ D'OTTAWA
UNIVERSITY OF OTTAWA

NUCLEAR STRUCTURE CALCULATIONS FOR ODD-MASS COPPER ISOTOPES

by

Jennifer Tan

Submitted in partial fulfillment of
the requirements for the degree of
MASTER OF SCIENCE
at the

Department of Physics
Faculty of Science and Engineering
University of Ottawa
Ottawa, Canada

July, 1972.

To My Father and Mother

ACKNOWLEDGMENTS

The author would like to express her most sincere gratitude to her advisor, Dr. R. J. W. Hodgson for suggesting this thesis topic and for providing continual professional guidance throughout the course of this investigation.

The author is also fortunate in having the opportunity to acquire some experimental experience under Dr. I. L. Fairweather. His interest in the work as well as financial assistance is deeply appreciated. Her appreciation is also extended to Dr. B. Hird, for his valuable comments and discussions.

Finally, the author would like to express her gratefulness to Mr. Samuel Tan for his encouragement and useful suggestions in computer programming. Special thanks are extended to Miss L. Sawyer for typing this thesis.

AN ABSTRACT

NUCLEAR STRUCTURE CALCULATIONS FOR ODD-MASS COPPER ISOTOPES

by

Jennifer Tan

Advisor: R. J. W. Hodgson

Submitted in partial fulfillment
of the requirements for the
degree of Master of Science.

The structure of the odd-mass copper isotopes are studied using the intermediate coupling model and the projected Hartree-Fock model. In the intermediate coupling model, each copper isotope is described as a proton in the $2p_{3/2}$, $1f_{5/2}$ and $2p_{1/2}$ orbits coupled to an even-even core of quadrupole vibrations. An anharmonic term is included in the phonon spectrum to describe the non-degeneracy of the two-phonon triplet. The effects of considering quasiparticles are also studied and comparison is made with the original version.

In the projected Hartree-Fock model, the variational procedure is carried out after the projection of angular momentum

from a deformed intrinsic state. An additional vibrational correlation of the hexadecapole type is included.

In each approach, calculated and observed energy levels and transition probabilities are discussed in detail. Comparison between results from different approaches is also carried out.

TABLE OF CONTENTS

LIST OF FIGURES

LIST OF TABLES

CHAPTER I INTRODUCTION

I. Purpose of Study

As we all know, the main difficulty behind theoretical studies of nuclear structure lies in the fact that the basic laws of nuclear forces are still unknown. One is faced with two problems: first, to find the laws of the nuclear forces and then, to calculate the nuclear properties resulting from those forces. The nature of these forces are not known at present, so it can only be studied by careful analysis of the properties of the nuclei. The basic problem now becomes the one in finding the law of force, which, when applied to the nuclei, can reproduce the observed properties. Since the nuclear interaction is not known, the exact Hamiltonian for a nuclear system cannot be written. A model Hamiltonian which is solvable is then used instead. The solution of this model Hamiltonian can offer a description of the behaviour of the real nuclei.

In recent years due to highly developed experimental technology, much work has been done successfully on odd mass nuclei whose double even neighboring nuclei exhibit a vibrational spectrum. The purpose of this investigation, is to account for a number of the experimentally observed properties such as energies, spins, and electromagnetic transition rates for the odd -A Cu isotopes in the

mass region $59 < A < 65$.

In this present study, the theory of intermediate coupling approach in the unified model developed by Chaudhury[1] from the outline of Bohr and Mottelson[2,3,4] is applied. This model has been applied extensively to light nuclei as well as heavy nuclei and is proven to be quite successful in general. Not many studies using this model have been conducted on the intermediate nuclei. Therefore the purpose of this study is to show that the application of intermediate coupling model to the odd-mass nuclei in the specific region of $59 < A < 65$ can meet with equal success.

Ample experimental information has been accumulated for Cu^{63} and Cu^{65} but very scarce experimental data is available for Cu^{59} and Cu^{61}, especially Cu^{59}. In calculating the 4 isotopes, and comparing the theoretical results of Cu^{63} and Cu^{65} with the experimentally observed properties, an attempt is made to predict the properties of Cu^{59} and Cu^{61} not yet observed.

In this study, an alternate approach is also used to investigate the odd Cu isotopes theoretically. This is the Hartree-Fock model and it has been applied mainly to light nuclei where the many-body system is simpler. Besides serving as a comparison to the intermediate coupling model approach, the Hartree-Fock calculation is also intended to show the degree of success in its application to the heavy nuclei.

II. Scope Covered

Some background material is presented in Chapter II, describing the historical developments and basic theories of the different models up to and including the unified model. The background around the Hartree-Fock model is also discussed.

The mathematical formulation of all the theory used in this investigation is given in Chapters III and IV. In Chapter III, the classical intermediate coupling model as well as an extended version in which quasiparticles are considered and discussed in parallel. In both cases, the even-even core is taken to include anharmonic effects. In Chapter IV, the projected Hartree-Fock model is developed mathematically. In addition to the classical theory, vibrational correlations of the quadrupole and hexadecapole types are included.

The theoretical results obtained from applying the theory discussed to the odd-mass Cu isotopes are given in the next two Chapters. Comparisons between the theoretical energy levels and electromagnetic transition rates, spectroscopic factors and the corresponding observed values are shown and analysed in all cases.

The last part of the thesis deals with the general conclusions that can be drawn from the entire study. Certain suggestions for future studies in this area are also presented..

Part of the author's time as a graduate student was spent in acquiring some experimental experience in the $Ni^{58}(p, \gamma)Cu^{59}$ reaction. The dynamitron was available for performing angular distribution experiments. Some experimental results were obtained and can be compared with the theoretical angular distributions. An additional Chapter (Chapter IX), is devoted to describing the experimental techniques studied. It is hoped that perhaps this may be of some use to future studies.

CHAPTER II BACKGROUND

I. Historical Background and Development of the Unified Model

1. Liquid-drop Model

Niels Bohr, Frenkel, Kalckar and Wheeler[5,6,7,8] were pioneers of the Nuclear Collective Theory. They postulated and developed the liquid drop model. This model associates the properties of a liquid drop with the nucleus. Certain analogies can be made, such as: the nucleus has closely-packed particles forming a well-defined nuclear surface like the liquid surface. The nucleus can also support surface oscillations as the liquid drop does. The binding energy of a nucleus (which is proportional to its mass number) is analogous to the energy needed to evaporate the drop of liquid into separate molecules (Which is proportional to the number of molecules).

The liquid drop model has met considerable success, treating the nucleus as a deformable body, in the theory of nuclear fission as well as in predictions of some static nuclear properties with atomic number.

The deficiency of this model is in certain unliquid-like features of nuclear matter. Molecules in liquids have short-range forces whereas nucleons have long-range forces. The liquid molecules

are much less mobile than the nucleons. The liquid-drop model therefore over simplifies the dynamical motion in the nucleus. It was indicated that:

> 'The liquid drop model of the nucleus is not very successful in describing the actual excited states. It gives too large level distances.'
>
> 'The liquid drop model is more successful when used to determined the stability of the ground states of nuclei against deformation. The limit for stability against fission is well reproduced, and the underlying idea is well borne out by the fact that nuclei near this limit show the phenomenon of induced fission.' [9]

According to the model, the fundamental modes of nuclear excitation correspond to collective types of motion, such as surface oscillations and elastic vibrations. These collective aspects as indicated by the liquid-drop model are considered significant despite the suspicion of the model itself.

2. Independent Particle Model

At the time when the liquid-drop model was developed, M. Mayer[10], Haxel et al.[11] (both in 1949) introduced the Independent Particle Model (IPM) as an alternative that was equally successful. The IPM assumes that the nucleons in a nucleus move independently in an average field of force created by all the other nucleons. The sum

of these internucleonic forces can be represented in a first order approximation by a static spherically symmetric potential.

Certain analogies can also be drawn between the nucleus and the atomic case in this model. Similar to the above assumption, the electrons in an atom move independently with respect to the other electrons. Another analogy is that the nucleus has a shell structure similar to the atomic shell structure. This conclusion was drawn as a result of the observed periodicities in the properties of the nuclei, after investigations of nuclear stability were made. First such indications were given by G. Gamow[12] and W. Elsasser[13]. Corresponding to the magic numbers of the periodic table are the magic numbers of the nucleus. Nuclei containing 2, 8, 20, 28, 50, 82 or 126 protons or neutrons are more stable than their neighbors. These magic numbers are not as strong as in the case of the atomic structure.

3. Nuclear Shell Model

The shell model can be divided into three sub-models according to their different principles, methods of treatment and their representation of different phases in the development of the shell model itself. They are: the extreme single-particle model (ESPM), the single-particle model (SPM) and the Individual (Independent)-Particle Model (IPM).

In the ESPM, nucleons are assumed to move independently in a central potential. It is found that a central potential intermediate between an infinite square-well potential and a harmonic-oscillator should be used. One such potential is the Woods-Saxon[15] Potential. Mayer[16] and Haxel, Jensen and Suess[17] showed that a strong spin-orbit potential should be added in order to split the degenerate levels with the same orbital angular momentum (i.e. the $j = \ell \pm 1/2$ levels). In this model, the nucleons are paired so that a pair of nucleons contribute zero spin and zero magnetic moment. The paired nucleons form an inert core with total angular momentum and magnetic moment being zero. This is the case with even-even nuclei. A nucleus with odd mass-number A is considered to consist of such a core with a single unpaired nucleon. The properties of the nucleus are ascribed to this single outer nucleon. The core angular momentum is zero while the angular momentum state of the single particle is determined by the level scheme of the central potential modified by a strong spin-orbit potential.

A refined version of the ESPM became the SPM. Instead of considering states of one single particle only, states of several particles are involved. The nucleus now consists of filled (or closed) shells containing the maximum number of protons and neutrons permitted by the Pauli exclusion principle. The remaining particles are in the unfilled (or open) shells and they contribute to the properties of the

nucleus just as the single outer nucleon before. States of these 'loose' particles are considered. Degeneracy of the states of these particles with the same quantum numbers n, ℓ, j is removed by using a two-particle interaction. This shell structure is related to the 'magic numbers' such that a shell closure occurs when there are 2, 8, 20, 50, 82 or 126 protons or neutrons. The energy level just above a closed-shell level has amuch larger spacing than that within a shell.

Progressing further, the IPM is developed. In this model, in contrast to the first two, all the particles in the nucleus are taken into account. It is therefore also known as the many-particle shell model. The potential consists of two parts: A single particle potential and an interparticle potential. To produce a complete set of wave functions, the L-S and j-j coupling schemes have been developed.

Significant contributions to the development of the nuclear shell model have been made after its introduction. Haxel et al.[16] and Mayer[17] established definite evidence for the shell structure in 1949. In 1954, Brueckner et al.[18] and later, Gomes, Walecka and Weisskoff (1958)[19] proved the coexistence of independent particles and hard cores. Before that, the main difficulty with the shell model was that the nucleon-nucleon interaction, having a hard repulsive core should scatter the nucleons far from their shell model orbitals, thus destroying the fundamental principle of the model itself. However, Brueckner theory shows that the Pauli principle restrains this scattering

action. In 1955 and 1959, Nilsson[20,21] introduced a successful form of potential consisting of an axially anisotropic, symmetric oscillator, a spin-orbit term and an additional term proportional to the square of the angular momentum. The first two terms represent a self-consistent, deformed potential. The last term depresses states of higher angular momentum.

4. Unified Model

As more and more experimental data was collected, some phenomena became evident:

1. The lifetimes of nuclear gamma transitions of electric quadrupole type predicted by the shell model are much longer than those observed in some heavy nuclei. The observed lifetimes are about a hundred times shorter than the single-particle estimates.[22]

2. Nuclear quadrupole moments definitely give evidence of shell structure. On the other hand, for some heavy nuclei, the quadrupole moments predicted by the shell model are much larger than the observed values. In some cases, the observed values are more than twenty times larger than the single-particle estimates.[23]

In both cases, the nuclei are in the regions away from the magic numbers or closed shells. Rainwater[24] offered an explanation in 1950, suggesting that deviation from the magic numbers results in deviation from the spherical shape (into spheroidal shape), and this

increases the electric quadrupole moments. This deformation is caused by the centrifugal pressure exerted by the nucleons in the unfilled shells and the filled shells (or core). The quadrupole moments calculated using this assumption have the same sign and the same order of magnitude as those observed.

Bohr and Mottelson[5] indicated that the existence of collective transitions with such short lifetimes is a characteristic feature of the excitation spectra of strongly deformed nuclei. The long lifetimes predicted by the shell model as described in the above phenomenon (1) is thus explained.

By then, it had become evident that even though the shell model and the liquid-drop model approach the problem of nuclear structure in opposite directions, each describes essential features which should be taken into account simultaneously to offer a more complete picture. The phenomena described above indicate that both the collective aspects of the liquid-drop model and the shell structure of the single particle model are equally significant and so there is the necessity of combining the two models.

A quantitative formulation of this combined model based on Rainwater's theory was developed by A. Bohr in 1952[2]. This became the Unified Collective Model and was further expanded in 1953-1955 by Bohr and Mottelson.[3,4] In this model, motions of the individual particles are coupled to nuclear surface oscillations. By shifting

the emphasis from the collective motion of the density to the corresponding motion of the shell model field, the Unified Model was able to incorporate both individual particle and collective effects.

The properties of the Unified Model are dependent on and hence categorized according to the strength of the coupling: i.e. strong coupling, weak coupling and intermediate coupling. The last was discussed in detail by Chaudhury in 1954.[1]

Properties of systems in the intermediate coupling region were analyzed in detail by Chaudhury[1] in 1954. He developed methods along the line of Tamm-Dancoff method of field theory[25] (1954-1950). States containing up to a certain number of quanta of the surface oscillations are included in the diagonalization of the Hamiltonian, and, representation of the uncoupled motion is used.

In recent years, much work has been done on nuclei in the mass region $A < 150$ and $190 < A < 222$ using Chaudhury's method.[26,27,28] with much success in accounting for a number of experimentally observed properties of the low-lying levels. In these calculations, an assumption that a quadrupole phonon spectrum underlies the core spectrum is made. In this phonon spectrum, there exists a triplet of degenerate states at twice the energy of the first excited state. However, the harmonic core vibrations used in these calculations do not describe the non-degeneracy of the two-phonon triplet. A definite improvement on the predictions of the classical mode can be brought about by including an

anharmonic term in the phonon spectrum.[29] In the present work, anharmonic core effects are therefore considered.

In 1956 and 1957, the BCS theory of superconductivity was established[30]. Bohr, Mottelson and Pines[31] suggested the adoption of the BCS theory to nuclear physics. This was later explored by Belyaev[32].

In this approach, nuclear properties are investigated, using a short-range pairing force and a long-range quadrupole force. The pairing forces destroy the independent-particle structure, causing a diffused Fermi surface. In the IPM, there is a sharp cutoff at the Fermi energy, so, all of the single-particle states below the Fermi energy are definitely occupied (hole states), and all of those above the Fermi energy are definitely unoccupied (particle states). The pairing forces cause some of the particles to be excited from the occupied states to the unoccupied states. The probability of occupation of a single-particle state is V^2 and the probability of non-occupation is U^2.

Hybrid particles known as the Independent Quasi-particles are introduced. They move in the pairing field and are generalized fermions which are partly particles (with probability amplitude V) and partly holes (with amplitude U).

Since a single-particle state does not have to be fully occupied or empty, quasiparticles are also considered in the present

work. The effects of this inclusion can then be compared with the calculation using the classical form. It was found that the modification could bring a definite improvement.[34]

5. Hartree-Fock Theory

In the present work, calculations outlined above are restricted to the simplest system of a single particle coupled to quadrupole nuclear surface oscillations (i.e. of the lowest order). For a fuller description of nuclear states, many-particle configuration should be considered. Also, particle states with different values of angular momentum j can be coupled due to the interaction with the surface oscillations. Calculations become complicated because now, the wave function must accomodate a number of unperturbed states. Searches into other branches of many-body theory were made in order to find solutions to the many-body problem in nuclear structure. Important advances were stolen from other fields, for example, the pairing force theory from the BCS theory of superconductivity, quantized field theory from elementary particles, etc. Atomic physics allowed the development of the Hartree-Fock Self-consistent field method. The HF theory provides an approximation for reducing the problem of many interacting particles to one of non-interacting particles in a field. This HF approximation is based on the assumption that each nucleon of the nucleus moves independently in a potential field. This

field consists of the sum of all the interactions of this nucleon with all the other nucleons, averaged over their wave functions.[35]

However, the nucleon interactions contain a strong short-range repulsive core which produces short-range two-body correlations. This 'residual interaction' is neglected in the independent particle wave functions used in the HF theory. As described above, the 'pairing force theory' or Quasiparticle theory is developed to take into account this short-range part of the residual interaction. It can therefore be regarded as a 'generalized HF (or Hartree-Bogolyubov (HB)) theory'.[36] The 'Random Phase Approximation (RPA) or time dependent (TDHF) theory' is also another extension of the HF theory to describe excited states and to consider the long-range part of the residual interaction. The advantages of these extensions are further developed, combining to give the quasi-particle RPA (QPRA) or generalized TDHF. Even though several theories branch out, there is the common theme throughout.

As we can see, collective motion is contained in the Unified Model while the HF theory implies the independent movement of nucleons with respect to each other in an averaged field. But it is established that the HF treatment is well-adapted for the description of collective motion. The explanation of the paradox lies in the fact that the averaged field summarized the effects of all other particles, so in this sense, the description is really collective. The self-consistent field becomes time-dependent when the nucleons vibrate or rotate collectively.

The Unified Model and HF theory also agree in certain aspects, the most important of which is the similar rotational spectrum of the type

$$E = \frac{J(J+1)}{2\mathcal{J}}$$

due to the non-spherical shape of the nucleus given by the model. The above formulation of rotation originates from Bohr and Mottelson's[3] description of the strong-coupling model. The two models differ only in their predictions of $\mathcal{J}$, the moment of inertia. The 'cranking model' is used in the strong-coupling approach to calculate $\mathcal{J}$ quantitatively but it is now believed that the HF theory offers a more correct expression for $\mathcal{J}$.[37]

The HF method has been used extensively to investigate the structure of light nuclei. It becomes a relatively simple method when both neutrons and protons are present outside closed shells, causing strong configuration mixing and hence making the shell-model calculations impractical. The main difficulty in HF calculations is the nucleon-nucleon interaction inside the nuclei. Various attempts have been made to solve this difficulty.[38] Calculations in which an effective internucleon potential inside the nucleus is assumed are also made,[39] thus, avoiding this problem (e.g. G. S. Warke and M. R. Gunye in 1966). Work limited to the closed- shell nuclei is widely explored.[40] In such calculations, the HF potential is assumed to be spherically

symmetric, thus simplifying the HF equations. For non-closed shell nuclei, it is inconsistent with the HF equations to assume such symmetry. Ripka[35] shows that the HF method is especially convenient for treating configuration interaction inside a closed shell, as well as to calculate the configuration interaction between major shells which produce quadrupole deformation and the effective charge.

One main feature of the HF theory is the variational principle used to derive the HF equations. A many body wave function is described as a product of single particle wave functions, ψ_j. Starting with some trial set of these single particle wave functions, the average potential, V_j, is calculated. This is inserted into the HF equations and recalculate the ψ_j. With the new ψ_j's, V_j's are recalculated. The cycle is continued until the same ψ_j's are obtained from successive calculations. Self-consistency is therefore achieved.

The HF Hamiltonian H is then defined by the variational equation

$$\delta \frac{\langle\phi|H|\phi\rangle}{\langle\phi|\phi\rangle} = 0$$

where ϕ are the trial wave functions.

Self-consistency ensures that the HF Hamiltonian will be invariant under rotation so that angular momentum can be preserved as a good quantum number. The solutions to the above equation mix several values of J. The description of a nuclear level thus requires the

use of a projection operator P_J to extract the component of a good quantum number J. The projection technique was developed by Peierls and Yoccoz[41] in 1957. If variation is done before projection, the procedure is the HFP process. An improved version is the variation after projection, the PHF process in which the angular momentum is projected from the trial wave functions, and the resulting projected determinants inserted in the variational equation.

Considerable interest in the HF calculations has been shown in recent years[42-48]. PHF theory is also studied in much detail[49-57]. The PHF and HFP processes are compared,[49,50,55,56,57] and it was concluded that the PHF method is superior over the HFP approach. In one case[57] however, the HFP was found to be a fairly good approximation.

The HF model tends to compress the energy spectrum, Das-Gupta and Harvey[58] suggested that there are residual correlations (β vibration) which are of importance. Rowe[59] has also discussed several methods of describing 'vibrational' correlations in finite nuclei.

In the present calculation, the PHF method is used and an additional vibrational correlation is included in the variational procedure, following the line of Castel and Parikh.[55]

CHAPTER III FORMULATION OF THE UNIFIED NUCLEAR MODEL

I. General Theory

It was mentioned before that the properties of the Unified Model can be divided into three systems depending on the coupling strength. This in turn depends on the correlation between nucleons in the nucleus. (Mottelson, 1960) There are two major types of correlation attributed to two different schemes by which the particles can couple. One type is favored by the tendency of each nucleon to align its orbit with the long-range average field produced by all the other nucleons. This gives rise to the 'aligned coupling' scheme. The other type is favored by the tendency of particles coupling in pairs to $J = 0$ configuration. The latter is due to short-range inter-nucleonic forces and gives rise to the 'pair coupling' scheme. The aligned coupling scheme produces a deformed equilibrium shape while the pair coupling scheme makes for a spherical equilibrium shape. Rowe[36] has developed in detail the wave functions in both cases.

These two kinds of forces tend to compete with each other and the equilibrium shape of the nucleus depends on the balance between them. It seems that the shell structure is definitely related to the domineering strength of the two opposing schemes. At the

beginning of the shell, pair coupling dominates whereas aligned coupling overrides towards the end of the shell. This conclusion can be drawn from the following:

If N particles in 2Ω more or less degenerate magnetic substates are considered and, if -F is the potential energy of a nucleon in the field created by one other, then the potential energy for aligned coupling is

$$\Delta E(\text{aligned}) \sim -\tfrac{1}{2}N(N-1)F \qquad (N \ll \Omega)$$

For pair coupling, the potential energy for a single-pair state in a $(j)^2$ configuration is $-\Omega G$. Therefore the potential energy for N/2 pairs is

$$\Delta E(\text{pairing}) \sim -\tfrac{1}{2}N\Omega G \qquad (N \ll \Omega)$$

Also $G < F$ since shell structure exists and this is only so if pairing forces dominated over field forces (Mottelson, 1960). From the above argument, it can be seen that pair coupling dominates when $N \ll \Omega G/F$, i.e. at the beginning of the shell and gives way to aligned coupling when $N > \Omega G/F$ near the end of the shell.

1. Strong Coupling Model

When the strength of the aligned force exceeds that of the pairing force, then the long range forces become strong and so does the coupling between the single particle and the core. This is then

the strong coupling system which covers the region of nuclear mass number A, where $150 < A < 190$ and $A > 222$. This is then the region of nuclei far from either neutron or proton closed-shells. Nuclei of large surface deformation are found in this region.

The mathematical formulation of the strong coupling model of Bohr and Mottelson is well presented in their works[3]. An approximate solution is obtained, depending on the condition that the particle motion is fast compared to that of the deformed nuclear surface. The relatively slow vibration and rotation of the entire system can then be considered. Certain spatial orientation stability of the nuclear surface is required due to the large deformation.

The particle exerts a centrifugal pressure, giving the surface an axially symmetric shape. The resulting nuclear coupling scheme is illustrated here,

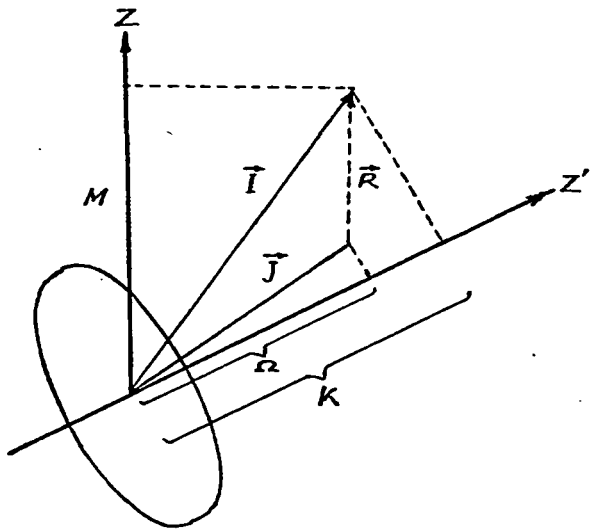

Fig. III.1 (from A. Bohr)

The angular momentum $\vec{j}$ of the particle precesses around the nuclear axis with a constant projection Ω. The total angular momentum $\vec{I}$ is the sum of $\vec{j}$ and the angular momentum $\vec{R}$ of the surface. The coupled system of particle and surface rotates like a symmetric top with quantum numbers I, k (i.e. projection of $\vec{I}$ on nuclear axis) and M (i.e. projection of $\vec{I}$ on space fixed axis).

The angular momentum components j_z and I_z are approximately constants of motion for existing solutions to the wave function. The Hamiltonian can be written as

$$H = H_o + U \qquad \text{(III.1)}$$

where H_o is the part of H commuting with j_z and I_z (the unperturbed Hamiltonian), while the perturbation U contains no diagonal elements in the j_z and I_z representation. It is found that[3] the perturbation term U can be neglected within the limit of this strong coupling approximation.

The strong coupled system is best described by means of the Eulerian angles θ_i, specifying a coordinate system fixed in the nucleus as well as the two surface coordinates β and δ where β is the deformation parameter and γ is an angular coordinate characterizing the eccentricity of the nuclear shape.

H_o consists of a kinetic energy part T and a function of β and γ, i.e. $W(\beta, \gamma)$

$$H_o = T + W(\beta, \gamma) \tag{III.2}$$

Since for each particle state, there is a spectrum of vibrational and rotational states,

$$T = T_{\text{vibrational}} + T_{\text{rotational}}$$

$$W(\beta, \gamma) = W_{\text{rotational}} + W_{\text{vibrational}} \tag{III.3}$$

For strong coupling, the dominant term is the vibrational energy $T_{\text{vibrational}}$, therefore;

$$H_o = T_{\text{vibrational}} + W_{\text{rotational}} + W_{\text{vibrational}} \tag{III.4}$$

and

$$H_{\text{strong coupling}} = H_o = T_{\text{vibrational}} + W(\beta,\gamma) \tag{III.5}$$

A Bohr and B. Mottelson give the wave functions for the strong coupling approximation as

$$\Psi_{\text{strong coupling}} = |\Omega; n_\beta n_\gamma; IkM\rangle$$

$$= \left(\frac{2I+1}{16^2}\right)^{\frac{1}{2}} \rho_{n_\beta n_\gamma}(\beta,\gamma) \{X_\Omega D^I_{Mk}(\theta_i) + (-)^{I-j} X_{-\Omega} D^I_{M-k}(\theta_i)\} \tag{III.6}$$

where X_n describes the motion of the particle with respect to the deformed nucleus, $\rho_{n_\beta n_\gamma}$ represents vibrations in β and γ characterized

by the quantum numbers n_β and n_γ , and D^I_{Mk} describes the nuclear rotations. They are also eigenfunctions of the symmetric top. This wave function $\Psi_{s.c.}$ is valid for $\omega_p >> \omega_c$ (i.e. for the precession frequency of the particle large compared to the collective frequencies).

Since the surface is invariant under the rotation of 180^o about an axis perpendicular to the nuclear symmetry axis, one can see the reason behind the simultaneous occurence of both signs for Ω and k in the $\Psi_{\text{strong coupling}}$. The total parity of $\Psi_{s.c.}$ is therefore made sure to be the same as that of the particle state.

The strong coupling model has been extremely successful in predicting the rotational spectra of heavy nuclei. It was shown above that the rotational spectrum consists of $W_{\text{rotational}}(\beta,\gamma)$ since $T_{\text{rotational}}(\beta,\gamma)$ i.e. the rotational part of the kinetic energy is negligible. $W_{\text{rotational}}(\beta,\gamma)$ is given as[3].

$$W_{\text{rotational}}(\beta,\gamma) = \frac{\hbar^2}{2\mathcal{J}_z}(k - \Omega)^2 + \left(\frac{\hbar^2}{4\mathcal{J}_x} + \frac{\hbar^2}{4\mathcal{J}_y}\right)\{I(I+1) - k^2 + j(j+1) - \Omega^2 - (-1)^{I-j}(j+\tfrac{1}{2})(I+\tfrac{1}{2}) \times \delta_{\Omega,\frac{1}{2}}\,\delta_{k\frac{1}{2}}\} \tag{III.7}$$

where $\mathcal{J}_x$, $\mathcal{J}_y$, $\mathcal{J}_z$ are the components of the effective moment of inertia .

For even-even nuclei, the total angular momentum I is equal to the surface angular momentum R. The above equation simplifies and the rotational spectrum is given by

$$E_{rotational} = \frac{\hbar^2}{2\mathcal{J}}(I(I+1) - k^2) \qquad \text{(III.8)}$$

for even particle number, k = 0, it follows that

$$E_{rotational} = \frac{\hbar^2}{2\mathcal{J}} I(I+1) \qquad \text{(III.9)}$$

The symmetrized wavefunction $\Psi_{s.c.}$ vanishes unless I = 0, 2, 4. So the allowed values of I are 0, 2, 4, 6,----

In an odd-A nucleus, the last odd particle has an angular momentum $\vec{j}$ and a projection Ω along the nuclear axis. If the ground state spin is I_o, then for $I_o > \frac{1}{2}$,

$$E_{rotational} = \frac{\hbar^2}{2\mathcal{J}} [I(I+1) - I_o(I_o+1)] \qquad \text{(III.10)}$$

where

$I > \Omega$ in magnitude,

therefore

$I_o = \Omega$

So, $I = I_o, I_o + 1, I_o + 2,$------where each I has only one rotational state.

For a $k = \frac{1}{2}$ band, the equation

$$E_{rotational} = \frac{\hbar^2}{2}[I(I+1) - k^2] \quad \text{generalizes to}$$

become

$$E_{rotational} = \frac{\hbar^2}{2}[I(I+1) + \delta_{k\frac{1}{2}}\, a(-1)^{I+\frac{1}{2}}(I+\tfrac{1}{2})] \qquad \text{(III.11)}$$

where a is the 'decoupling parameter'[36] which measures the breakdown of the strong coupling of the particle to the deformed core. Using the above sequence the rotational states are: 1/2, 3/2, 5/2, 7/2, 9/2---

2. Weak Coupling Model

In the weak coupling region, i.e. in the immediate vicinity of closed-shells, the pair coupling scheme dominates. The short-range pairing forces override the long-range forces, hence the weak coupling between the single particle and the core.

In the weak coupling model, the motions of the particle and the surface are approximated to be independent of each other. The particle is described by the same shell model quantum numbers, while the surface oscillations are represented by N phonons, each with total angular momentum R and its z- component M_R. Usually, two additional quantum numbers are required to describe the state of the surface completely, but for small N ($N < 3$), R and M_R are sufficient.

The wave function can be expanded in the representation of uncoupled motion even though the effect of the coupling implies a certain interweaving of particle and surface motion.

$$\Psi_{\text{weak coupling}} = \sum_{jNR} |\, j;NR;IM\rangle\langle j;NR;IM|\rangle \qquad \text{(III.12)}$$

The weak coupling causes the angular momentum j to be shared between the particle and the surface, which is reflected in a reduction of the expectation value of j_z. If j remains a constant of motion,

$$\langle j_z\rangle = (1 - \frac{15}{128\pi} \frac{(2j - 1)(2j + 3)}{j^2(j + 1)^2} \frac{k^2}{\hbar\omega C})M \qquad \text{(III.13)}$$

where k is the coupling constant, ω the surface frequency and C the deformability.

From here, a dimensionless parameter x is extracted

$$x = \sqrt{\frac{5}{16\pi}} \quad \frac{1}{\sqrt{j}} \quad \frac{k}{\sqrt{\hbar\omega C}} \qquad \text{(III.14)}$$

x is a measure of the strength of the coupling.

$$\langle j_z\rangle = (1 - \text{cons.} \quad (x\sqrt{j})^2)M \qquad \text{(III.15)}$$

where $x\sqrt{j}$ becomes the relevant parameter for perturbation expansion. One sees that the validity of the weak-coupling approximation is determined by the smalless of x. $x\sqrt{j}$ also represents the order of

magnitude of the amplitude of the one-phonon state. Inversely, for $x >> 1$, the strong coupling approximate solution becomes valid.

3. Intermediate Coupling Model

This model is applied to the gap between the regions of validity of the perturbation approximation ($x\sqrt{j} << 1$) and the strong coupling approximation($x >> 1$). Intermediate coupling is especially important for large j. Increasing number of phonons are required to achieve the strong coupling situation for increasing j.

By illustrating the process of transfer of angular momentum to the surface as a function of x, it has been shown [36] that a coupling strength of $x = 0.9\sqrt{j}$ for A = 20 increases rather slowly with A to a value of $x = 1.4\sqrt{j}$ for A = 200. This then corresponds to the intermediate region in which neither the weak coupling perturbation nor the strong coupling approximation would work.

In this region, the weak coupling wave function can be used, with the expansion carried sufficiently far for an adequate representation of the nuclear state. The determination of the coefficients of the wave function requires the solution of the corresponding secular determinant. In 1945 and 1950, Tamm and Dancoff[25] developed the method of field theory. In 1954, Chaudhury[1] explored techniques to analyze the properties of the intermediate coupling system, using the representation of the uncoupled

motion and diagonalizing the Hamiltonian, including states containing up to a certain number of quanta of the surface oscillations. His method is somewhat similar to that of Tamm-Dancoff. Later,[28] Chaudhury and Bailey refined the method but complication still arises in the calculation when the number of unperturbed states included in the wave function becomes too many. The simplest system which is studied here consists of a single particle coupled to quadrupole nuclear surface oscillations. This technique has proven to be very successful in calculations of low-lying levels of odd-A nuclei in the regions $A < 150$ and $190 < A < 222$.

In the next section, the mathematical formulation of the ICM is discussed.

II. Mathematical Formulation of the ICM

The basic concept of the ICM is that the nucleus is a system consisting of single nucleons coupled to an even-even core. As a result of the interaction between the nucleons outside the core and the core the nuclear surface supports oscillations about a spherical shape when certain modes of oscillation are excited. Since the core exhibits collective motion, its oscillation is analogous to that of the classical liquid-drop. In other words, the even-even nucleus can be visualised as

a quantized liquid drop.

The mathematical formulation of the ICM is concerned basically with three parts, i.e. the part describing the motion of the nucleons outside the core, the part describing the collective motion of the core surface and the part describing the interaction between the core and the nucleons outside it. Along this line, A Bohr[2] has developed the explicit Hamiltonian which is given in the following section. The nuclear spin of the nucleus is therefore the vector sum of the spins of the core and the nucleons outside the core, i.e. for an odd-mass nucleus,

$$\vec{I} = \vec{R} + \vec{j} \qquad \text{(III.16)}$$

where

I is the resultant spin of the nucleus

R is the spin of the core

j is the spin of the nucleon outside the core.

In the ICM, the coupling between the core and the single particles is strong enough to cause splitting of the energy levels of the nucleus but not to deform the nuclear surface appreciably from its equilibrium shape.

1. Hamiltonian in the ICM

The Hamiltonian in its classical form[1] is separated into three parts:

$$H = H_c + H_{s.p.} + H_{int.} \qquad \text{(III.17)}$$

where H_c is the usual Hamiltonian for the core vibrations, modified in this study to take into account the splitting of the two-phonon states, $H_{s.p.}$ is the usual single-particle shell-model Hamiltonian describing the motion of the nucleons outside the core, and $H_{int.}$ is the interaction Hamiltonian describing the interaction between these outside nucleons and the core.

2. H_c, the core Hamiltonian

From the analogy to the liquid-drop mentioned above, the classical solution is developed, which is then quantized to give the explicit surface Hamiltonian.

The shape of a liquid-drop, having a constant density throughout can be described in terms of its radius in polar coordinates $R(\theta, \zeta)$. Assuming that oscillations from a spherical shape are small, this can be expanded in terms of the spherical harmonics,

$$R(\theta, \zeta) = R_o(1 + \sum_{\lambda\mu} \alpha_{\lambda\mu} Y_{\lambda\mu}(\theta, \zeta)) + O(\alpha^2) \qquad \text{(III.18)}$$

where

R_o radius of the nucleus in its spherical equilibrium shape

$Y_{\lambda\mu}$ normalized spherical harmonic function of order λ, μ and with the Condon and Shortley phase convention

$\alpha_{\lambda\mu}$ expansion parameters which are coordinates describing the deformation of the nuclear surface.

Unlike the liquid-drop, nuclear density is not constant throughout, but has a radial shape. Assuming that the density maintains its radial shape as it oscillates for collective modes known as 'volume conserving modes' or 'irrotational flow', then the above expression for $R(\theta, \zeta)$ applies to each equi-density surface and is hence still valid.

(λ) can take on all non-negative integers while (μ) for a given (λ) can assume all integers from $(-\lambda)$ to (λ) including zero. Terms corresponding to $\lambda = 0$ and $\lambda = 1$ can be omitted because they both occur at high excitation energies only. The former represents an isotropic volume change of the nucleus, whereas the latter, of three terms, correspond to the collective dipole oscillations of the neutrons with respect to the protons. There are five terms corresponding to $\lambda = 2$, representing the quadrupole oscillations of the core and

seven terms corresponding to $\lambda = 3$, representing the octupole vibrations of the core. The terms for $\lambda = 2$ are the leading terms and will be the only ones considered in this study. Hence from now on (λ) will only assume the value (2) and the subscript can be neglected.

For small coefficients $\alpha_{2\mu}$ (where $\{\alpha_{2\mu}\}$ are much less than unity), it is possible to show that the potential energy for such a system of small deformation, to first order, is given by

$$V = \tfrac{1}{2} \sum_{\mu=-2}^{2} C|\alpha_\mu|^2 \qquad \text{(III.19)}$$

and the kinetic energy by

$$T = \tfrac{1}{2} \sum_{\mu=-2}^{2} B|\dot{\alpha}_\mu|^2 \qquad \text{(III.20)}$$

B and C are hydrodynamic parameters because pure surface oscillation is assumed. B is the 'mass parameter' and C is the 'nuclear deformability'.

$$C = 4R_o^2 S - \frac{3}{2\pi} \frac{1}{5} \frac{Z^2 e^2}{R_o} \qquad \text{(III.21)}$$

where Ze is the uniformly distributed electrostatic charge of the nucleus.

S is the surface tension and

$$4\pi R_o^2 S = 15.4\ A^{2/3}\ \text{MeV} \quad [61] \qquad \text{(III.22)}$$

$$B = \frac{3}{8\pi} AMR_o^2 \qquad \text{(III.23)}$$

where A is the atomic number and M the nucleon mass. The collective Hamiltonian of the core surface is:

$$H_c = \tfrac{1}{2} \sum_{\mu=-2}^{2} (B|\dot{\alpha}_\mu|^2 + C|\alpha_\mu|^2) \qquad \text{(III.24)}$$

Such a harmonic oscillator Hamiltonian has the familiar classical solution

$$\omega = \sqrt{\frac{C}{B}} \qquad \text{(III.25)}$$

$$\alpha_\mu = \varepsilon_\mu \cos \omega t \qquad \text{(III.26)}$$

$$E = \sum_{\mu=-2}^{2} \tfrac{1}{2}|\varepsilon_\mu|^2 \omega^2 B \qquad \text{(III.27)}$$

The motion is quantized, in the usual way, by introducing momentum coordinates

$$P_\mu = \frac{\partial H_c}{\partial \dot{\alpha}_\mu} = B\dot{\alpha}_\mu^* \qquad \text{(III.28)}$$

P_μ and α_μ are now quantum mechanical operators required to obey the following commutation relations:

$$[\alpha_\mu, \alpha_{\mu'}] = [\alpha_\mu^*, \alpha_{\mu'}^*] = 0 \qquad \text{(III.29)}$$

$$[P_\mu, P_{\mu'}] = [P_\mu^*, P_{\mu'}^*] = 0$$

$$[\alpha_\mu, P_{\mu'}] = [\alpha^*_\mu, P^*_{\mu'}] = +i\hbar\delta_{\mu\mu'}$$

with solution,

$$P_\mu = -i\hbar \frac{\partial}{\partial \alpha_\mu} \tag{III.30}$$

The quantized Hamiltonian is now,

$$H_c = \sum_{\mu=-2}^{2} \left(\frac{1}{2B} |P_\mu|^2 + \frac{C}{2}|\alpha_\mu|^2\right) \tag{III.31}$$

Following the usual procedure, for solution of the harmonic oscillator problem, the creation and annihilation operators are introduced: (Villars, 1963)

$$b^*_\mu = \left(\frac{C}{2\hbar\omega}\right)^{\frac{1}{2}} \alpha^*_\mu - i \left(\frac{1}{2\hbar\omega B}\right)^{\frac{1}{2}} P_\mu \tag{III.32}$$

$$b_\mu = \left(\frac{C}{2\hbar\omega}\right)^{\frac{1}{2}} \alpha_\mu + i \left(\frac{1}{2\hbar\omega B}\right)^{\frac{1}{2}} P^*_\mu \tag{III.33}$$

It follows directly from the above two expression that (b^*_μ) and (b_μ) satisfy the usual commutation rules:

$$[b_\mu, b_{\mu'}] = [b^*_\mu, b^*_{\mu'}] = 0 \tag{III.34}$$

$$[b_\mu, b^*_{\mu'}] = \delta_{\mu\mu'}$$

By inversion of the expressions for the creation and annihilation operators, the coordinates and momenta can be expressed as:

$$\alpha_\mu = \left(\frac{\hbar}{2B\omega}\right) \left(b_\mu + (-)^\mu b_{-\mu}\right) \tag{III.35}$$

$$P_\mu = i \frac{\hbar B\omega}{2} \left(b^*_\mu - (-)^\mu b_{-\mu}\right) \tag{III.36}$$

Substituting these into the expression for H_c, yields

$$H_c = \sum_{\mu=-2}^{2} \frac{\hbar\omega}{2} \left(b^*_\mu b_\mu + b_\mu b^*_\mu\right)$$

$$= \sum_{\mu=-2}^{2} \hbar\omega \left(b^*_\mu b_\mu + \tfrac{1}{2}\right) \tag{III.37}$$

It is apparent now that the quantized liquid-drop behaves as a collection of independent harmonic oscillators with energies $\hbar\omega$.

The creation and annihilation operators are connected to the occupation numbers n_μ by:

$$b_\mu b^*_\mu = n_\mu + 1 \tag{III.38}$$

$$b^*_\mu b_\mu = n_\mu$$

The surface Hamiltonian H_c is diagonal in the n_μ representation and the corresponding eigenvalues become:

$$E_N = \hbar\omega \sum_{\mu=-2}^{2} (n_\mu + \tfrac{1}{2}) \qquad \text{(III.39)}$$

But,

$$N = \sum_{\mu=-2}^{2} n_\mu = 0, 1, 2, \ldots\ldots$$

Therefore,

$$E_N = \hbar\omega(N + 5/2) \qquad \text{(III.40)}$$

From the equation of motion,

$$[H_c, b_\mu^*] = \hbar\omega b_\mu^* \qquad \text{all } \mu, \qquad \text{(III.41)}$$

it follows that, a band of excited states can be generated from the ground state, by the successive application of the step-up operators b_μ^*. This band gives rise to a harmonic spectrum of energy levels, i.e. the quadrupole vibrational spectrum:

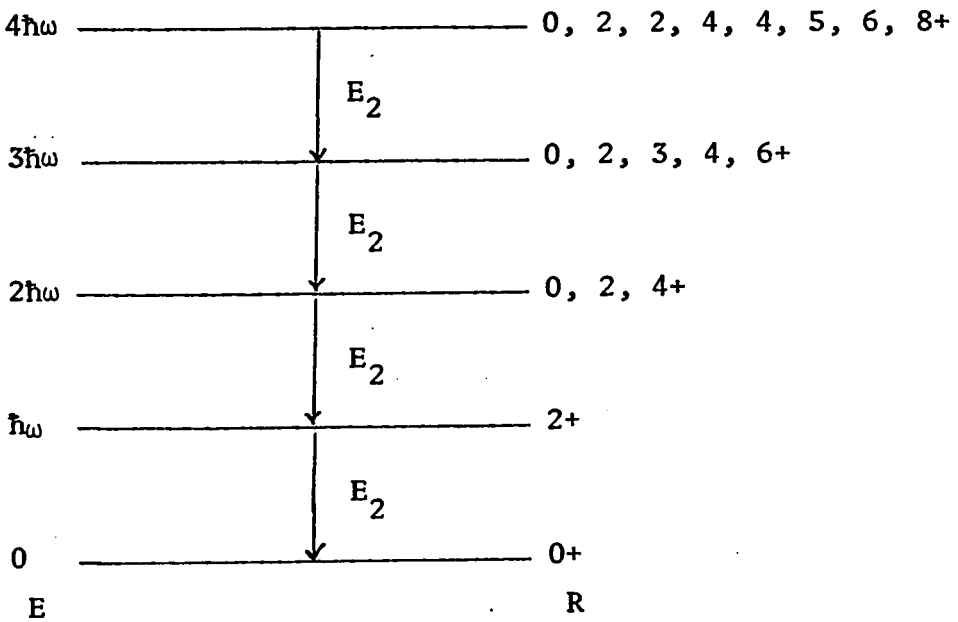

Fig. III.2

The energy levels are equally spaced with each energy difference being $\hbar\omega$. Each level is as many times degenerate as there are ways to distribute the N excitation quanta among the five degrees of freedom. Each quanta is a Bose-Einstein particle or phonon of spin (2). n_μ is the number of phonons with a μ_z component of angular momentum $\mu\hbar$. Therefore the surface having N phonons each of angular momentum $2\hbar$, has a resultant angular momentum $R\hbar$ due to the coupling of these phonons. Only certain R's are allowed because the N oscillator quanta are identical bosons and consequently can only couple such that the combination is symmetric. The possible angular momentum states can be obtained by a tedious counting scheme discussed by Hecht[62] (1964) in his lecture notes.

The spectrum shown in the diagram is actually the general form of the experimental excitation spectra in even-even nuclei in a broad region of the nuclear mass spectrum, $50 < A < 150$.

From the above diagram, it can be seen that for each N, the allowed values of R are:

N	R
0	0
1	2
2	0, 2, 4
3	0, 2, 3, 4, 6
4	0, 2, 2, 4, 4, 5, 6, 8

For N less than 3, the surface state can be completely described by the number of phonons N and the surface angular momentum Rħ. For N greater than 3, degeneracy results and it is necessary to include another quantum number (seniority) for a complete description.

In the present calculations, only cases of N < 3 are considered.

3. $H_{s.p.}$, the particle Hamiltonian

In the present study, only the case of a single nucleon outside an even-even core is studied. This nucleon can occupy several shell-model single particle states. The odd nucleon has an orbital angular momentum quantum number ℓ and an intrinsic spin quantum number such that $\vec{j} = \vec{\ell} + \vec{s}$, where j is now the total angular momentum quantum number. The z-component of j is m. Again, using the formalism

of second quantization, the set of fermion creation and annihilation operators a^*_{jm} and a_{jm}, respectively, is introduced:

$$[a^*_{jm'}, a_{jm}]_+ = \delta_{jj'} \delta_{mm'} \qquad \text{(III.42)}$$

$$[a_{j'm'}, a_{jm}]_+ = 0 = [a^*_{j'm'}, a_{jm}]_+$$

$$a^*_{jm} |0> = |jm> \qquad \text{(III.43)}$$

Therefore, the particle Hamiltonian can be written as:

$$H_{s.p.} = \sum_{jm} \varepsilon_j a^*_{jm} a_{jm} \qquad \text{(III.44)}$$

where ε_j is the excitation energy of the j level.

E_J is the single particle eigenvalue of H_p, and is used as an adjustable parameter, being varied around the single-particle excitation energy ε_j, taken from experiments.

4. $H_{int.}$, the Interaction Hamiltonian

A first order estimate of the interaction between the last odd nucleon and the collective oscillations of the nuclear surface was derived by Milford [63] and is presented here.

The interaction between nucleons is taken to be a two-body

interaction, depending only on the internucleonic distance. The core is also taken to be a liquid-drop of A-1 nucleons. The interaction between the last odd nucleon and the core is then a function of the coordinates (r_p, Ω_p) of the nucleon and the collective coordinates (α_μ) of the core surface,

$$\text{INT.} = \int_{\text{core}} V(\vec{\rho})\,dV \qquad \text{(III.45)}$$

where

$$V(\vec{\rho}) = V(|\vec{r}_p - \vec{r}_c|) = \sum_{\ell=0}^{\infty} g_\ell(r_p, r_c) P_\ell(\cos\gamma) \qquad \text{(III.46)}$$

$\vec{r}_p$ is the radius vector of the last odd nucleon

$\vec{r}_c$ is the radius vector of a volume element dV of the core

γ is the angle between $\vec{r}_p$ and $\vec{r}_c$

$P_\ell(\cos\gamma)$ is the set of Legendre Polynomials. (Rose 1957)

Using the spherical Harmonic Addition Theorem, this is expressed as:

$$\text{INT.} = \sum_{\ell=0}^{\infty} \sum_{m=-\ell}^{\ell} \left(\frac{4\pi}{2\ell+1}\right)^{\frac{1}{2}} \int d\Omega_c \int_0^{R(\Omega_c)} g_\ell(r_p, r_c) r_c^{\,2} dr_c$$

$$\times\ Y^*_{\ell m}(\Omega_c) Y_{\ell m}(\Omega_p) \qquad \text{(III.47)}$$

or

$$\text{INT.} = \sum_{\ell=0}^{\infty} \sum_{m=-\ell}^{\ell} \left(\frac{4\pi}{2\ell+1}\right)^{\frac{1}{2}} \int d\Omega_c \; G_\ell(r_p, R(\Omega_c)) \; Y^*_{\ell m}(\Omega_c)$$

$$\times \; Y_{\ell m}(\Omega_p) \qquad \text{(III.48)}$$

where

$$G_\ell(r_p, R(\Omega_c)) = \int_o^{R(\Omega_c)} g_\ell(r_p, r_c) r_c^2 dr_c \qquad \text{(III.49)}$$

and

$$R(\Omega_c) = R_o\left(1 + \sum_{\lambda\mu} \alpha_{\lambda\mu} Y_{\lambda\mu}(\Omega_c)\right) + O(\alpha^2) \qquad \text{(III.50)}$$

and

$$\Omega_p = (\theta_p, \phi_p) \qquad \Omega_c = (\theta_c, \phi_c)$$

Assuming the surface oscillations to be small, $G_\ell(r_p, R(\Omega_c))$ can be expanded in a Taylor series about R_o, and to first order,

$$G_\ell(r_p, R(\Omega_c)) \sim G_\ell(r_p, R_o) + g_\ell(r_p, R_o) R_o^3 \sum_{\mu=-2}^{2} \alpha_\mu Y_{2\mu}(\Omega_c)$$

(III.51)

Substituting back into eq. (III.48) and using the orthogonality of the spherical harmonics,

$$\text{INT} = \sqrt{4\pi}\, G_o(r_p, R_o) + \left(\frac{4\pi}{5}\right)^{\frac{1}{2}} R_o^3 \sum_{\mu=-2}^{2} G_2(r_p, R_o)$$

$$\times \; \alpha_\mu \; Y_{2\mu}(\Omega_p) \qquad \text{(III.52)}$$

The first term is the effective single-particle potential, representing the interaction of the odd nucleon with the undistorted core. This is included in H_p. The second term is the particle-core coupling interaction, and is usually written in the form:

$$H_{INT.} = -k(r_p) \sum_{\mu=-2}^{2} \alpha_\mu Y_{2\mu}(\Omega_p) \qquad \text{(III.53)}$$

The matrix elements of $k(r_p)$ depend on the initial and final state of the system, but this dependence is negligible so that if a nucleus is assumed to have a sharp boundary, $k(r_p)$ becomes a surface delta function:

$$k(r_p) = R_o V_o \delta(r_p - R_o) \qquad \text{(III.54)}$$

where V_o is the nuclear potential. If n is the principal quantum number and ℓ the orbital quantum number, $\phi_{n\ell}(r)$ the radial wave function, then

$$\langle n'\ell' | k(r_p) | n\ell \rangle = V_o R_o^3 \phi^*_{n'\ell'}(R_o) \phi_{n\ell}(R_o) \qquad \text{(III.55)}$$

According to Bohr and Mottelson, this is approximately independent of n and ℓ for binding energies in the range of 5 - 10 MeV. This can be treated as a constant of 40 MeV, assuming a kinetic energy of 25 MeV inside the nucleus.

Expressing α_μ in terms of the creation or annihilation operators, H_{INT} can now be written as:

$$H_{INT.} = -k \left(\frac{\hbar\omega}{2C}\right)^{\frac{1}{2}} \sum_{\mu=-2}^{2} (b_\mu + (-)^\mu b_\mu^*) Y_{2\mu}(\Omega_p) \qquad \text{(III.56)}$$

OR

$$H_{INT.} = -\left(\frac{\pi}{5}\right)^{\frac{1}{2}} \hbar\omega\zeta \sum_{\mu=-2}^{2} (b_\mu + (-)^\mu b_\mu^*) Y_{2\mu}(\Omega_p) \qquad \text{(III.57)}$$

where

$$\zeta \equiv k \left(\frac{5}{2\pi\hbar\omega C}\right)^{\frac{1}{2}} ,$$

a dimensionless coupling parameter defined by Chaudhury[27].

5. Explicit Hamiltonian In the Classical Model

Combining H_c, $H_{s.p.}$ and $H_{INT.}$, the total Hamiltonian becomes:

$$H = \sum_{\mu=-2}^{2} \hbar\omega \left(b_\mu^* b_\mu + \tfrac{1}{2}\right) + \sum_{jm} \varepsilon_j a_{jm}^* a_{jm}$$

$$- \left(\frac{\pi}{5}\right)^{\frac{1}{2}} \hbar\omega\zeta \sum_{\mu=-2}^{2} (b_\mu + (-)^\mu b_{-\mu}^*) Y_{2\mu}(\Omega_p) \qquad \text{(III.58)}$$

The basis vectors for the space are chosen following Chaudhury's standard technique in order to obtain the eigenfunctions and eigenvalues of the Hamiltonian in the ICM. These are formed from the eigenvectors of the uncoupled system in the angular momentum representation, and are of the form:

$$|j;NR:IM> = \sum_{m_j, m_R} C(jRI;m_j m_R M)\,|jm_j>|NRm_R> \qquad \text{(III.59)}$$

where

$j\hbar$ is the angular momentum of the last odd nucleon

$R\hbar$ is the angular momentum of the surface vibration

N is the number of phonons in the vibrational surface

$I\hbar$ is the total angular momentum of the system

and $\vec{I} = \vec{j} + \vec{R}$.

$m_j\hbar$ is the z-projection of the odd nucleon and

$m_R\hbar$ is the z-projection of the core surface

$M\hbar$ is the z-projection of the total system

and

$C(jRI;m_j m_R M)$ is the Clebsch-Gordan coefficient. The following eigenvalue equation is satisfied by the basic eigenvectors:

$$H_c|j;NR;IM> = (N + 5/2)\hbar\omega|j;NR;IM> \qquad \text{(III.60)}$$

$$H_{s.p.}|j;NR;IM> = E_j|j;NR;IM> \qquad \text{(III.61)}$$

such that

$$(H_C + H_{s.p.})|j;NR;IM> = [(N + 5/2)\hbar\omega + E_j]\,|\,j;NR;IM> \qquad \text{(III.62)}$$

As we can see, both H_C and $H_{s.p.}$ are diagonal in the basis chosen, and the diagonal matrix elements of the total Hamiltonian are contributed by them:

$$\langle j;NR;IM|H_C + H_{s.p.}|j;NR;IM\rangle = (N + 5/2)\hbar\omega + E_j \qquad \text{(III.63)}$$

The off-diagonal elements due to H_C and $H_{s.p.}$ are zero, but the elements of $H_{INT.}$ are given by:

$$\langle j', N'R';I'M'|H_{INT.}|j;NR;IM\rangle = -\sqrt{\frac{\pi}{5}}\,\hbar\omega\,\zeta$$

$$\times \langle j';N'R';I'M'|\sum_{\mu=-2}^{2}(b_\mu + (-)^\mu b^*_{-\mu})Y_{2\mu}(\Omega_p)|j;NR;IM\rangle \qquad \text{(III.64)}$$

Since the creation and annihilation operators do not connect states with the same N, all the diagonal elements due to $H_{INT.}$ are zero.

A complete matrix of the total Hamiltonian can now be obtained, where the diagonal elements are completely and only given by H_C and $H_{s.p.}$ and the off-diagonal elements by $H_{INT.}$. Certain selection rules must be obeyed, they are,

$$\Delta N = 1$$

$$\Delta R \leq 2$$

$$\Delta j \leq 2$$

$$\Delta \ell = 0 \text{ or } 2.$$

In the actual calculation of $\langle j';N'R';I'M'|H_{INT.}|j;NR;IM\rangle$, b_μ is

redefined in terms of an irreducible tensor, $A_{-\mu}$, so that it can be dealt with just as $b^*_{-\mu}$ and $Y_{2\mu}$ are components of irreducible tensors of second rank;

$$\text{i.e.} \quad b_\mu = (-)^\mu A_{-\mu} \,, \tag{III.65}$$

so that

$$\langle j';N'R';I'M'|H_{INT.}|j;NR;IM\rangle = -\sqrt{\frac{\pi}{5}}\,\hbar\omega\,\delta\,\langle j';N'R';IM|$$

$$\sum_\mu ((-)^\mu A_{-\mu} + (-)^\mu b^*_{-\mu}) Y_{2\mu}(\Omega_p)|j;NR;IM\rangle \tag{III.66}$$

$H_{INT.}$ now is the sum of two scalar products of two irreducible tensors of second rank operating on two independent spaces. $A_{-\mu}$, $b^*_{-\mu}$ operate on the collective space whereas $Y_{2\mu}$ acts on the single nucleon space.

Using the following general relationship derived by Bailey from Racah Algebra, i.e. †

$$\langle j_1'j_2'j'm'|T_L(1)\cdot T_L(2)|j_1j_2m\rangle = \delta_{jj'}\delta_{mm'}\,(-)^{j_1+j_2-j}$$

$$\sqrt{(2j_1'+1)(2j_2'+1)}\;\; x\;\; W(j_1j_2j_1'j_2';jL)\langle j_1'||T_L(1)||j_1\rangle$$

$$x\;\langle j_2'||T_L(2)||j_2\rangle \tag{III.67}$$

where $T_L(1)$ and $T_L(2)$ are spherical tensor operators operating in different spaces, the matrix elements of $H_{INT.}$ for $N' < N$ becomes:

† Bailey, Appendix A1, eq. 17. See Reference no. 64.

$$\langle j';N'R';I'M'|H_{INT.}|j;NR;IM\rangle = (-)^{j' + R' - I + 1}$$

$$\times\ \delta_{MM'}\delta_{II'}\sqrt{\frac{\pi}{5}}\ \hbar\omega\delta\ \sqrt{(2j' + 1)(2R + 1)}\ W(jRj'R';I2)$$

$$\times\ \langle \ell's'j'||Y_2||\ell s_j\rangle\ \langle N'R'||b||NR\rangle \qquad \text{(III.68)}$$

$W(jRj'R';I2)$ is a Racah coefficient, $\langle \ell's'j'||Y_2||\ell sj\rangle$ and $\langle N'R'||b||NR\rangle$ are reduced matrix elements. The latter two can be derived† since,

$$\langle \ell's'j'||Y_2||\ell sj\rangle = (-)^{\ell - j' + \frac{1}{2}}\left[\frac{5}{4\pi}(2\ell + 1)(2j + 1)\right]^{\frac{1}{2}}$$

$$\times\ \langle \ell\ 2\ 000|\ell'0\rangle W(\ell_j\ell'j';\tfrac{1}{2}\ 2) \qquad \text{(III.69)}$$

$$\langle j;N'R';I'M'|H_{INT.}|j;NR;IM\rangle = (-)^{j' + R' - I + 1}$$

$$\times\ \delta_{MM'}\delta_{II'}\sqrt{\frac{\pi}{5}}\ \hbar\omega\delta\ \sqrt{(2j' + 1)(2R + 1)}\ W(jRj'R';I2)$$

$$\times\ (-)^{\ell - j + \frac{1}{2}}\sqrt{\frac{5}{4\pi}}\ \sqrt{(2\ell + 1)(2j + 1)}\ \langle \ell\ 2\ 000|\ell'0\rangle$$

$$\times\ W(\ell j\ell'j';\tfrac{1}{2}\ 2)\ \langle N'R'||b||NR\rangle = (-)^{R' - I + 3/2 + \ell}$$

$$\times\ \delta_{MM'}\delta_{II'}\ \tfrac{1}{2}\hbar\omega\delta\ \sqrt{(2j' + 1)(2R + 1)}\ \sqrt{(2\ell + 1)(2j + 1)}$$

† Bailey, Appendix III and IV.

$$\times\ W(jRj'R';I2)\ W(\ell j\ell' j';\tfrac{1}{2}\ 2)\ \langle \ell 2\ 000|\ell' 0\rangle\langle N'R'||b||NR\rangle \qquad \text{(III.70)}$$

Since $H_{INT.}$ is Hermitian, its matrix is symmetric in (N,R) and (N',R').

The eigenvectors of the total Hamiltonian H can be expressed as a linear combination of the basis vectors.

$$|E;IM\rangle = \sum_{jNR} A(jNRI|E)|j;NR;IM\rangle \qquad \text{(III.71)}$$

where A(jNRI|E) are expansion coefficients representing the amplitudes of the basis states. The eigenvalue equation of H is:

$$H|E;IM\rangle = E|E:IM\rangle \qquad \text{(III.72)}$$

where E is the eigenvalue of the nuclear state $|E;IM\rangle$.

This equation can be solved by diagonalizing the total Hamiltonian H in the space of the basis states. In the present calculation, computation of this sort is done on an IBM-360/65 computer system.

6. Inclusion of Anharmonic Core Effects

In the classical version of the ICM, one basic assumption is that there is a quadrupole phonon spectrum underlying the core spectrum, (Fig. 2). The first excited state (R = 2+) has an energy of $\hbar\omega$. The second excited state consists of a triplet of degenerate states (R = 0+, 2+, 4+) at $2\hbar\omega$.

In the present study, an anharmonic term is included in the phonon spectrum to describe the non-degeneracy of the two-phonon triplet[29, 34]. Before, it is assumed that each triplet states has an energy of $2\hbar\omega$. Now, it is taken to have an energy $(2 + \eta_R)\hbar\omega$, where η_R is not necessarily zero, and is defined by the core spectrum, i.e.:

$$N = 2 \left\{ \begin{array}{l} \text{———— } R = 4 \\ \text{———— } R = 2 \\ \text{———— } R = 0 \end{array} \right\} \quad (2 + \eta_R)\hbar\omega \quad \begin{array}{l} E_{24} \\ E_{22} \\ E_{20} \end{array}$$

$$N = 1 \quad \text{———— } R = 2 \quad \hbar\omega \quad E_{12}$$

$$N = 0 \quad \text{———— } R = 0 \quad 0 \quad 0$$

core spectrum

$$\begin{aligned} E_{12} &= \hbar\omega \\ (2 + \eta_o)\hbar\omega &= E_{20} \\ (2 + \eta_2)\hbar\omega &= E_{22} \\ (2 + \eta_4)\hbar\omega &= E_{24} \end{aligned} \qquad \text{(III.73)}$$

From the above equations, η_o, η_2 and η_4 can be determined. The core Hamiltonian H_C can now be written as:

$$H_C = \hbar\omega \sum_{\mu} (b^*_\mu b_\mu) + \frac{1}{4} \sum_{R=0,2,4} \hbar\omega\eta_R (b^*_\mu b^*_\mu)^R (b_\mu b_\mu)^R \qquad \text{(III.74)}$$

(c.f. eq. (III.37))

and

$$E_{N=1} = \hbar\omega$$

$$E_{N=2} = (2 + \eta_R)\hbar\omega.$$

$H_{s.p.}$ and $H_{INT.}$ of course remain unchanged. The total Hamiltonian becomes

$$H = \sum_{\mu=-2}^{2} \hbar\omega(b^*_\mu b_\mu) + \frac{1}{4} \sum_{R=0,2,4,} \hbar\omega\eta_R (b^*_\mu b^*_\mu)^R (b_\mu b_\mu)^R +$$

$$\sum_{jm} \varepsilon_j a^*_{jm} a_{jm} - \sqrt{\frac{\pi}{5}}\, \hbar\omega\zeta \sum_{\mu=-2}^{2} (b_\mu + (-)^\mu b^*_{-\mu}) Y_{2\mu}(\Omega_p)$$

(III.75)

The diagonal elements are given by:

$$\langle j;NR;IM | (H_C + H_{s.p.}) | j;NR;IM\rangle = [E_N + E_j] \qquad \text{(III.76)}$$

where E_N is defined above for N = 1 and N = 2. The off diagonal elements are the same as before (eq. (III.70).

III. Nuclear Electromagnetic Transitions in the Intermediate Coupling Model

In addition to the theoretical prediction of energy levels, spins and eigenfunctions, the theoretical analysis of electromagnetic properties is important because it yields further insight into the nuclear structure. For example, the magnitude of the electromagnetic transition rates is strongly dependent on the nature of the wave functions describing the levels.

The theory describing the quantized electromagnetic radiation from a nuclear source is presented in detail by Blatt and Weisskopf (1952),[65] Preston (1962)[66] as well as de-Shalit and Talmi (1963)[67]. In the present study, the electric quadrupole (E2) and magnetic dipole (M1) transitions are of main concern between low-lying levels of the same parity. Expressions for calculating these within the ICM will be developed.[3] First, the matrix elements of the multipole operator $M(\lambda, \mu)$ are calculated. Then, the explicit expressions for the multipole transition rates are presented in terms of the expansion coefficients of the nuclear eigenfunctions.

The transition probability $T(\lambda)$ for electromagnetic radiation of multipole order, λ, and angular frequency ω is derived by means of the standard long-wavelength approximation to be:-

$$T(\lambda) = \frac{8\pi(\lambda + 1)}{\lambda[(2\lambda + 1)!!]^2} \frac{1}{\hbar} \left(\frac{\omega}{C}\right)^{2\lambda + 1} B(\lambda) \qquad \text{(III.77)}$$

where $B(\lambda)$ is the reduced transition probability between the initial state $|E;IM\rangle$ and the final state $|E';I'M'\rangle$ given by:-

$$B(\lambda) = \Sigma|\langle E';I'M'|\ M(\lambda, \mu)|E;IM\rangle|^2 \qquad \text{(III.78)}$$

The summation should be over the final states and the average over the initial states since the orientation of these states is unknown. Therefore,

$$B(\lambda) = \frac{1}{2\lambda + 1} \sum_{M\mu M'} |\langle E';I'M'|M(\lambda, \mu)|E;IM\rangle|^2 \qquad \text{(III.79)}$$

1. Electric Quadrupole Transitions

Matrix elements of the Electric Quadrupole Operator.

The electric multipole operator for this model is given as:[3]

$$m_e(\lambda, \mu) = \frac{Ze}{A^2}\ r^\lambda Y_{\lambda\mu}(\theta, \phi) + \frac{3}{4\pi} ZeR_o^\lambda \alpha^*_{\lambda\mu} \qquad \text{(III.80)}$$

According to Kisslinger and Sorenson[68] and others[69], an effective charge e_{eff} is required for the last odd nucleon so that polarization is accounted for, therefore,

$$m_e(\lambda, \mu) = (e_{eff} + \frac{Ze}{A^2})\ r^\lambda Y_{\lambda\mu}(\theta, \phi) + \frac{3}{4\pi} ZeR_o^\lambda \alpha^*_{\lambda\mu} \qquad \text{(III.81)}$$

where R_o is the equilibrium radius given by:

$$R_o = 1.18 \times 10^{-13} A^{1/3} \text{cm}.$$

The eq. above can be separated into two parts, i.e. one contributed by the odd nucleon and the other by the core surface:

$$m_{pe}^{(p)}(\lambda, \mu) = (e_{eff} + \frac{Ze}{A^2}) r^{\lambda} Y_{\lambda\mu}(\theta, \phi) \qquad \text{(III.82)}$$

$$m_e^{(e)}(\lambda, \mu) = \frac{3}{4\pi} ZeR_o^{\lambda} \alpha_{\lambda\mu}^{*} \qquad \text{(III.83)}$$

For $\lambda = 2$, the matrix elements between the initial state $|E;IM\rangle$ and the final state $|E';I'M'\rangle$ are:

$$\langle E';I'M'|m_e(2, \mu)|E;IM\rangle = \langle E';I'M'|m_e^{(p)}(2, \mu)|E;IM\rangle + \langle E';I'M'|m_e^{(e)}(2, \mu)|E;IM\rangle \qquad \text{(III.84)}$$

Using eqs. (III.82) and (III.83) and expressing in terms of the expansion coefficients,

$$\langle E';I'M'|m_e^{(p)}(2, \mu)|E;IM\rangle = \sum_{\substack{j'N'R' \\ jNR}} A(j'N'R'I'|E')A(jNRI|E)$$

$$\times \langle j';N'R';I'M'|m_e^{(p)}(2, \mu)|j;NR;IM\rangle = (e_{eff} + \frac{Ze}{A^2}) \sum_{\substack{j'N'R' \\ jNR}}$$

$$A(j'N'R'I'|E')A(jNRI|E) \langle r^2\rangle \langle j';N'R';IM|Y_{2\mu}(\theta, \phi)|j;NR;IM\rangle \qquad \text{(III.85)}$$

$$\langle E';I'M'|m_e^{(e)}(2,\mu)|E;IM = \sum_{\substack{j'N'R'\\jNR}} A(j'N'R'I'|E')A(jNRI|E)$$

$$\times \langle j';N'R';I'M'|m_e^{(e)}(2,\mu)|j;NR;IM\rangle = \frac{3}{4\pi} ZeR_o^2 \sum_{\substack{j'N'R'\\jNR}}$$

$$A(j'N'R'I'|E')A(jNRI|E)|j';N'R';I'M'|\alpha^*_{\lambda\mu}|j;NR;IM\rangle$$

$$= \frac{3}{4\pi} Ze R_o^2 \left(\frac{h}{2B\omega}\right)^{\frac{1}{2}} \sum_{\substack{j'N'R'\\jNR}} A(j'N'R'I'|E')A(jNRI|E)$$

$$\times \langle j';N'R';I'M'|(b^*_\mu + A_\mu)|j;NR;IM\rangle \qquad \text{(III.86)}$$

According to Moszkowski[70], $\langle r^2\rangle$ can be assumed to be independent of the quantum number n and ℓ so that

$$r^2 = \frac{3}{5} R_o^2 \,. \qquad \text{(III.87)}$$

Re-expressing eq. (III.85) in terms of the reduced matrix elements $\langle j'||Y_2||j\rangle$,† using the expression

$$\langle j_1'j_2'j'm'|T_{LM}(1)|j_1j_2m\rangle = C(jLj';mMm') \quad (-)^{j_2 + L - j_1 - j'}$$

$$\times \delta_{j_2j_2} \left((2j+1)(2j'+1)\right)^{\frac{1}{2}} W(j_1jj_1'j';j_2L) \quad \langle j_1'||T_L||j_1\rangle$$

† Bailey Appendix I eq. A.I.14.

where $\vec{j} = \vec{j}_1 + \vec{j}_2$, we get

$$\langle E';I'M'|m_e^{(p)}(2,\mu)|E;IM\rangle = \frac{3}{5}\left(e_{eff} + \frac{Ze}{A^2}\right)R_o^2\,(2I+1)^{\frac{1}{2}}$$

$$\times\; C(I2I';M\,M') \sum_{\substack{j'N'R'\\ jNR}} A(j'N'R'I'|E')A(jNRI|E)$$

$$\times\; (-)^{R-j-I'}\sqrt{2j'+1}\,\langle j'||Y_2||j\rangle W(jIj'I';R2) \qquad \text{(III.88)}$$

Re-expressing eq. (III.86) in terms of the reduced matrix elements $\langle N'R'||b||NR\rangle$ and $\langle N'R'||A||NR\rangle$, using the expression[†]

$$\langle j_1'j_2'j'm'|T_{LM}(2)|j_1j_2jm\rangle = C(jLj';mMm')\;(-)^{2j_1-j+j_1'+j_2'-2j+L}$$

$$\times\; \delta_{j_1j_1'} \times \sqrt{(2j+1)(2j_2'+1)}\; W(j_2jj_2'j';j_1L)\langle j_2'||T_L||j_2\rangle$$

we get

$$\langle E';I'M'|m_e^{(e)}(2,\mu)|E'\;IM\rangle = \frac{3}{5}Z_eR_o^2\,\frac{\hbar\omega}{k}\sqrt{2I+1}\,\sqrt{\frac{5}{16}}$$

$$\times\; C(I2I';M_\mu M') \sum_{\substack{j'N'R'\\ jNR}} A(j'N'R'I'|E')A(jNRI|E)\;(-)^{I-j'}\delta_{jj'}\delta_{\ell\ell'}$$

$$\times\; \left[(-)^{R'}\sqrt{(2R'+1)}\,\langle N'R'||b^*||NR\rangle + (-)^{R}\sqrt{(2R+1)}\,\langle N'R'||b||NR\rangle\right.$$

$$\left.\times\; W(RIR'I';j2)\right] \qquad \text{(III.89)}$$

[†] Bailey, Appendix I, eq. A.I.15.

where ζ has been introduced.

Reduced Electric Quadrupole Transition Probability

Using the expression for $B(\lambda)$ and the above expressions for $\langle E';I'M'|m_e(2,\mu)|E;IM\rangle$, the reduced transition probability for electric quadrupole transitions, B(E2) can be obtained. In this case, $\lambda = 2$, therefore,

$$B(E2) = \frac{1}{2I+1} \sum_{M\mu M'} \Big| C(I2I';M\mu M') \sqrt{2I+1} \sum_{\substack{j'N'R' \\ jNR}} A(j'N'R'I'|E') \times A(jNRI|E) \Big[\frac{3}{5} (e_{eff} + \frac{Ze}{A^2}) R_o^2 (-)^{\frac{1}{2}+\ell+j'+j+R-I'} \delta_{NN'} \delta_{RR'} \times C(\ell 2\ell';000) \times \sqrt{\frac{5}{4\pi}(2j'+1)(2j+1)(2\ell+1)} W(jIj'I';R2) \times W(\ell j\ell' j';\tfrac{1}{2}2) + \frac{3}{4\sqrt{5\pi}} \frac{ZeR_o^2}{k} \zeta \hbar\omega (-)^{I-j'} \delta_{jj'} \delta_{\ell\ell'} W(RIR'I';j2) \times \left((-)^{R'} \sqrt{2R'+1} \langle N'R'||b^*||NR\rangle + (-)^{R} \sqrt{2R+1} \langle N'R'||b||NR\rangle \right) \Big]^2 \quad \text{(III.90)}$$

The Clebsch-Gordan coefficient $C(I2I';M\mu M')$ can be taken outside the summation over j', N', R' and j,N,R. Squaring and summing over M, μ, and M', as a result of the orthogonality of the Clebsch-Gordan

coefficients, a factor (2I' + 1) is obtained so that the above expression becomes:

$$B(E2) = (2I' + 1)\Big| \sum_{\substack{jN'R' \\ jNR}} A(j'N'R'I'|E')A(jNRI|E)$$

$$x \left[\frac{3}{5} \left(e_{eff} + \frac{Ze}{A^2}\right) R_o^2 (-)^{\frac{1}{2}+\ell+j'+j+R-I'} \delta_{NN'} \delta_{RR'} \right.$$

$$x\ C(\ell 2\ell;000) \sqrt{\frac{5}{4\pi}\,(2j' + 1)(2j+ 1)(2\ell + 1)}$$

$$x\ W(jIj'I';R2)\ W(\ell j\ell'j';\tfrac{1}{2}2) + \frac{3}{4\sqrt{5\pi}} \frac{ZeR_o^2}{k}$$

$$x\ \zeta\hbar\omega(-)^{I-j'} \delta_{jj'}\delta_{\ell\ell'}\ W(RIR'I';j2) \left((-)^{R'} \sqrt{2R' + 1}\right.$$

$$\left. x\ \langle N'R'||b^*||NR\rangle + (-)^{R} \sqrt{2R + 1}\ \langle N'R'||b||NR\rangle)\right]\Big|^2$$

(III.91)

according to eq. (II.77),

$$T(E2) = \frac{12\pi}{[\,5!!\,]^2} \frac{1}{\hbar} \left(\frac{\omega}{C}\right)^5 B(E2) \qquad \text{(III.92)}$$

2. Magnetic Dipole Transitions

Matrix Elements of the Magnetic Dipole Operator

The magnetic dipole operator is given by:

$$m_m(1, \mu) = \frac{\mu_N}{2}\sqrt{\frac{3}{\pi}}\,(g_\ell \ell_{1z} + g_{s_{eff}} S_{1z} + g_R R_{1z}) \qquad \text{(III.93)}$$

where

μ_N is the nuclear magneton

g_ℓ is the orbital gyromagnetic ratio

g_R is the effective gyromagnetic ratio of the core and

$$g_R = \left(\frac{Z}{A}\right)$$

$g_{s_{eff}}$ is the effective spin gyromagnetic factor introduced to account for polarization effects phenomenologically

ℓ_{1z}, S_{1z} and R_{1z} are spherical tensors corresponding to ℓ, S and R. Similar to the matrix elements of the electric quadrupole operator,

$$\langle E',I'M'|m_m(1, \mu)|E;IM\rangle = \frac{\mu_N}{2}\sqrt{\frac{3}{\pi}} \sum_{\substack{j'N'R' \\ jNR}} A(j'N'R'I'|E')A(jNRI|E)$$

$$\times \langle j';N'R';I'M'|\, g_\ell \ell_{1z} + g_{s_{eff}} S_{1z} + g_R R_{1z}|j;NR;IM\rangle \qquad \text{(III.94)}$$

Separating into three parts, we get:

$$\langle E';I'M'|m_m(1,\mu)|E;IM\rangle = \frac{\mu_N}{2}\sqrt{\frac{3}{\pi}}\,[g_\ell\langle E';I'M'|\ell_{1z}|E;IM\rangle$$

$$+ g_{s_{eff}}\langle E';I'M'|S_{1z}|E;IM\rangle + g_R\langle E';I'M'|R_{1z}|E;IM\rangle] \qquad \text{(III.95)}$$

Each part is now considered separately.

$$\langle E';I'M'|\ell_{1z}|E;IM\rangle = \sum_{\substack{j'N'R'\\ jNR}} A(j'N'R'I'|E')A(jNRI|E)$$

$$\times\ \langle j';N'R';I'M'|\ell_{1z}|j;NR;IM\rangle$$

where

$$\langle j'N'R';I'M'|\ell_{1z}|j;NR;IM\rangle = C(I1I';M\mu M')\,(-)^{R+1-j-I'}$$

$$\times\ \delta_{NN'}\delta_{RR'}\sqrt{(2I+1)(2j'+1)}\ W(jIj'I';R1) \qquad \langle j'||\ell||j\rangle$$

$$= C(I1I';M\mu M')\,(-)^{\frac{1}{2}+R+j+j'-\ell-I'}\,\delta_{\ell\ell'}\sqrt{(2I+1)(2j+1)(2j'+1)\ell(\ell+1)(2\ell+1)}$$

$$\times\ W(jIj'I';R1)\ W(\ell j\ell' j';\tfrac{1}{2}1) \qquad \text{(III.97)}$$

Therefore, substituting into eq. (III.95), the first term is calculated

$$\langle E';I'M'|\ell_{1z}|E;IM\rangle = C(I1I';M\mu M') \sum_{\substack{j'N'R'\\ jNR}} A(j''N'R'I'|E')$$

$$\times\ A(jNRI|E)\ (-)^{R+1-j-I'}\ \delta_{\ell\ell}\ \sqrt{(2I+1)(2j+1)(2j'+1)\ell(\ell+1)(2\ell+1)}$$

$$\times\ \delta_{NN'}\delta_{RR'}\ W(jIj'I';R1)\ W(\ell j\ell'j';\tfrac{1}{2}1) \qquad \text{(III.98)}$$

$$\langle E';I'M'|S_{1z}|E';IM\rangle = \sum_{\substack{j'N'R'\\ jNR}} A(j'N'R'I'|E')A(jNRI|E)$$

$$\times\ \langle j';N'R';I'M'|S_{1z}|j;NR;IM\rangle \qquad \text{(III.99)}$$

Again, using ref. * and ref.† .

$$\langle j';N'R';I'M'|S_{1z}|j\ ;NR\ ;IM\rangle = C(I1I';M\mu M')(-)^{R+1-j-I'}$$

$$\times\ \delta_{\ell\ell'}\sqrt{(2I+1)(2j'+1)}\ W(jIj'I';R1) \qquad \langle j'||S||j\rangle$$

$$= C(I1I';M\mu M')(-)^{R+\ell'+\frac{1}{2}-I'}\ \delta_{\ell\ell'}\sqrt{\tfrac{3}{2}(2I+1)(2j+1)(2j'+1)}$$

$$\times\ W(jIj'I';R1)\ \ W(\tfrac{1}{2}j\tfrac{1}{2}j';\ell 1) \qquad \text{(III.100)}$$

* Bailey, Appendix IV. eq. (A.IV.24).

Substituting into eq. (III.99), one obtains the second term,

$$\langle E';I'M'|S_{1z}|E;IM\rangle = C(I1I';M\mu M') \sum_{\substack{j'N'R' \\ jNR}} A(j'N'R'I'|E')A(jNRI|E)$$

$$x\ (-)^{R+\ell'+\frac{1}{2}-I'}\ \delta_{\ell\ell'}\sqrt{\frac{3}{2}(2I+1)(2j+1)(2j'+1)}\ \delta_{NN'}\delta_{RR'}$$

$$x\ W(jIj''I'';R1)\ W(\tfrac{1}{2}j\tfrac{1}{2}j';\ell 1) \qquad \text{(III.101)}$$

Proceeding to the third term, we have,

$$\langle E';I'M'|R_{1z}|E;IM\rangle = \sum_{\substack{j'N'R' \\ jNR}} A(j'N'R'I'|E)A(jNRI|E)$$

$$x\ \langle j';N'R';I'M'|R_{1z}|j;NR;IM\rangle \qquad \text{(III.102)}$$

By the expression of * and † $\langle j';N'R';I'M'|R_{1z}|j;NR;IM\rangle$ becomes:

$$\langle j';N'R';I'M'|R_{1z}|j;NR;IM\rangle = C(I1I';M\mu M')\ (-)^{2j-I+j'+R'-2I'+1}$$

$$\delta_{\ell\ell'}\delta_{jj'}\sqrt{(2I+1)(2R'+1)}\ W(RIR'I';j1)\ \langle N'R'||R||NR\rangle$$

(III.103)

Using the expression $\langle N'R'||R||NR\rangle = \delta_{NN'}\delta_{RR'}\sqrt{R(R+1)}$**, this is expressed as:

** Bailey, Appendix IV. eq. (A.IV.24)

$$\langle j';N'R';I'M'|R_{1z}|j;NR;IM\rangle = C(I1I';M\mu M')(-)^{I+j-R'}\,\delta_{\ell\ell'}\delta_{jj'}$$

$$\sqrt{(2I+1)(2R'+1)R(R+1)}\quad W(RIR'I';j1)\delta_{NN'}\delta_{RR'} \qquad \text{(III.104)}$$

Substituting this into the eq. (III.102), the third term is obtained as:

$$\langle E';I'M'|R_{1z}|E;IM\rangle = C(I1I';M\mu M') \sum_{\substack{j'N'R'\\ jNR}} A(j'N'R'I'|E')A(jNRI|E)$$

$$\times\,(-)^{I+j'-R'}\,\delta_{\ell\ell'}\delta_{jj'}\,\sqrt{(2I+1)(2R'+1)R(R+1)}$$

$$\times\, W(RIR'I';j1)\delta_{NN'}\delta_{RR'} \qquad \text{(III.105)}$$

Inserting there three terms into eq. (III.95), we can get the matrix elements:

$$\langle E';I'M'|m_m(1,\mu)|E;IM\rangle = \frac{\mu_N}{2}\sqrt{\frac{3}{\pi}} \sum_{M\,M'} C(I1I';M\mu M') \sum_{\substack{j'N'R'\\ jNR}}$$

$$A(j'N'R'I'|E')A(jNRI|E) \quad [g_\ell(-)^{R+1-j-I'}\delta_{\ell\ell'}$$

$$\sqrt{(2I+1)(2j+1)(2j'+1)\ell(\ell+1)(2\ell+1)}\,\delta_{NN'}\delta_{RR'}\, W(jIj'I';R1)\quad W(\ell j\ell' j';\tfrac{1}{2}1)$$

$$+\; g_{s_{eff}}(-)^{R+\ell'+\frac{1}{2}-I'}\delta_{\ell\ell'}\sqrt{\tfrac{3}{2}(2I+1)(2j+1)(2j'+1)}\,\delta_{NN'}\delta_{RR'}$$

$$W(jIj'I';R1)\; W(\tfrac{1}{2}j\tfrac{1}{2}j';\ell') + g_R(-)^{I+j'-R'}\delta_{\ell\ell'}\delta_{jj'}$$

$$\sqrt{(2I+1)(2R'+1)R(R+1)}\,\delta_{NN'}\delta_{RR'}\, W(RIR'I';j1)\;\delta_{NN'}\delta_{RR'}]$$

(III.105)

Reduced Magnetic Dipole Transition Probability

Using the above expression into the eq. (III.78), where $\lambda = 1$ we can obtain B(M1).

$$B(M1) = \frac{3\mu N^2}{4\pi} \frac{1}{2I+1} \sum_{M\mu M'} |C(I1I';M\mu M') \sqrt{2I+1}$$

$$\sum_{\substack{j'N'R' \\ jNR}} A(j'N'R'I'|E')A(jNRI|E) \times \left[g_\ell (-)^{\frac{1}{2}+R+j+j'-\ell-I'} \delta_{NN'}\delta_{RR'}\delta_{\ell\ell'}\right.$$

$$\sqrt{(2j'+1)(2j+1)(2\ell+1)\ell(\ell+1)} \quad W(jIj'I';R1)\, W(\ell j\ell' j';\tfrac{1}{2}1)$$

$$+ g_{s_{eff}} (-)^{R+\ell'+\frac{1}{2}-I'} \delta_{NN'}\delta_{RR'}\delta_{\ell\ell'} \sqrt{\frac{3}{2}(2j+1)(2j'+1)} \quad W(jIj'I';R1)$$

$$\times \quad W(\tfrac{1}{2}j\tfrac{1}{2}j';\ell 1) + g_R (-)^{I+j'-R'} \delta_{NN'}\delta_{RR'}\delta_{jj'}\delta_{\ell\ell'}$$

$$\left.\sqrt{(2R'+1)R(R+1)} \quad W(RIR'I';j1)\right]\Big|^2 \qquad \text{(III.107)}$$

Again, using the same procedure on the Clebsch-Gordan coefficient C(I1I';M M'), the final expression for B(M1) is:

$$B(M1) = \frac{3\mu_N^2}{4\pi}(2I'+1)\Big| \sum_{\substack{j'N'R' \\ jNR}} A(j'N'R'I'|E')A(jNRI|E)$$

$$\times \Big[g_\ell (-)^{\frac{1}{2}+R+j+j'-\ell-I'} \delta_{NN'}\delta_{RR'}\delta_{\ell\ell'} \sqrt{(2j'+1)(2j+1)(2\ell+1)\ell(\ell+1)}$$

$$\times W(jIj'I';R1)\, W(\ell j\ell' j';\tfrac{1}{2}1) + g_{s_{eff}} (-)^{R+\ell'+\frac{1}{2}-I'} \delta_{NN'}\delta_{RR'}\delta_{\ell\ell'}$$

$$\times \sqrt{\tfrac{3}{2}(2j'+1)(2j+1)}\; W(jIj'I';R1)\, W(\tfrac{1}{2}j\tfrac{1}{2}j';\ell 1) + g_R (-)^{I+j'-R'}$$

$$\times \delta_{NN'}\delta_{RR'}\delta_{jj'}\delta_{\ell\ell'} \sqrt{(2R'+1)R(R+1)}\; W(RIR'I';j1)\Big]\Big|^2 \qquad \text{(III.108)}$$

Using eq. (III.77), T(M1) is obtained, i.e.:

$$T(M1) = \frac{16\pi}{[3!!]^2} \frac{1}{\hbar} \left(\frac{\omega}{c}\right)^3 B(M1) \qquad \text{(III.109)}$$

IV. Quasiparticles

In the classical version of the ICM discussed above, two basic assumptions are made. One is that the single particle states are either fully occupied or empty. The other assumption is that the quadrupole operator $\alpha_{2\mu}$ which is approximately equal to $\gamma^2 Y^2_{2\mu}$ is simply proportional to the phonon operator, i.e. $\alpha_\mu \propto (b_\mu + (-)^\mu b^*_\mu)$. Or, specifically, α_μ is defined to be (see eq. (III.35)

$$\alpha_\mu = \frac{\hbar}{2B\omega} (b_\mu + (-)^\mu b^*_\mu) \qquad \text{(III.35)}$$

According to this latter assumption, the quadrupole moments of phonon states are zero and electric quadrupole transitions only exist between states differing by one phonon, i.e. $|N' - N| = 1$.

Data gathered from vibrating nuclei show evidence that these assumptions are not entirely valid. In Chapter I, quasiparticles have already been introduced. The short-range pairing forces cannot be neglected and they destroy the Fermi picture of single particle states, causing a diffusion in the Fermi surface. Quasiparticles are then the hybrid particles which are partly particles, with probability amplitude v and partly holes, with probability amplitude u, such that

$$u^2 + v^2 = 1 \qquad \text{(III.110)}$$

The Bogolubov-Valatin[71,72] canonical transformation can be used to replace the actual system of interacting nucleons by a system of non-interacting quasiparticles. The quasiparticle creation or annihilation operator becomes a linear combination of a shell model particle and a shell model hole creation or annihilation operator.

Since quadrupole moments are definitely observed in the core nuclei studied in the present work, the second assumption should be dropped. Hence in this modified version of the ICM, the phonon states are allowed to have the experimental quadrupole moments. Instead of dealing with the phonon operator b_μ, the explicit quadrupole operator $\alpha_{2\mu}$ is used.

In the following, the mathematical formulation used in this modified version is presented.

1. Explicit Hamiltonian and its matrix Elements in the Modified ICM

The total Hamiltonian still consists of $H_{s.p.}$, H_c and $H_{INT.}$. $H_{s.p.}$ remains the usual single-particle shell-model Hamiltonian, and H_c is the same Hamiltonian for the core vibrations, with anharmonicity included, i.e. eqs. (III.44) and (III.74).

The effects of including quasiparticles appear in the interaction Hamiltonian $H_{INT.}$.

$$H_{INT.} = -\sqrt{\frac{\pi}{5}}\ \hbar\omega\ \zeta \sum_\mu (b_\mu + (-)^\mu b^*_\mu) Y_2 (\Omega_p) \qquad \text{(III.57)}$$

Replacing $(b_\mu + (-)^\mu b^*_{-\mu})$ by $\alpha_{2\mu}$, the revised form becomes:

$$H_{INT.} = -\zeta\hbar\omega\sqrt{\pi/5} \sum_\mu \alpha_{2\mu} Y_{2\mu}(\Omega_p) \quad \text{where} \quad \Omega_p = \theta_p, \phi_p$$

$Y_{2\mu}$ is the angular part of the quadrupole operator α.

The total Hamiltonian now becomes:

$$H = H_{s.p.} + H_c + H_{INT.}$$

$$= \sum_{jm} \epsilon_j a^*_{jm} a_{jm} + \sum_\mu \hbar\omega(b^*_\mu b_\mu) + \tfrac{1}{4} \sum_{R=0,2,4} \hbar\omega\eta_R (b^*_\mu b^*_\mu)^R (b_\mu b_\mu)^R$$

$$- \sqrt{\pi/5}\, \zeta\hbar\omega \sum_\mu \alpha_{2\mu} Y_{2\mu}(\Omega_p) \qquad \text{(III.111)}$$

The matrix elements of H_c and $H_{s.p.}$ remain the same as in the classical form and contribute the diagonal elements in the total matrix of H.

The matrix elements of $H_{INT.}$ contribute the off-diagonal members again, and in the revised form, are given by:

$$\langle j';N'R';IM \,|H_{INT.}|\, j;NR;IM\rangle = (-)^{j'-R'-I+1} \delta_{MM'} \delta_{II'} \sqrt{\pi/5}\, \hbar\omega\delta$$

$$\times \sqrt{(2j'+1)(2R+1)} \quad W(jRj'R';I2) \; (-)^{\ell-j+\frac{1}{2}} \quad \sqrt{5/4\pi}\, \sqrt{(2\ell+1)(2j+1)}$$

$$\times \quad \langle \ell 2000 | \ell' 0\rangle \; W(\ell j \ell' j';\tfrac{1}{2}2) \quad \langle N'R' || \alpha || NR\rangle (u_j u_{j'} - v_j v_{j'}) \qquad \text{(III.112)}$$

where u_j and v_j represent the quasiparticle and quasihole amplitudes in state j, respectively.

In its classical form, $\langle N'R'||b||NR\rangle$ is non-zero only when $|N' - N| = 1$, and is taken to be the pure harmonic value. In the revised model, $\langle N'R'||\alpha||NR\rangle$ is dependent upon the observed transition rates and quadrupole moments of the core nucleus,[73] i.e., for $N' \neq N$,

$$\langle N'R'||\alpha||NR\rangle \propto \sqrt{2R + 1}\ \sqrt{B(E2:R \to R')} \qquad \text{(III.113)}$$

For $N' = N$,

$$\langle NR||\alpha||NR\rangle \propto \frac{5}{4}\sqrt{\frac{7}{2\pi}}\ e\, Q_{NR} \qquad \text{(III.114)}$$

where Q_{NR} is the observed quadrupole moment for the state $|NR\rangle$. These values are normalized, so that $\langle 12||\alpha||00\rangle = \sqrt{5}$ which is its pure harmonic value. The normalization is required so that the coupling parameter ζ has similar magnitude to that in the classical model.

2. Nuclear Electromagnetic Transition Rates in the Modified ICM

The reduced electric quadrupole and magnetic dipole transition rates are as given in the classical form (eqs. (III.91) and (III.108)), with the addition of the factor $(u_j u_{j'} - v_j v_{j'})$ for E2 and $(u_j u_{j'} + v_j v_{j'})$ for M1[24] in the summation over j and j'. Again the matrix elements $\langle N'R'||b||NR\rangle$ are replaced by $\langle N'R'||\alpha||NR\rangle$ defined as above. The explicit expressions for B(E2) and B(M1) in the modified model are

given here:

$$B(E2) = (2I'+1)\Big| \sum_{\substack{j'N'R' \\ jNR}} A(j'N'R'I'|E')A(jNRI|E)$$

$$\Big[\frac{3}{5} \left(e_{eff} + \frac{Z}{A^2} e\right) R_o^2 (-)^{\frac{1}{2}+\ell+j'+j+R-I'} \delta_{NN'}\delta_{RR'}$$

$$\times C(\ell 2\ell;000)\sqrt{\frac{5}{4\pi}(2j'+1)(2j+1)(2\ell+1)}\ W(jIj'I';R2)$$

$$\times W(\ell j\ell'j';\tfrac{1}{2}2)\ (u_j u_{j'} - v_j v_{j'}) + \frac{3}{4\sqrt{5\pi}} \frac{ZeR_o^2}{k}$$

$$\times \zeta\hbar\omega(-)^{I-j'} \zeta_{jj'}\zeta_{\ell\ell'}\ W(RIR'I';j2)\ (-)^R \sqrt{2R+1}\ \langle N'R'||\alpha||NR\rangle\Big]\Big|^2$$

(III.115)

$$B(M1) = \frac{3\mu_N^2}{4\pi}(2I'+1) \sum_{\substack{j'N'R' \\ jNR}} A(j'N'R'I'|E')A(jNRI|E)$$

$$\times \Big[g_\ell (-)^{\frac{1}{2}+R'+j+j'-\ell-I'} \delta_{NN'}\delta_{RR'}\delta_{\ell\ell'}\sqrt{(2j'+1)(2j+1)(2\ell+1)\ell(\ell+1)}$$

$$\times W(jIj'I';R1)\ W(\ell j\ell j';\tfrac{1}{2}1)(u_j u_{j'} + v_j v_{j'})$$

$$+ g_{s_{eff}}(-)^{R+\ell'+\frac{1}{2}-I'} \delta_{NN'}\delta_{RR'}\delta_{\ell\ell'}\sqrt{\frac{3}{2}(2j'+1)(2j+1)}$$

$$\times W(jIj'I';R1)\ W(\tfrac{1}{2}j\tfrac{1}{2}j';\ell 1)(u_j u_{j'} + v_j v_{j'}) + g_R(-)^{I+j'-R'}$$

$$\times \delta_{NN'}\delta_{RR'}\delta_{jj'}\delta_{\ell\ell'}\sqrt{(2R'+1)R(R+1)}\ W(RIR'I';j1)\Big]\Big|^2$$

(III.116)

Using the same expressions for T(E2) and T(M1) as before, (eqs. (III.92) and (III.109)) the respective transition probabilities can be obtained.

3. Spectroscopic factors

One of the most useful methods of studying the low-energy structure of the odd-mass nuclei (comprised of A nucleons) is to investigate stripping reactions on the adjacent (A-1) even-even nucleus and/or pickup reactions on the adjacent (A+1) even-even nucleus. Since we are studying the case of a single nucleon coupled to an even-even nuclear core, we are only concerned with the stripping reactions. The application of pairing theory to these reactions was studied by Yoshida (1961)[74]. After applying stripping theory, single-particle transfer experiments determine the spectroscopic factor leading to a state of angular momentum :

$$S(I_\alpha) = |< \Psi_{IM} | \Psi_{IM}(j, R)>|^2 \qquad \text{(III.117)}$$

where Ψ_{IM} is the odd-mass parent nucleus and $\Psi_{IM}(j;R)$ is the (unnormalized) coupled-channel state of nucleon j and even daughter R:

$$\Psi_{IM} = \sum_\alpha A_\alpha(jNR|I)\ a^*_{jm}|\ \Psi_{NR} \qquad \text{(III.118)}$$

where

$A_\alpha(jNR|I)$ are the expansion coefficients in eq. (III.71). Suppose the daughter nucleus is the quasi-particle vacuum and the

parent a quasi-particle state:

$$|\Psi_{jm}> = \alpha^*_{jm}|> \text{ and } |\Psi_{NR}> = |> \qquad \text{(III.119)}$$

where

α^*_{jm} here is a creation operator.

The targets are usually residing in the ground state, therefore,

$$N = R = 0.$$

$$S(I_\alpha) = |<|\alpha_{jm} A_\alpha (j00|I) a^*_{jm}|\Psi_{NR}>|^2 \delta_{Ij}$$

$$= |<|\alpha_{jm} A_\alpha (j00|I) a^*_{jm}|>|^2 \delta_{Ij}$$

$$= A^2_\alpha (j00|I) |<| \alpha_{jm} a^*_{jm}|>|^2 \delta_{Ij} \qquad \text{(III.121)}$$

But:

$$\alpha_{jm} = u_j a_{jm} - v_j a^*_{j-m} \quad \text{(Bogolyubov-Valatin transformation)} \qquad \text{(III.121)}$$

$$\alpha_{jm} a^*_{jm} = u_j - v_j a^*_{j-m} a_{jm}$$

In the first order,

$$S(I_\alpha) = A^2_\alpha (j00|I)\ \delta_{Ij}\ u^2_j \qquad \text{(III.122)}$$

Thus single-particle transfer reactions provide a means of measuring the coefficients u_j, v_j directly.

CHAPTER IV FORMULATION OF THE HARTREE-FOCK CALCULATIONS

I. Hamiltonian Wave Functions and Energy in the Hartree-Fock Method

The Hartree-Fock theory is based on the theory of a self-consistent field which is an approximation for reducing the problem of many interacting particles to one of non-interacting particles in an average nuclear field. A large part of the internucleon forces, i.e. residual interaction is neglected in this approximation. In Chapter I, we have already discussed how the Hartree-Fock theory serves as a basis for extended ideas which take into consideration the residual interaction.

The physical principles of self-consistent field theory are illustrated by deriving it intuitively and neglecting particle exchange first, as in Hartree theory and then including particle exchange, as in Hartree-Fock Theory.[36]

Some basic ideas of the Hartree-Fock theory will be presented here and then developed to a full mathematical formulation specifically for our present study.

1. Basic Hartree-Fock Theory

The fundamental assumption of HF theory is that the nuclear

wave function is an antisymmetrized product of independent particle wave functions:

$$\phi(12....A) = A\psi_1(1)\psi_2(2) \ldots \psi_A(A) \qquad \text{(IV.1)}$$

where A represents an antisymmetrization operation generating the normalized Slater determinant:

$$A\psi_1(1)\psi_2(2) \ldots\psi_A(A) \equiv \frac{1}{(A!)^{\frac{1}{2}}} \begin{vmatrix} \psi_1(1) & \psi_2(1) & \ldots\psi_A(1) \\ \psi_1(2) & \psi_2(2) & \ldots\psi_A(2) \\ \vdots & \vdots & \\ \psi_1(A) & \psi_2(A) & \ldots\psi_A(A) \end{vmatrix} \qquad \text{(IV.2)}$$

OR

$$\phi(12....A) \equiv \frac{1}{(A!)^{\frac{1}{2}}} \det|\psi_i(j)| \qquad \text{(IV.3)}$$

where $\psi_i(j)$ are the single-particle wave-functions. The ground state has the first (lowest) A orbits filled. The most general wave function must be a linear combination of infinitely many such wave functions, due to the interaction-potential. The best possible wave function of this form is determined by application of a variational principle. The variational principle states that for small variations of an eigenstate, the energy expectation is stationary; for the ground state in particular it is a minimum, i.e.:

$$\delta\langle\phi|H|\phi\rangle = \langle\delta\phi|H|\phi\rangle = 0 \qquad \text{(IV.4)}$$

for small variations $\delta\phi$ which preserve the normalization of the single-particle wave functions:

$$\int |\psi_i(r)|^2 \, d\vec{r} = 1 \qquad \text{(IV.5)}$$

Assuming a two-body potential, V, the Hamiltonian is:

$$H = T + V \qquad \text{(IV.6)}$$

where T is the kinetic energy. Therefore,

$$H = \sum_{i=1}^{A} T_i + \tfrac{1}{2} \sum_{ij}^{A} V(ij)$$

$$= \sum_{i\neq 1}^{A} \frac{p_i^2}{2m} + \tfrac{1}{2} \sum_{i\neq j}^{A} V(ij) \qquad \text{(IV.7)}$$

In order to reveal explicitly the residual two-body interaction, Wick's Theorem is used (Appendix C of D. J. Rowe[36]) to derive a general Hamiltonian in the language of second quantization:

$$H = \sum_{ij} T_{ij} \, a_i^\dagger a_j + \tfrac{1}{4} \sum_{ij\kappa\ell} \langle ij|V|\kappa\ell\rangle \; a_i^\dagger a_j^\dagger a_\ell a_\kappa$$

$$= \sum_{ij} \varepsilon(i,j) a_i^\dagger a_j + \tfrac{1}{2} \sum_{ij\kappa\ell} \langle ij|V|\kappa\ell\rangle a_i^\dagger a_j^\dagger a_\ell a_\kappa \qquad \text{(IV.8)}$$

with $a_j^\dagger|0\rangle = |j\rangle$ and $\varepsilon(i,j)$ is the single-particle energy, and

where $\langle ij|V|\kappa\ell\rangle$ is between antisymmetrized two-particle states. It has the antisymmetry properties:

$$\langle ij|V|\kappa\ell\rangle = -\langle ij|V|\kappa\ell\rangle = \langle ij|V|\widetilde{\kappa\ell}\rangle \qquad \text{(IV.9)}$$

The notation of second quantization is used again in the A-body wave function $|\phi\rangle$ which can be defined as:

$$|\phi\rangle = b^{\dagger}_{\alpha_1} b^{\dagger}_{\alpha_2} b^{\dagger}_{\alpha_3} \ldots b^{\dagger}_{\alpha_A}|0\rangle \ , \quad b^{\dagger}_{\alpha_i}|0\rangle = |\alpha_i\rangle \qquad \text{(IV.10)}$$

where $b^{\dagger}_{\lambda_1}$ is a creation operator creating a particle in orbit λ_1 and b_{λ_1} is the corresponding annihilation operator. These obey the anti-commutation rules:

$$[b_\alpha, b^{\dagger}_\beta]_+ = \delta_{\alpha\beta} \ , \quad [b_\alpha, b_\beta]_+ = [b^{\dagger}_\alpha, b^{\dagger}_\beta]_+ = 0 \qquad \text{(IV.11)}$$

The orbits α described by the nucleons are eigenstates of a single-particle Hamiltonian h.

$$h|\alpha\rangle = e_\alpha|\alpha\rangle \qquad \text{(IV.12)}$$

The single-particle orbits $b^{\dagger}_{\alpha_i}|0\rangle$ have been chosen to minimize the total energy E_{HF} so that:

$$E_{HF} = \langle\phi|H|\phi\rangle = \sum_{\alpha=1}^{A} \langle\alpha|t|\alpha\rangle + \tfrac{1}{2} \sum_{\alpha,\beta=1}^{A} \langle\alpha\beta|V|\alpha\beta\rangle \qquad \text{(IV.13)}$$

where E_{HF} is the H.F. energy, and $\langle\alpha|t|\alpha\rangle$ is the kinetic energy of the orbit α and

$$\langle\alpha\beta|V|\alpha\beta\rangle = - \langle\alpha\beta|V|\beta\alpha\rangle \qquad \text{(IV.14)}$$

It is advantageous to expand the orbits $|\alpha\rangle$ in terms of a complete basis j of known wave functions, i.e. $|j\rangle = a^{\dagger}_j|0\rangle$ and $|i\rangle = a^{\dagger}_i|0\rangle$

(IV.15)

$$|\alpha> = \sum_i C_i^\alpha |i> \qquad \text{(IV.16)}$$

OR

$$b_\alpha^\dagger = \Sigma C_i^\alpha a_i^\dagger \qquad \text{(IV.17)}$$

with

$$\sum_j C_j^{\alpha *} C_j^{\alpha'} = \delta_{\alpha\alpha'}, \qquad \sum_\alpha C_j^{\alpha *} C_{j'}^{\alpha} = \delta_{jj'} \qquad \text{(IV.18)}$$

therefore,

$$\Sigma |C_j^\alpha|^2 = 1 \qquad \text{(IV.19)}$$

so now,

$$E_{HF} = \sum_{\alpha=1}^{A} \sum_{i,j} C_i^{\alpha *} (i|t|j> C_j^\alpha + \tfrac{1}{2} \sum_{\alpha,\beta=1}^{A} \sum_{ij\kappa\ell} C_i^{\alpha *} C_\kappa^{\beta *}$$

$$x \quad <i\kappa|C|\widetilde{j\ell}> C_j^\alpha C_\ell^\beta \qquad \text{(IV.20)}$$

The stationary condition is then given by,

$$\frac{\partial}{\partial C_i^{\alpha *}} * [E_{HF} - e_\alpha (\Sigma |C_j^\alpha|^2 - 1)] = 0 \qquad \text{(IV.21)}$$

where e_α is introduced as a Lagrange multiplier, with the help of expansion (IV.16) of the orbits, the energy E_{HF} in eq. (IV.20) can be expressed in terms of the known matrix elements of t and V in the known basis j. The derivatives of (eq. (IV.21) may then be calculated directly, so one obtains:

$$\sum_j \left[\langle i|t|j\rangle + \sum_{\alpha=1}^{A} \langle i\alpha|V|j\alpha\rangle \right] C_j^\alpha = e_\alpha C_i^\alpha \qquad \text{(IV.22)}$$

where

$$\langle i\alpha|V|j\alpha\rangle = \sum_{\kappa\ell} C_\kappa^{\alpha *} \langle i\kappa|V|j\ell\rangle C_\ell^\lambda \qquad \text{(IV.23)}$$

This is an eigenvalue problem and can be restated as:

$$\sum_j \langle i|h|j\rangle C_j^\alpha = e_\alpha C_i^\alpha \qquad \text{(IV.24)}$$

since $h|\alpha\rangle = e_\alpha|\alpha\rangle$

where h is a Hamiltonian given by its matrix elements.

$$\langle i|h|j\rangle = \langle i|t|j\rangle + \sum_{\alpha=1}^{A} \langle i\alpha|V|j\alpha\rangle \qquad \text{(IV.25)}$$

Eqs. (IV.24) and (IV.25) are the H.F. equations for the orbits α. They can be solved by the Iteration Procedure:

1) An initial set of coefficients C_j^α is chosen, as well as the orbits occupied.

2) With this set of coefficients, C_j^α, $\langle i|h|j\rangle$ can be computed

3) The Hamiltonian matrix (eq. (IV.25)) is diagonalized.

4) A new set of coefficients C_j^α is obtained and A orbits are chosen to be filled by nucleons (often the ones with lowest energy)

5) One returns to step 2), 3) and 4). This process is repeated until the change in C_j is negligible.

The iteration process is somewhat complicated by the fact that there are many local minima of the energy E_{HF} and therefore many solutions of the HF equations. Various minima can be reached by various initial guesses which then become crucial. Furthermore, after each diagonalization, new filled orbits have to be chosen and the energies of the orbits vary from one solution to another. The HF Hamiltonian h can have various symmetries, which, when assumed in a given step of the iteration process (and in particular in the initial guess), are preserved in the successive iterations. These symmetries, e.g. axial symmetry, parity symmetry, spherical symmetry, and time-reversal symmetry are discussed in detail, by Ripka.[35] We can see that 'educated' initial guesses lend some control over the iteration process.

The basis j on which the HF orbits of eq. (IV.15) are expanded is chosen to be the shell model states in this study, i.e.

$$|j\rangle \equiv |n\ell jm\tau\rangle \qquad \text{(IV.26)}$$

These are convenient to use because of the general availability of matrix elements of the two-body interaction in this representation. n and ℓ are the radial and orbital angular momentum quantum numbers of the harmonic-oscillator wave function; j and m are the total angular

momentum and its projection on the z-axis of the intrinsic frame of reference attached to the nucleus, and τ the third component of isospin, distinguishes proton and neutron states. Eq. (IV.15) becomes:

$$|\alpha\rangle = \sum_{jm} C^{\alpha}_{jm} |jm\,\tau_{\alpha}\rangle \qquad \text{(IV.27)}$$

Hartree-Fock calculations at this point are usually divided into two classes depending on the number of terms included in the above expansion of the orbits α.

1. Single major-shell calculations in which the expansion of each orbit is limited to states $|jm\tau\rangle$ belonging to a major shell of the spherical oscillator.
2. Major-shell mixing calculations which can include states of several major shells in the expansion.

In the present work, we are only concerned with class 1, and shall discuss it in the following section.

2. Single Major-Shell Hartree-Fock Calculations

In eq. (IV.26), j is limited such that:

$j = 1s_{1/2}$ for 1s shell orbits

$j = 1p_{3/2}$ and $1p_{1/2}$ for 1p shell orbits

$j = 1d_{5/2}$, $2s_{1/2}$ and $1d_{3/2}$ for 2s-1d shell orbits

$j = 1f_{7/2}$, $2p_{3/2}$, $2p_{1/2}$ and $1f_{5/2}$ for 2p-1f shell orbits, etc. (IV.28)

It is found that nuclei with a filled major shell, e.g. O^{16}, Ca^{40} and Ni^{56}, etc., can be used as reference nuclei because the wave functions of their orbits are known. The filling of the orbits in another nucleus can be compared with the filling in a closed-shell nucleus by writing the sum over occupied orbits,

$$\sum_{\alpha=1}^{A} = \sum_{\substack{\alpha=1s,1p \\ \text{or} \\ \alpha=1s,1p,2s,1d, \\ \text{etc.}}} + \sum_{\beta=1}^{M} - \sum_{\gamma=1}^{N} \qquad \text{(IV.29)}$$

where β are the orbits that are filled in the nucleus in question but empty in the reference nucleus. These are particle orbits. The orbits γ are empty in the nucleus under consideration but filled in the reference nucleus and are the hole orbits. Another way of representing this is

$$|\phi\rangle = \prod_{i=1}^{M} \prod_{j=1}^{N} b_{\beta i}^{\dagger} \, b_{\alpha j} | \text{ Ref. Nucleus}\rangle \qquad \text{(IV.30)}$$

where

$$|\beta\rangle = \sum_{j} C_{j}^{\beta} | jm \; \tau_{\beta}\rangle$$

and

$$|\alpha\rangle = \sum_{i} C_{j}^{\alpha} | jm \; \tau_{\alpha}\rangle$$

Similar to C_j^α, the coefficients C_j^β may be found by solving the HF eqs. by iteration,

$$\sum_j \langle i|h|j|C_j^\beta\rangle = e_\beta C_i^\beta \qquad \text{(IV.31)}$$

provided axial symmetry is assumed.

For example, let us consider O^{16} as the reference nucleus with four 1s-shell orbits and twelve 1p-shell orbits filled. Thus Ne^{20} would consist of M = 4 particle orbits and no hole orbit in its ground state and C^{12} would consist of N = 4 hole orbits.

The HF Hamiltonian matrix now becomes:

$$\begin{aligned}\langle jm\tau|h|j'm'\tau\rangle &= \langle jm\tau|t|j'm'\tau\rangle + \sum_{\alpha=1}^{A} \langle jm\tau,\alpha|V|j'm'\tau,\alpha\rangle \\ &= \langle jm|t|j'm'\rangle + \sum_{\alpha=1s,1p} \langle jm\tau,\alpha|V|j'm'\tau,\alpha\rangle \\ &\quad + \sum_{\beta=1}^{M} \langle jm\tau,\beta|V|j'm'\tau,\beta\rangle - \sum_{\gamma=1}^{N} \langle jm\tau,\gamma|V|j'm'\tau,\gamma\rangle\end{aligned} \qquad \text{(IV.32)}$$

where O^{16} is used as a reference. Since

$$\langle jm|t|j'm'\rangle + \sum_{\alpha=1s,1p} \langle jm\tau,\alpha|V|j'm'\tau,\alpha\rangle = \varepsilon_j \delta_{jj'}\delta_{mm'} \qquad \text{(IV.33)}$$

i.e., this is the HF Hamiltonian of the closed-shell solution of O^{16}, therefore we have,

$$\langle jm\tau|h|j'm'\tau\rangle = \varepsilon_j \delta_{jj'}\delta_{mm'} + \sum_{\beta=1}^{M} \langle jm\tau,\beta|V|j'm'\tau,\beta\rangle$$

$$- \sum_{\gamma=1}^{N} \langle jm\tau,\gamma|V|j'm'\tau,\gamma\rangle \qquad \text{(IV.34)}$$

where

ε_j is the single particle energy of the O^{16} field.

$$\langle jm\tau,\alpha|V|j'm'\tau,\alpha\rangle = \sum_{j_1 j_2} C^{\alpha *}_{j1} \langle jm\tau,\ j_1 m_\alpha \tau_\alpha|V|j'm'\tau, j_2 m_\beta \tau_\beta\rangle C^{\beta}_{j_2}$$

(IV.35)

and

$$\langle jm\tau,\beta|V|j'm'\tau,\beta\rangle = \sum_{j_1 j_2} C^{\beta *}_{j_1} \langle jm\tau,\ j_1 m_\beta \tau_\beta|V|j'm'\tau,\ j_2 m_\beta \tau_\beta\rangle C^{\beta}_{j_2}$$

(IV.36)

$$\langle jm\tau,\ j_1 m_1 \tau_\alpha|V|j'm'\tau,\ j_2 m_2 \tau_\alpha\rangle = \sum_{JM} \sum_{TM_T} \langle jj_1 mm_1|JM\rangle\langle j'j_2 m'm_2|JM\rangle$$

$$\times \langle \tfrac{1}{2}\ \tfrac{1}{2}\ \tau\ \tau_\alpha|TM_T\rangle^2 \langle jj_1|V|j'j_2\rangle_{JT} \qquad \text{(IV.37)}$$

and

$$\langle jm\tau,\ j_1 m_1 \tau_\beta|V|j'm'\tau,\ j_2 m_2 \tau_\beta\rangle = \sum_{JM} \sum_{TM_T} \langle jj'mm'|JM\rangle\langle j'j_2 m'm_2|JM\rangle$$

$$\times \langle \tfrac{1}{2}\ \tfrac{1}{2}\ \tau\ \tau_\beta|TM_T\rangle^2 \langle jj_1|V|j'j_2\rangle_{JT} \qquad \text{(IV.38)}$$

In terms of the O^{16} closed-shell Slater determinant $|\phi_o\rangle$ the HF state of eq. (IV.10) may be written as:

$$|\phi\rangle = b_{\beta_1} b_{\beta_2} \ldots b_{\beta_M} b_{\gamma_1} b_{\gamma_2} \ldots b_{\gamma_N} |\phi_o\rangle \tag{IV.39}$$

The HF energy of the intrinsic state is then given by:

$$E_{HF} = \langle\phi|H|\phi\rangle$$

$$= E_o + \sum_{\beta} \langle\beta|T|\beta\rangle - \sum_{\gamma} \langle\gamma|T|\gamma\rangle + \tfrac{1}{2} \sum_{\beta\beta'} \langle\beta\beta'|V|\beta\beta'\rangle$$

$$+ \tfrac{1}{2} \sum_{\gamma\gamma'} \langle\gamma\gamma'|V|\gamma\gamma'\rangle - \sum_{\beta\gamma} \langle\beta\gamma|V|\beta\gamma\rangle \tag{IV.40}$$

where E_o is the ground state energy of O^{16}

$$E_o = \langle|\phi_o|H|\phi_o\rangle \tag{IV.41}$$

and T is the O^{16} spherical field operator defined by its matrix elements

$$\langle jm\tau|T|j'm'\tau\rangle = \varepsilon_j \delta_{jj'} \delta_{mm'} \tag{IV.42}$$

which is usually taken from experiments.

The expression for E_{HF} can be simplified as follows:

$$\sum_{\beta} \langle\beta|T|\beta\rangle = \sum_{\beta} \sum_{jj'} C_j^{\beta} C_{j'}^{\beta *} \langle j'|T|j\rangle$$

$$= \sum_{\beta} \sum_{j} |C_j^{\beta}|^2 \varepsilon_j \tag{IV.43}$$

$$e_\beta = \langle\beta|h|\beta\rangle = \sum_{j,j'} C_j^{\beta*} C_{j'}^{\beta} \langle j|h|j'\rangle$$

$$= \sum_j |C_j|^2 \varepsilon_j + \sum_{\beta'} \sum_{jj'} C_j^{\beta*} C_{j'}^{\beta} \langle j,\beta'|v|j',\beta'\rangle$$

$$- \sum_\gamma \sum_{jj'} C_j^{\gamma*} C_{j'}^{\gamma} \langle j,\gamma|v|j',\gamma\rangle \qquad \text{(IV.44)}$$

Therefore

$$e_\beta = \sum_j |C_j|^2 \varepsilon_j + \sum_{\beta'} \langle\beta\beta'|v|\beta\beta'\rangle - \sum_\gamma \langle\beta\gamma|v|\beta\gamma\rangle \qquad \text{(IV.45)}$$

Similarly,

$$e_\gamma = \sum_j |C_j^\gamma|^2 \varepsilon_j + \sum_\gamma \langle\gamma\beta|v|\gamma\beta\rangle - \sum_{\gamma'} \langle\gamma\gamma'|v|\gamma\gamma'\rangle \qquad \text{(IV.46)}$$

Thus, we can write:

$$E_{HF} = E_o + \tfrac{1}{2} \sum_{\beta=1}^{M} (e_\beta + \tilde{\varepsilon}_\beta) - \tfrac{1}{2} \sum_{\gamma=1}^{N} (e_\gamma + \tilde{\varepsilon}_\gamma) \qquad \text{(IV.47)}$$

with

$$\tilde{\varepsilon}_\beta = \langle\beta|T|\beta\rangle = \sum_j |C_j^\beta|^2 \varepsilon_j \qquad \text{(IV.48)}$$

and

$$\tilde{\varepsilon}_\gamma = \langle\gamma|T|\gamma\rangle = \sum_j |C_j^\gamma|^2 \varepsilon_j \qquad \text{(IV.49)}$$

II. Angular Momentum Projection

The intrinsic states $|\phi>$ constructed in the manner discussed above are not eigenfunctions of the total angular momentum J of the nuclear state. The HF energy E_{HF} is not the eigenvalue then. Such eigenfunctions are constructed by a so-called projection operator P^J_k to a state $|\phi>$.

In the following sections, the projected wave functions and projected energy levels are calculated.

1. Projected Wave Function

Applying the projection operator, we obtain:

$$\psi^J_k = P^J_k|\phi_k> \qquad \text{(IV.50)}$$

where k is the projection of J_z on the z axis of the intrinsic frame.

Theoretical discussions of the rotational spectra thus produced are based on the unified model of Bohr and Mottelson[3] in which single-particle and collective rotational motions are distinguished and uncoupled. For example, the state of spin J belonging to the ground-state rotational band of an even-even nucleus is described by the product wave functions,

$$|JM> = \frac{2J+1}{8\pi^2} D^{J*}_{M0}(\Omega)|\phi_o> \quad J = 0, 2, 4... \qquad \text{(IV.51)}$$

The rotational motion is described by the symmetric top wave function[4];

$$D^{J*}_{Mo}(\Omega) = \left(\frac{4\pi}{2J+1}\right)^{\frac{1}{2}} Y^J_M(\beta, \gamma) \tag{IV.52}$$

The single-particle motion is described in the intrinsic state $|\phi_o\rangle$.

Similarly, rotational bands in deformed nuclei are generated by the HF intrinsic states.

$$|\psi^J_k\rangle = P^J_k|\phi_k\rangle$$

$$= \left(\frac{2J+1}{16\pi^2}\right)^{\frac{1}{2}}\{D^J_{Mk}(\Omega)|\phi_k\rangle + (-)^{J+k} D^{J*}_{M-k}(\Omega)|\phi_{-k}\rangle\} \tag{IV.53}$$

where

$$|\phi_{-k}\rangle = e^{-i\pi J_y}|\phi_k\rangle \tag{IV.54}$$

An alternative way is by using the projection method of Peierls and Yoccoz[41] which uses the Hill Wheeler integral[75]:

$$|\psi^J_{Mk}\rangle = \frac{2J+1}{8\pi^2 N^{\frac{1}{2}}_{Jk}} \int d\Omega D^{J*}_{Mk}(\Omega) R(\Omega)|\phi_k\rangle \tag{IV.55}$$

where $R(\Omega)$ is the rotation operator.

$$R(\Omega) = e^{-i\pi J_z} e^{-i\pi J_y} e^{-i\pi J_z} \tag{IV.56}$$

Ω stands for the Euler angles α, β and γ.

and $$D^{J}_{Mk}(\Omega) = \langle JM|R(\Omega)|Jk\rangle \qquad \text{(IV.57)}$$

The projected wave function of Peierls and Yoccoz is the projection of the intrinsic deformed wave function on the subspace of angular momentum J.

N_{Jk} is a normalization constant defined as:

$$N_{Jk} = \frac{2J+1}{8\pi^2} \int d\Omega D^{J*}_{kk}(\Omega) \langle \phi_k|R(\Omega)|\phi_k\rangle \qquad \text{(IV.58)}$$

It can be shown that

$$\frac{2J+1}{8\pi^2} \int d\Omega D^{J*}_{kk}(\Omega) R(\Omega) = \sum_{\alpha} |\alpha Jk\rangle\langle \alpha Jk| \qquad \text{(IV.59)}$$

where α is any complete set of quantum numbers other than J and k.

$|\psi^{J}_{Mk}\rangle$ projected from $|\phi_k\rangle$ by eq. (IV.55) are then the eigenfunctions of the nuclear state of the total angular momentum J and projection M in the laboratory frame.

2. Projected Energies

From the wave functions $|\psi^{J}_{Mk}\rangle$, one can obtain projected energies for the low-lying states in the nucleus. The energy spectrum is given in the Peierls-Yoccoz theory by:

$$E_J = \frac{\langle\phi_k|H|\psi^J_{Mk}\rangle}{\langle\phi_k|\psi^J_{Mk}\rangle}$$

$$= \frac{\langle\phi_k|H\ P^J_k|\phi_k\rangle}{\langle\phi_k|P^J_k|\phi_k\rangle}$$

$$= \langle\psi^J_{Mk}|H|\psi^J_{Mk}\rangle \qquad \text{(IV.60)}$$

It can be shown that when projected wave functions are used, a tensor operator T^k_g has the following matrix element: (see Appendix A(B)).

$$\langle\psi^{J_1}_{M_1k_1}|T^k_g|\psi^{J_2}_{M_2k_2}\rangle = \frac{2J_2+1}{8\pi^2 N^{\frac{1}{2}}_{J_1k_1} N^{\frac{1}{2}}_{J_2k_2}} \begin{bmatrix} J_2 & k & J_1 \\ M_2 & g & M_1 \end{bmatrix} \sum_{\mu\nu} \begin{bmatrix} J_2 & k & J_1 \\ k_2 & \nu & \mu \end{bmatrix}$$

$$\times \int d\Omega D^{*J_1}_{k_1\mu}(\Omega)\langle\phi_{k_1}|R(\Omega)T^k_\nu|\phi_{k_2}\rangle \qquad \text{(IV.61)}$$

The intrinsic state $|\phi_k\rangle$ are eigenstates of J_z with eigenvalues k due to axial symmetry. The normalization constant (eq. (IV.58)) and the integral in expression (IV.59) then reduce to:

$$N_{Jk} = \frac{2J+1}{2}\int_0^\pi d\beta \sin\beta\ d^J_{kk}(\beta)\langle\phi_k|e^{-i\beta J_y}|\phi_k\rangle \qquad \text{(IV.62)}$$

and

$$\frac{2J+1}{8\pi^2}\int d\Omega D^{J_1^*}_{k_1\mu}(\Omega)\,|\phi_{k_1}|R(\Omega)T^k_\nu|\phi_{k_2}>$$

$$= \frac{2J+1}{2}\int_0^\pi d\beta\,\sin\beta\; d^{J_1}_{k_1\mu}(\beta)\,|\phi_{k_1}|e^{-i\beta J_y}\,T^k_\nu|\phi_{k_2}> \qquad \text{(IV.63)}$$

where the reduced matrix $d^J_{Mk}(\beta)$ is defined as:

$$d^J_{Mk}(\beta) = <\alpha JM|e^{-i\beta J_y}|\alpha J_k> \qquad \text{(IV.64)}$$

The nuclear Hamiltonian H is a tensor operator of rank zero, can then be substituted for T^k_g in eq. (IV.61). The projected energy E_J of the state of spin J belonging to the rotational band generated by the intrinsic state $|\phi_k>$ can be obtained readily,

$$E_J = \frac{\int_0^\pi d\beta\,\sin\beta\; d^J_{kk}(\beta)<\phi_k|e^{-i\beta J_y}\,H|\phi_k>}{\int_0^\pi d\beta\,\sin\beta\; d^J_{kk}(\beta)<\phi_k|e^{-i\beta J_y}|\phi_k>} \qquad \text{(IV.65)}$$

These overlap integrals are usually assumed to be small, for largely deformed nuclei, except in the region of $\beta \sim 0$. Expanding $d^J_{kk}(\beta)$ in powers of β, we get:

$$d^J_{kk}(\beta) = 1 - \tfrac{1}{4}[J(J+1) - k^2]\beta^2 + \ldots\ldots \qquad \text{(IV.66)}$$

Inserting this into the above expression for E_J, a rotational spectrum of $J(J + 1)$ in leading order is obtained.

The overlap integrals are also sizeable[76] in the region of $\beta \sim \pi$, i.e. when the overlapping nuclei are pointing in almost opposite directions. Thus there are contributions from $d^J_{kk}(\pi - \beta)$.

For $k = \frac{1}{2}$, for example,

$$d^J_{\frac{1}{2}\,\frac{1}{2}}(\pi - \beta) = -\tfrac{1}{2}(-1)^{J + \frac{1}{2}}(J + \tfrac{1}{2})\beta + \ldots\ldots \qquad \text{(IV.67)}$$

giving an energy spectrum of rotational model form,

$$E_{Jk=\frac{1}{2}} = E_o + \frac{\hbar^2}{2\mathcal{J}}\left[J(J + 1) + a(-1)^{J+\frac{1}{2}}(J + \tfrac{1}{2})\right] + \ldots. \qquad \text{(IV.68)}$$

where

$$a = \sum_j |C^\alpha_j|^2 \, (j + \tfrac{1}{2})(-)^{j + \frac{1}{2}} \qquad \text{(IV.69)}$$

III. Projected Hartree-Fock Method

So far we have discussed the HF method followed by projection of angular momentum (HFP). An improvement over this is the PHF method which is the projected Hatree-Fock method. The reason and proof of it being an improved method was already introduced in Chapter I.

1. PHF Method

In the HFP method, the intrinsic state $|\phi>$ remains the same for all the states in a band. This has the disadvantage of being restrictive. The PHF method is an improved variational procedure where the variation is carried out after the angular momentum projection. Different states in a band are then allowed to have various deformed determinants, thus giving important corrections to the HFP method. The resulting self-consistent wave function is a better approximation to the eigenstate of the Hamiltonian.

In the HFP method, variational procedure is first carried out, i.e.:

$$\delta<\phi|H|\phi> = 0 \qquad \text{(IV.70)}$$

so that an intrinsic state $|\phi>$ can be chosen. This is then used to project the eigenfunction $|\psi^J_{Mk}>$ of the nuclear state with angular momentum J.

In the PHF method, projection is first carried out on different intrinsic states $|\phi(i)>$, so that for each $|\phi_i>$, there is a projected wave function $|\psi^J_{Mk}(i)>$. Then the variational procedure is practiced on these eigenfunctions, i.e.:

$$\delta<\psi^J_{Mk}|H|\psi^J_{Mk}>= 0 \qquad \text{(IV.71)}$$

At the end, the best $|\psi^J_{Mk}>$ is chosen and hence the corresponding energy level.

2. Vibrational Correlations and Modified Hamiltonian

Calculations using the HF model have exhibited two short comings in general: the energy levels are too dense and the electromagnetic transition rates are not in good agreement. Das Gupta and Harvey (1967)[58] suggest that this indicates residual correlations (β- vibration) which are of importance. Recently, Rowe[59,77,78] discussed several methods describing vibrational correlations of the quadrupole and octupole nature. These correlations are found to be responsible for considerable enhancement of some electromagnetic transition rates. The inclusion of these correlations have been used in the calculation of nuclear collective vibrational excitations.

A modified Hamiltonian H' can now be defined as:[55]

$$H' = H - \lambda_2^o Q_{20} - \lambda_4^o Q_{40} = H - H_v \qquad \text{(IV.72)}$$

where H is the usual Hamiltonian defined in eq. (IV.8).

$$Q_{20} = \sqrt{\frac{16\pi}{5}}\, r^2 Y_{20} \qquad \text{(quadrupole operator)} \qquad \text{(IV.73)}$$

$$Q_{40} = \sqrt{\frac{4\pi}{9}}\, r^4 Y_{40} \qquad \text{(hexadecapole operator)} \qquad \text{(IV.74)}$$

and λ_2^o and λ_4^o are Lagrange multipliers.

The vibrational correlations are embodied in H_v, i.e.:

$$H_v = \lambda_2^o Q_{20} + \lambda_4^o Q_{40} \qquad \text{(IV.75)}$$

A PHF calculation is calculated for different values of the Lagrange multipliers λ_2^o and λ_4^o. Separate minima with respect to the parameters λ_2^o and λ_4^o for each angular momentum state in the band are obtained. Axial symmetry is preserved in this two-parameter variation while the important quadrupole and hexadecapole correlations are still allowed for.

CHAPTER V RESULTS AND ANALYSIS OF Cu ISOTOPES APPLYING THE UNIFIED NUCLEAR MODEL

I. Anharmonic Core and Particle

In this section, the ICM is applied to the odd Cu isotopes with the inclusion of anharmonic core effects discussed in section 6. Chapter III. The classical line based on the assumption that a single particle state is either fully occupied or empty is followed here.

1. Energy Levels and Eigenfunctions

The following odd mass Cu isotopes: Cu^{59}, Cu^{61}, Cu^{63} and Cu^{65} were investigated using the theory discussed in Chapter II. Ni^{58}, Ni^{60}, Ni^{62} and Ni^{64} are the respective neighbouring doubly-even core nuclei. Each odd mass nucleus is described in terms of a core coupled to a last odd proton, which has available to it the $2p_{3/2}$, $2p_{1/2}$ and $1f_{5/2}$ single-particle shell model states. Since the excited states of the doubly-even nuclei show quadrupole vibrational character, the core surface is taken to be susceptible to collective quadrupole vibrations. The coupling between the doubly-even core and the single-particle states of the last odd proton is assumed to be of intermediate strength, strong enough to cause splitting of energy levels but not enough to deform the

nucleus appreciably from its equilibrium shape.

a) Parameters used in the Calculation

All collective states up to and including three phonon states were included. The summations over j, N and R include the following values:

$j = 1/2, 3/2, 5/2$

$N = 1, 2, 3$

$R = 0, 2, 3, 4, 6$

From the independent-particle spectrum as given by the shell model, one would expect the spin of the ground state of the nuclei investigated to be $3/2^-$. This is verified by experimentally observed values. To be consistent, the ground state spin of these isotopes Cu^{59}, Cu^{61}, Cu^{63} and Cu^{65} is taken to be $3/2^-$. The following spins are expected:

$I = 3/2, 5/2, 7/2, 9/2, 11/2$

There are seven parameters which enter into these calculations, i.e. $\varepsilon, \varepsilon'$, ζ, $\hbar\omega$, η_o, η_2 and η_4. ε and ε' are the "effective" spacings in energy between the $2p_{3/2}$ and $1f_{5/2}$ states, the $2p_{1/2}$ and $2p_{3/2}$ states respectively. These are in units of $\hbar\omega$ in this study. The parameter ζ is the coupling strength between the odd proton and the core vibrations.

The last four parameters $\hbar\omega$, η_o, η_2 and η_o are extracted from the collective surface vibrations of the core. $\hbar\omega$ is the phonon energy and its value is taken to be the experimental energy of the first

excited (2+) state of the neighbouring doubly-even nucleus. The η_J values (J = 0, 2, 4) are obtained from the N = 2 triplet in the even-even vibrational spectrum as seen from the following diagram:

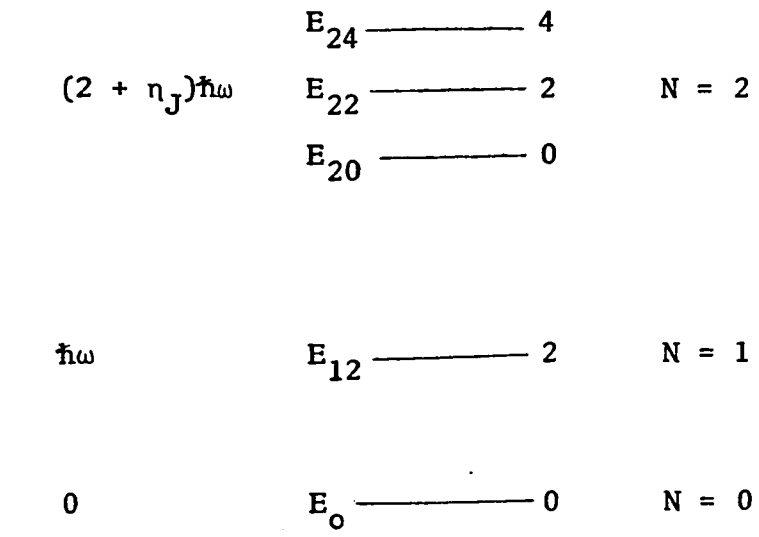

Figure V.1

$E_{12} = \hbar\omega$

$E_{20} = (2 + \eta_o)\hbar\omega$

$E_{22} = (2 + \eta_2)\hbar\omega$

$E_{24} = (2 + \eta_4)\hbar\omega$

Figs. V.2, V.3, V.4, and V.5 are the experimental doubly-even vibrational spectra of the core nuclei Ni^{58}, Ni^{60}, Ni^{62} and Ni^{64} respectively, from which the data $\hbar\omega$, η_o, η_2 and η_4 are extracted for the calculation of the Cu isotopes.

The above seven parameters are regarded as adjustable, being varied within reasonable limits, around the values extracted from the experimental core spectrum. The values of these parameters are chosen when the agreement is best between the calculated energy levels and those determined by experiments. Table I lists two sets of parameters, one giving the original experimental parameters before any variations are made and the other set giving the best-fit parameters after adjusting.

b) Results and Analysis

For each isotope, the total Hamiltonian was diagonalized in a truncated Hilbert space for each value of spin I between 1/2 and 11/2 for various reasonable values of $\varepsilon, \varepsilon'$ and ζ. Finer adjustments are given by variations in η_o, η_2 and η_4. These diagonalizations yielded the energy eigenvalues and the expansion coefficients of the eigenvectors. The phonon energy $\hbar\omega$ was also varied. The values of these parameters were then chosen when they gave the best agreement between theoretical energy levels and experimental ones.

Figs. V.6, V.7, V.8 and V.9 show the energy eigenvalues of Cu^{59}, Cu^{61}, Cu^{63} and Cu^{65}, respectively, plotted as functions of the coupling strength ζ for fixed values of $\varepsilon, \varepsilon'$, $\hbar\omega$, and η_J, indicated in

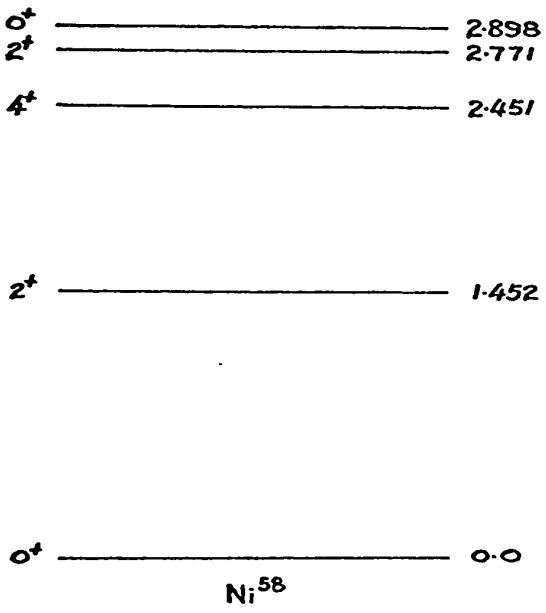
0+
2+
4+
2+
0+
2.898
2.771
2.451
1.452
0.0
Ni58

Fig. V.2

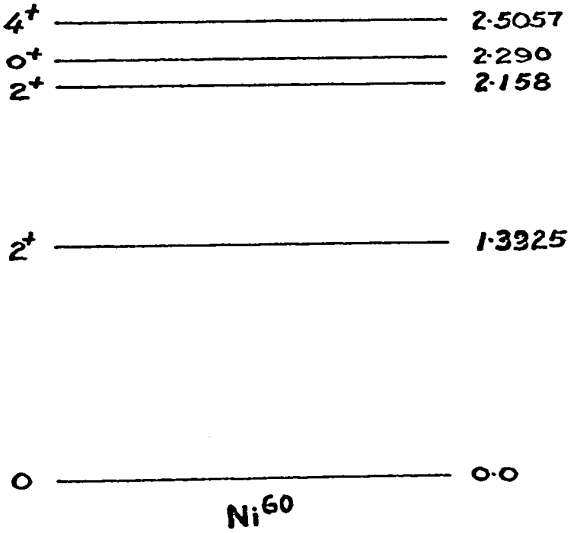
4+
0+
2+
2+
0
2.5057
2.290
2.158
1.3325
0.0
Ni60

Fig. V.3

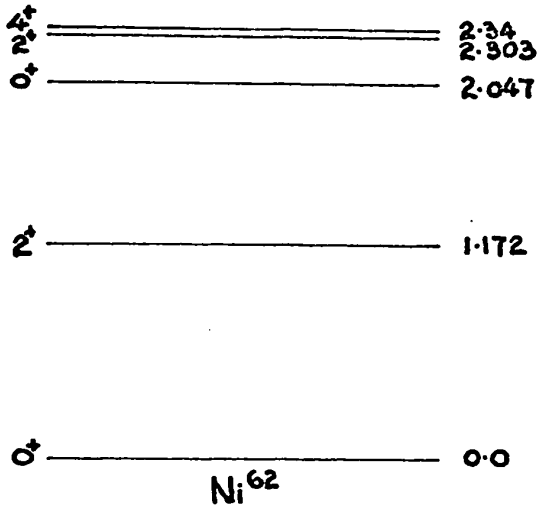

Fig. V.4

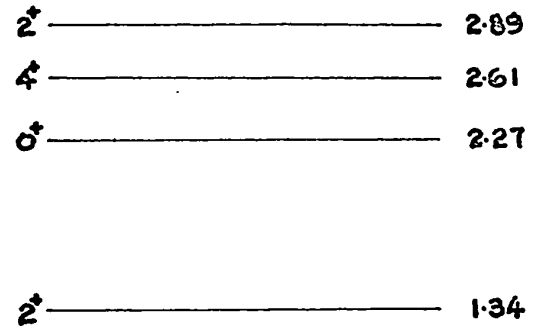

Fig. V.5

Table V. I Parameters used in the Classical ICM

(Anharmonic Core and Particles)

Isotope	Core	$\hbar\omega$ (MeV)	ε ($\hbar\omega$)	ε' ($\hbar\omega$)	ζ	η_o	η_2	η_4
Cu^{59}	Ni^{58}	1.450	0.537	0.744	1.4	-0.307	-0.092	-0.004
Cu^{61}	Ni^{60}	1.333	0.585	0.810	1.4	-0.281	-0.381	-0.120
Cu^{63}	Ni^{62}	1.172	0.665	0.922	1.0	-0.253	-0.035	-0.0034
Cu^{65}	Ni^{64}	1.340	0.582	0.806	1.0	-0.306	-0.157	-0.0522
Cu^{59}	Ni^{58}	1.452	0.830	0.956	1.80	-0.660	-0.085	0.12
Cu^{61}	Ni^{60}	1.400	0.895	0.840	1.70	0.36	-0.360	0.30
Cu^{63}	Ni^{62}	1.200	0.963	0.970	1.20	-0.20	-0.400	0.10
Cu^{65}	Ni^{64}	1.377	0.965	1.540	1.89	0.55	0.22	2.20

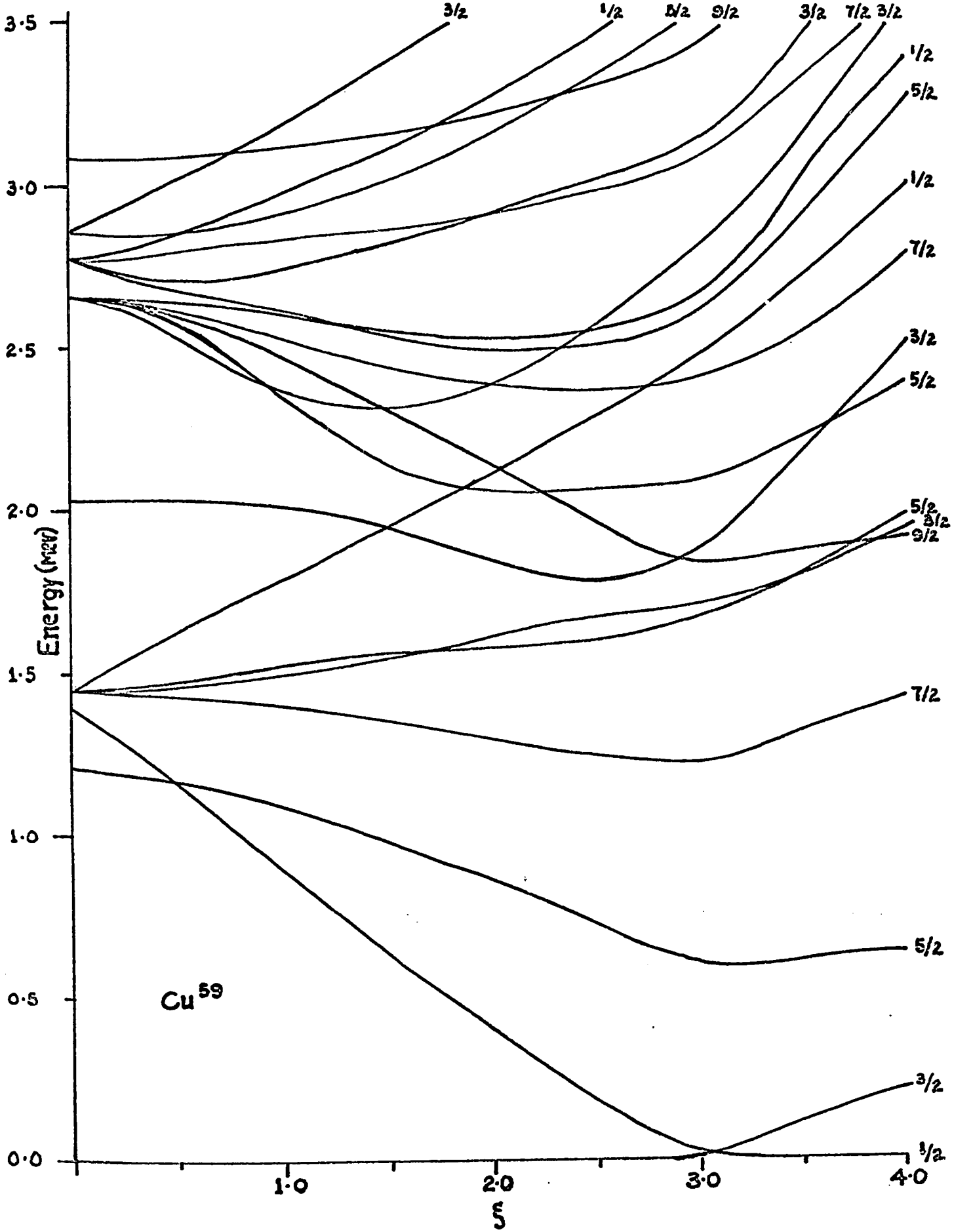
3·5
3·0
2·5
2·0
1·5
1·0
0·5
0·0
Energy (MeV)
1·0
2·0
3·0
4·0
ξ
Cu 59
3/2
1/2
5/2
9/2
3/2
7/2
3/2
1/2
5/2
1/2
7/2
3/2
5/2
5/2
3/2
9/2
7/2
5/2
3/2
1/2

Fig. V.6

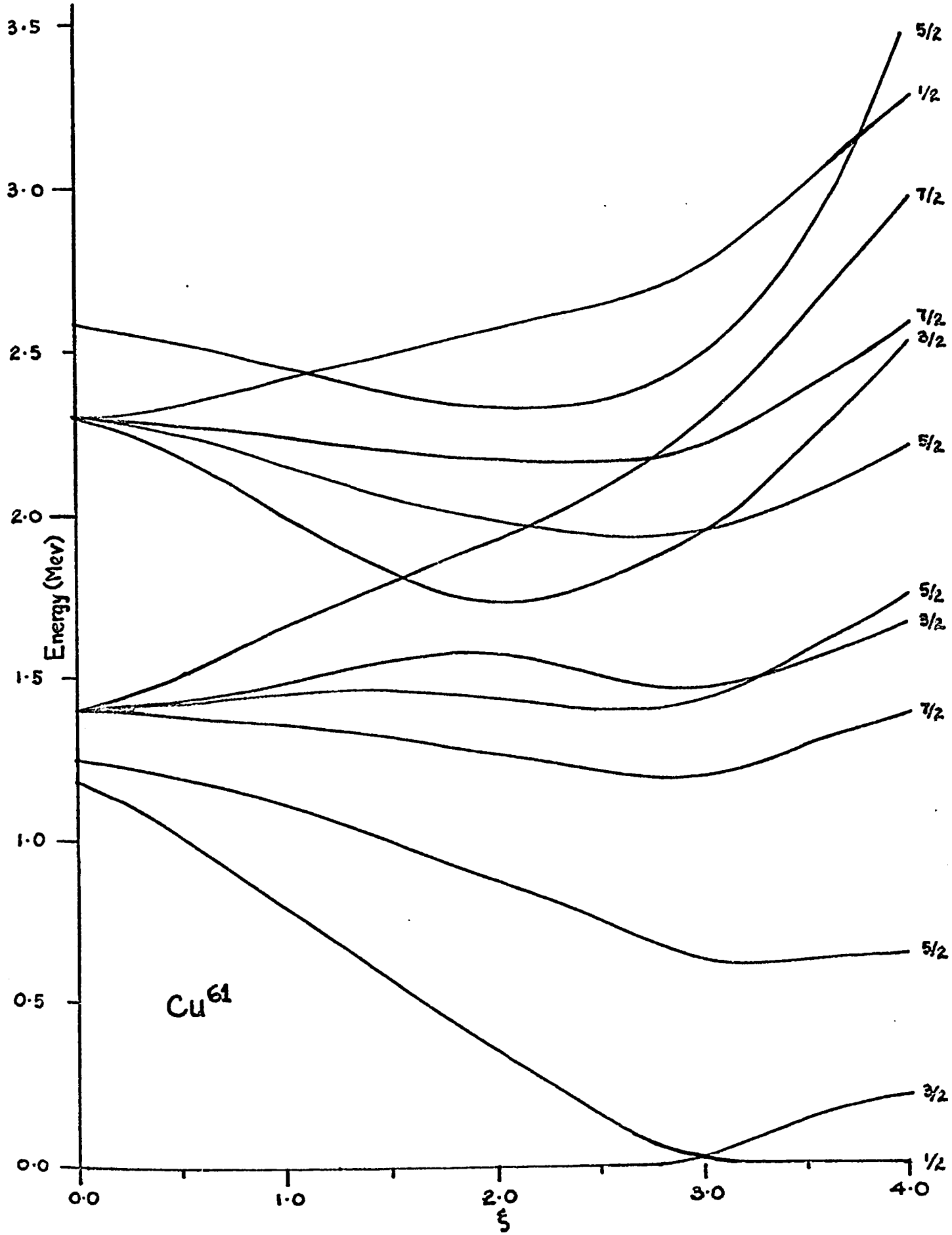
3·5
3·0
2·5
2·0
1·5
1·0
0·5
0·0
Energy (Mev)
0·0
1·0
2·0
3·0
4·0
ξ
5/2
1/2
7/2
7/2
3/2
5/2
5/2
3/2
7/2
5/2
3/2
1/2
Cu61

Fig. V.7

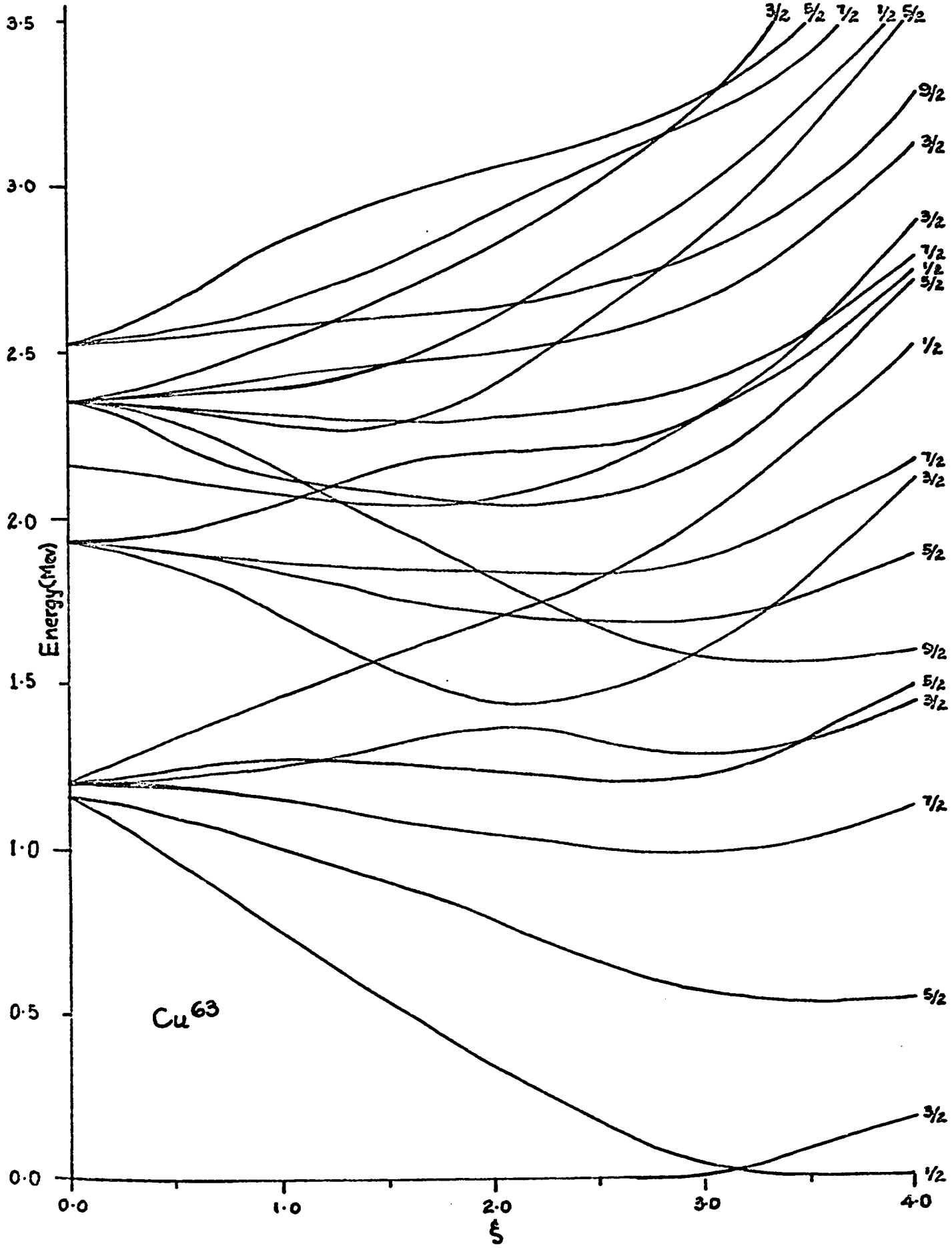
3·5
3·0
2·5
2·0
1·5
1·0
0·5
0·0
Energy(Mev)
0·0
1·0
2·0
3·0
4·0
ξ
Cu63
3/2 5/2 7/2 1/2 5/2
9/2
3/2
3/2
7/2
1/2
5/2
1/2
7/2
3/2
5/2
9/2
5/2
3/2
7/2
5/2
3/2
1/2

Fig. V.8

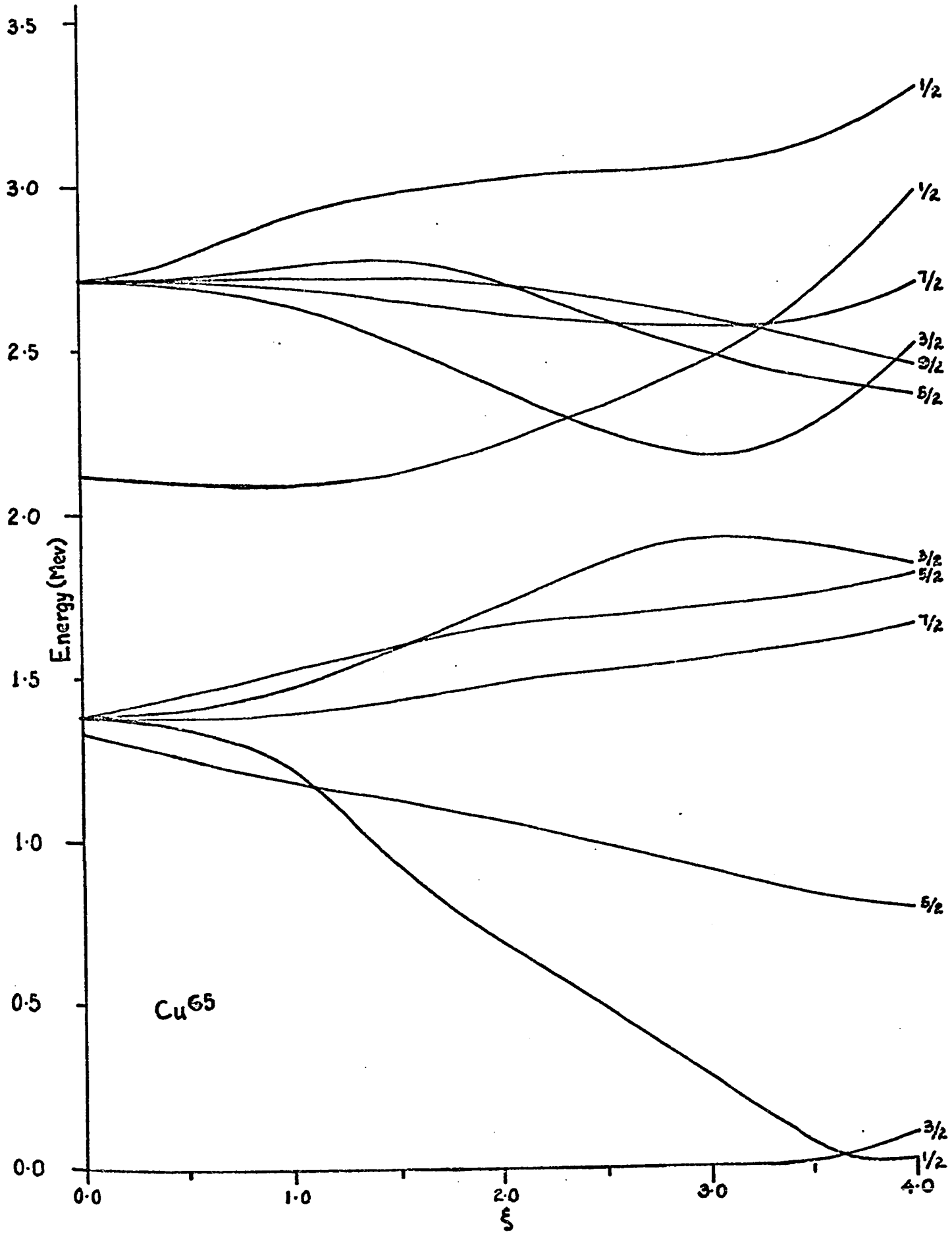
3·5
3·0
2·5
2·0
1·5
1·0
0·5
0·0
Energy (Mev)
1/2
1/2
7/2
3/2
3/2
5/2
3/2
5/2
7/2
5/2
3/2
1/2
Cu65
0·0
1·0
2·0
3·0
4·0
ξ

Fig. V.9

Table I. The energy level diagrams are shown in figs. V.10 through to V.13. These were constructed using the two sets of parameters as shown in Table I. Comparisons were made with the experimentally determined levels in each isotope.

2. Electromagnetic Transition Rates

As discussed previously in section III.1 of Chapter III, an effective charge should be assigned to the last odd proton to account for polarization effects of the core. In calculating the electromagnetic reduced transition rates, two sets of values are given for each isotope, one with the last odd proton having its normal charge and the other set with the last odd proton assigned an effective charge $e_p = 0.5e$ For a similar reason, an effective spin gyromagnetic ratio should be used as discussed in section III.2 of Chapter III. Hence $gs_{eff} = 0.5gs$.

a) Parameters used in the Calculation

In the calculations of both B(E2) and B(M1), we can see from eqs.(III.91) and (III.108) that expansion coefficients A(jNRI|E) are required for the actual computations. The reduced transition probabilities of the first six levels for each isotope are studied here, so the expansion coefficients A(jNRI|E) for I = $(3/2)_1$, $(1/2)_1$, $(5/2)_1$, $(7/2)_1$, $(3/2)_2$, $(5/2)_2$ are listed for all 4 Cu isotopes in Tables V.II, V.III, V.IV and V.V.

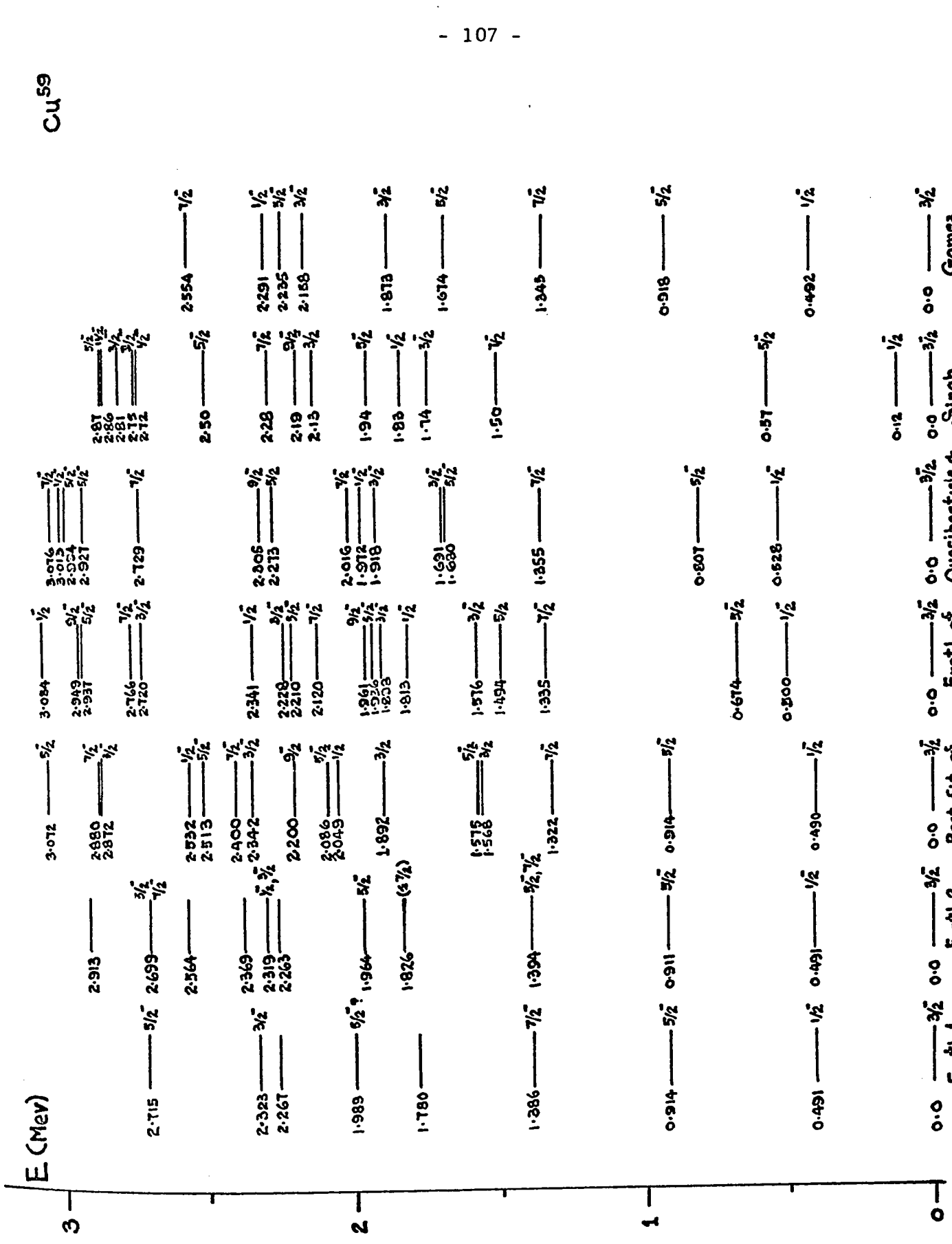
Cu59
E (Mev)
3
2
1
0
Expt 1
Expt 2
Best fit of Particle Harmonic Core
Expt of Quasiparticle + Anaharmonic Core
Singh et al
Gomez

Fig. V.10

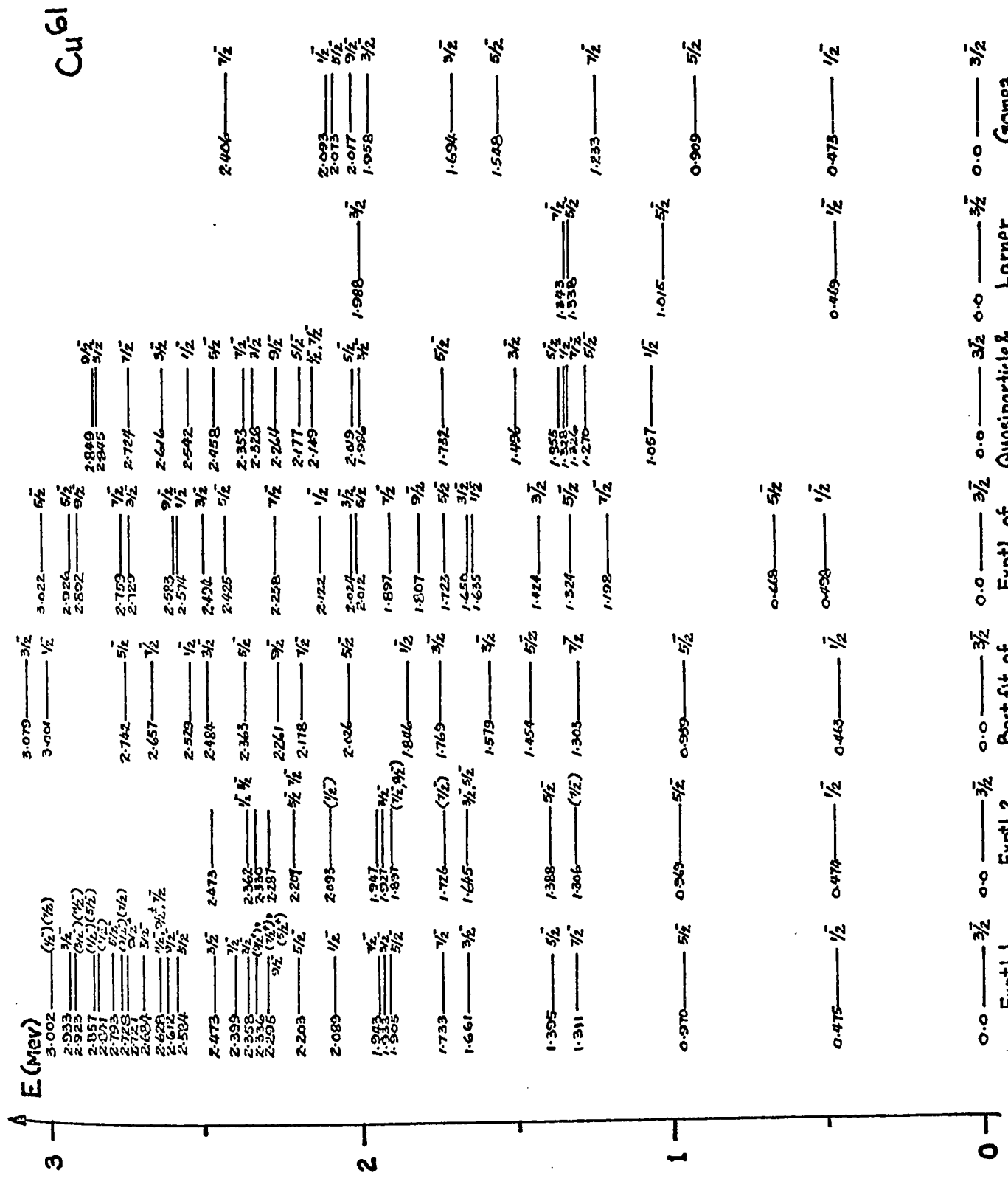
Cu 61
E (Mev)
3
2
1
0
Expt 1
Expt 2
Best fit of Particle & Harmonic Core
Expt of Harmonic Core
Quasiparticle & Anharmonic Core
Larner
Gomez

Fig. V.11

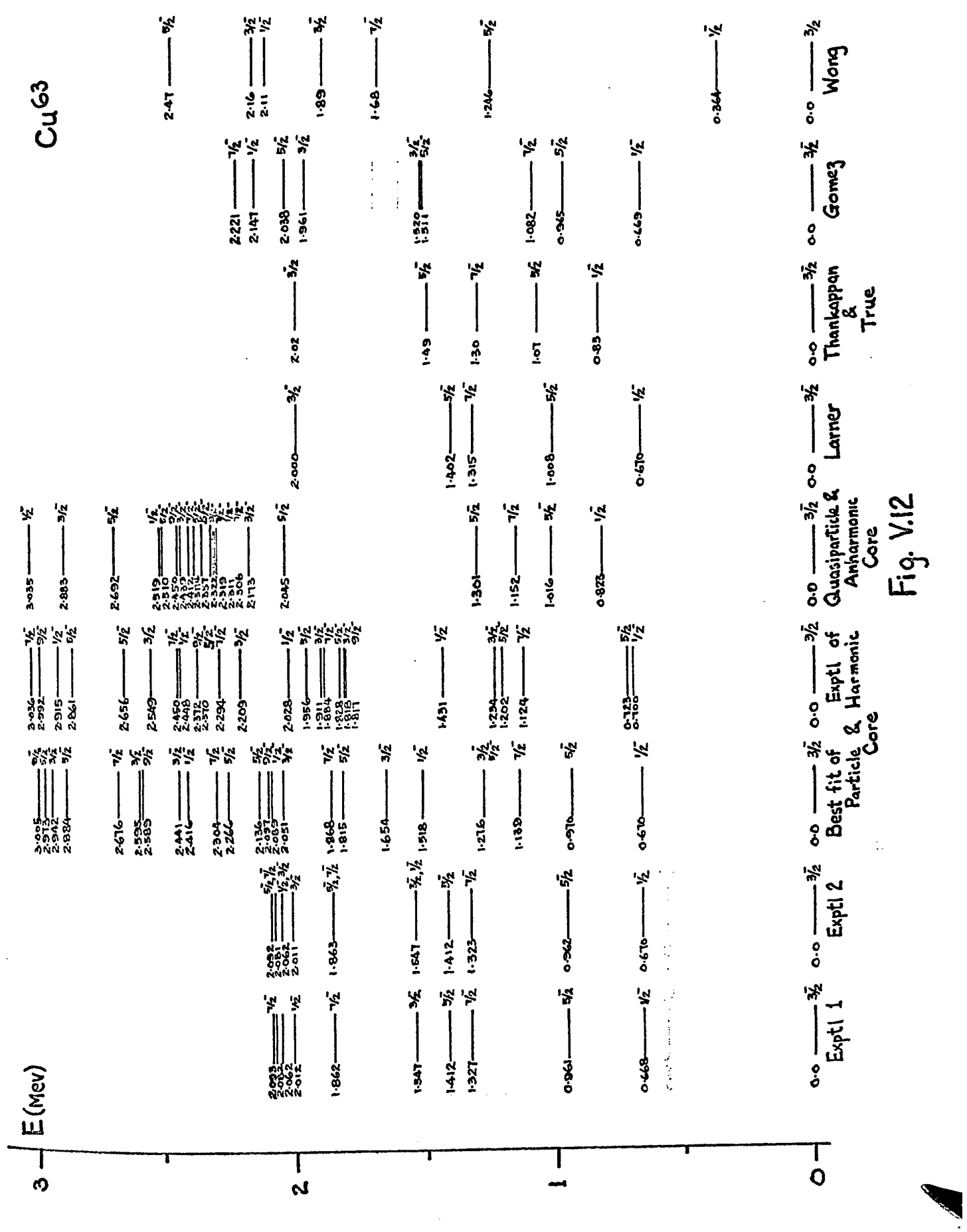
Cu63
E(Mev)
3
2
1
0
Exptl 1
Exptl 2
Best fit of Particle & Harmonic Core
Exptl of Anharmonic Core
Quasiparticle & Core
Larner
Thankappan & True
Gomez
Wong

Fig. V.12

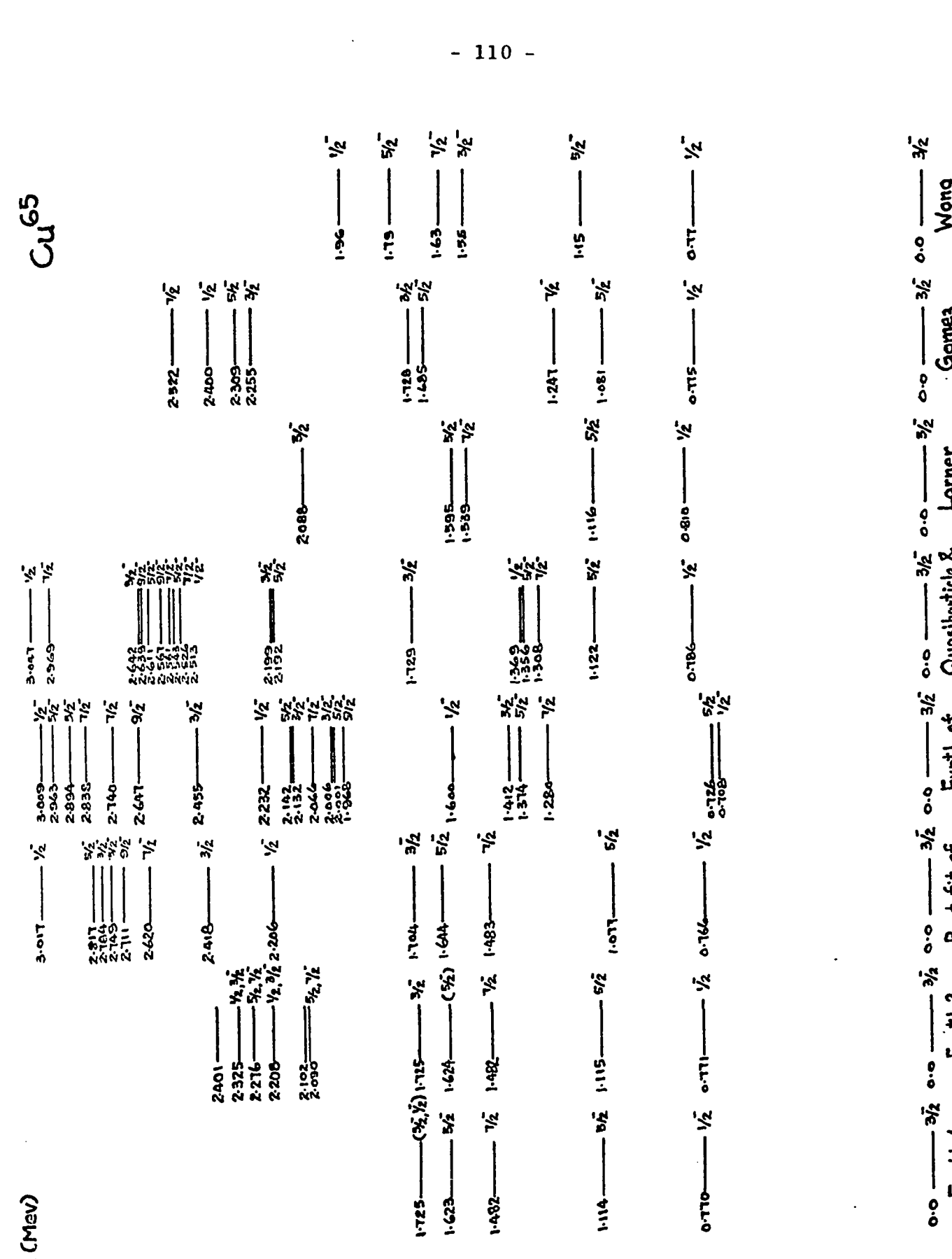
Cu65
E (Mev)
3
2
1
0
Exptl 1
Exptl 2
Best fit of Particle & Harmonic Core
Exptl of Harmonic Core
Quasiparticle & Anharmonic Core
Larner
Gomez
Wong

Fig. V.13

Table V.II Expansion Coefficients Corresponding to States $|E(MeV);I>$ of Cu^{59} in the Classical ICM using Best-fitting Parameters

Basic states $\|\ell_j;NR>$	$\|0;\ 3/2->$	$\|0.4900;1/2->$	$\|0.9139;5/2->$	$\|1.3215;7/2->$	$\|1.5675;3/2->$
$\|2p_{3/2};00>$	0.8906	0.0000	0.0000	0.0000	0.3871
$\|2p_{3/2};12>$	-0.3409	0.5877	0.4330	0.8834	0.6384
$\|2p_{3/2};20>$	0.1120	0.0000	0.0000	0.0000	-0.5583
$\|2p_{3/2};22>$	0.0373	-0.2055	0.0203	-0.1337	-0.0502
$\|2p_{3/2};24>$	0.0000	0.0000	-0.2375	-0.3128	0.0000
$\|2p_{3/2};30>$	-0.0109	0.0000	0.0000	0.0000	0.0338
$\|2p_{3/2};32>$	-0.0247	0.0674	0.0362	0.0749	0.1558
$\|2p_{3/2};33>$	-0.0008	0.0000	-0.0042	-0.0149	0.0208
$\|2p_{3/2};34>$	0.0000	0.0000	0.0565	0.0324	0.0000
$\|1f_{5/2};00>$	0.0000	0.0000	-0.7142	0.0000	0.0000
$\|1f_{5/2};12>$	0.1329	0.3600	0.2865	-0.0266	-0.0569
$\|1f_{5/2};20>$	-0.0000	0.0000	-0.1430	0.0000	0.0000
$\|1f_{5/2};22>$	-0.0071	-0.1247	-0.0790	0.0831	-0.0486
$\|1f_{5/2};24>$	-0.0854	0.0000	-0.0526	0.1055	0.1385
$\|1f_{5/2};30>$	0.0000	0.0000	0.0179	0.0000	0.0000
$\|1f_{5/2};32>$	0.0122	0.0583	0.0332	-0.0054	-0.0693

Table V.II

$\|1f_{5/2};33\rangle$	0.0033	0.0095	0.0024	-0.0026	-0.0343
$\|1f_{5/2};34\rangle$	0.0230	0.0000	0.0367	-0.0256	0.0699
$\|1f_{5/2};36\rangle$	0.0000	0.0000	0.0000	-0.1013	0.0000
$\|2p_{1/2};00\rangle$	0.0000	0.6459	0.0000	0.0000	0.0000
$\|2p_{1/2};12\rangle$	-0.2104	0.0000	-0.3284	0.0000	0.0867
$\|2p_{1/2};20\rangle$	0.0000	0.2011	0.0000	0.0000	0.0000
$\|2p_{1/2};22\rangle$	0.0738	0.0000	0.1268	0.0000	-0.2206
$\|2p_{1/2};24\rangle$	0.0000	0.0000	0.0000	-0.2497	0.0000
$\|2p_{1/2};30\rangle$	0.0000	-0.0404	0.0000	0.0000	0.0000
$\|2p_{1/2};32\rangle$	-0.0233	0.0000	-0.0494	0.0000	0.1634
$\|2p_{1/2};33\rangle$	0.0000	0.0000	0.0184	-0.0212	0.0000
$\|2p_{1/2};34\rangle$	0.0000	0.0000	0.0000	0.0669	0.0000

Table V.III Expansion Coefficients Corresponding to States |E(MeV);I> of Cu^{61} in the Classical ICM using Best-fitting Parameters

Basic states |ℓj;NR>	|0;3/2⁻>	|0.4628;1/2⁻>	|0.9593;5/2⁻>	|1.3029;7/2⁻>	|1.4539;5/2⁻>
$\|2p_{3/2};00\rangle$	0.9060	0.0000	0.0000	0.0000	0.2856
$\|2p_{3/2};12\rangle$	-0.3238	0.5750	0.4737	0.8972	0.8171
$\|2p_{3/2};20\rangle$	0.0624	0.0000	0.0000	0.0000	-0.1345
$\|2p_{3/2};22\rangle$	0.0401	-02212	0.0414	-0.1781	0.1900
$\|2p_{/32};24\rangle$	0.0000	0.0000	-0.2169	-0.2707	0.0000
$\|2p_{3/2};30\rangle$	-0.0108	0.0000	0.0000	0.0000	0.0058
$\|2p_{3/2};32\rangle$	-0.0164	0.0491	0.0321	0.0670	0.0738
$\|2p_{3/2};33\rangle$	-0.0012	0.0000	0.0020	-0.0047	0.0921
$\|2p_{3/2};34\rangle$	0.0000	0.0000	0.0542	0.0384	0.0000
$\|1f_{5/2};00\rangle$	0.0000	0.0000	-0.7078	0.0000	0.0000
$\|1f_{5/2};12\rangle$	0.1208	0.3311	0.2640	-0.0276	-0.0601
$\|1f_{5/2};20\rangle$	0.0000	0.0000	-0.0867	0.0000	0.0000
$\|1f_{5/2};22\rangle$	-0.0069	-0.1193	-0.0878	0.0901	-0.1451
$\|1f_{5/2};24\rangle$	-0.0717	0.0000	-0.0393	0.0917	0.0142
$\|1f_{5/2};30\rangle$	0.0000	0.0000	0.0186	0.0000	0.0000
$\|1f_{5/2};32\rangle$	0.0076	0.0393	0.0239	0.0056	-0.0328
$\|1f_{5/2};33\rangle$	0.0038	0.0106	0.0063	-0.0055	-0.0832

Table V.III

$\|1f_{5/2};34\rangle$	0.0205	0.0000	0.0375	-0.0279	-0.0583
$\|1f_{5/2};36\rangle$	0.0000	0.0000	0.0000	-0.0863	0.0000
$\|2p_{1/2};00\rangle$	0.0000	0.6891	0.0000	0.0000	0.0000
$\|2p_{1/2};12\rangle$	-0.2058	0.0000	-0.3306	0.0000	-0.2008
$\|2p_{1/2};20\rangle$	0.0000	0.1265	0.0000	0.0000	0.0000
$\|2p_{1/2};22\rangle$	0.0750	0.0000	0.1477	0.0000	-0.3266
$\|2p_{1/2};24\rangle$	0.0000	0.0000	0.0000	-0.2318	0.0000
$\|2p_{1/2};30\rangle$	0.0000	-0.0406	0.0000	0.0000	0.0000
$\|2p_{1/2};32\rangle$	-0.0162	0.0000	-0.0391	0.0000	-0.0009
$\|2p_{1/2};33\rangle$	0.0000	0.0000	0.0221	-0.0178	0.0000
$\|2p_{1/2};34\rangle$	0.0000	0.0000	0.0000	0.0674	0.0000

Table V.IV Expansion Coefficients Corresponding to States $|E(MeV);I>$ of Cu^{63} in the Classical ICM using Best-fitting Parameters

Basic states $\|\ell j;NR>$	$\|0;3/2^->$	$\|0.6695;1/2^->$	$\|0.9695;5/2^->$	$\|1.1386;7/2^->$	$\|1.2764;5/2^->$
$\|2p_{3/2};00>$	0.9521	0.0000	0.0000	0.0000	0.2568
$\|2p_{3/2};12>$	-0.2489	0.6363	0.6010	0.9371	0.9087
$\|2p_{3/2};20>$	0.0417	0.0000	0.0000	0.0000	-0.2116
$\|2p_{3/2};22>$	0.0192	-0.2131	0.1467	-0.1377	0.0165
$\|2p_{3/2};24>$	0.0000	0.0000	-0.1743	-0.2415	0.0000
$\|2p_{3/2};30>$	-0.0039	0.0000	0.0000	0.0000	0.0138
$\|2p_{3/2};32>$	-0.0072	0.0355	0.0241	0.0405	0.0556
$\|2p_{3/2};33>$	-0.0005	0.0000	0.0045	-0.0031	0.0252
$\|2p_{3/2};34>$	0.0000	0.0000	0.0230	0.0204	0.0000
$\|1f_{5/2};00>$	0.0000	0.0000	-0.7049	0.0000	0.0000
$\|1f_{5/2};12>$	0.0866	0.2627	0.1897	-0.0116	-0.0189
$\|1f_{5/2};20>$	0.0000	0.0000	-0.0667	0.0000	0.0000
$\|1f_{5/2};22>$	-0.0015	-0.0849	-0.0519	0.0681	-0.0859
$\|1f_{5/2};24>$	-0.0373	0.0000	0.0023	0.0684	0.0646
$\|1f_{5/2};30>$	0.0000	0.0000	0.0063	0.0000	0.0000
$\|1f_{5/2};32>$	0.0033	0.0256	0.0115	-0.0022	-0.0218
$\|1f_{5/2};33>$	0.0015	0.0094	0.0060	-0.0043	-0.0308

Table V.IV

$\|1f_{5/2};34\rangle$	0.0075	0.0000	0.0223	-0.0139	-0.0342
$\|1f_{5/2};36\rangle$	0.0000	0.0000	0.0000	-0.0485	0.0000
$\|2p_{1/2};00\rangle$	0.0000	0.6771	0.0000	0.0000	0.0000
$\|2p_{1/2};12\rangle$	-0.1375	0.0000	-0.2114	0.0000	-0.0225
$\|2p_{1/2};20\rangle$	0.0000	0.1112	0.0000	0.0000	0.0000
$\|2p_{1/2};22\rangle$	0.0384	0.0000	0.1006	0.0000	-0.2091
$\|2p_{1/2};24\rangle$	0.0000	0.0000	0.0000	-0.1700	0.0000
$\|2p_{1/2};30\rangle$	0.0000	-0.0264	0.0000	0.0000	0.0000
$\|2p_{1/2};32\rangle$	-0.0065	0.0000	-0.0181	0.0000	0.0239
$\|2p_{1/2};33\rangle$	0.0000	0.0000	0.0217	-0.0114	0.0000
$\|2p_{1/2};34\rangle$	0.0000	0.0000	0.0000	0.0392	0.0000

Table V.V Expansion Coefficients Corresponding to States $|E(MeV);I>$ of Cu^{65} in the Classical ICM using Best-fitting Parameters

Basis states $\|\ell j;NR>$	$\|0;3/2^->$	$\|0.7659;1/2^->$	$\|1.0771;5/2^->$	$\|1.4833;7/2^->$	$\|1.6435;5/2^->$
$\|2p_{3/2};00>$	0.9102	0.0000	0.0000	0.0000	0.3472
$\|2p_{3/2};12>$	-0.3461	0.7109	0.5513	0.9630	0.8806
$\|2p_{3/2};20>$	0.0614	0.0000	0.0000	0.0000	-0.1698
$\|2p_{3/2};22>$	0.0224	-0.2374	0.0741	-0.1285	0.0423
$\|2p_{3/2};24>$	0.0000	0.0000	-0.1009	-0.1465	0.0000
$\|2p_{3/2};30>$	-0.0081	0.0000	0.0000	0.0000	0.0131
$\|2p_{3/2};32>$	-0.0158	0.0624	0.0286	0.0459	0.0766
$\|2p_{3/2};33>$	-0.0028	0.0000	0.0131	0.0049	0.0440
$\|2p_{3/2};34>$	0.0000	0.0000	0.0305	0.0280	0.0000
$\|1f_{5/2};00>$	0.0000	0.0000	-0.7341	0.0000	0.0000
$\|1f_{5/2};12>$	0.1265	0.3355	0.2782	-0.0160	0.0094
$\|1f_{5/2};20>$	0.0000	0.0000	-0.0798	0.0000	0.0000
$\|1f_{5/2};22>$	0.0001	-0.1228	-0.0458	0.0818	-0.1117
$\|1f_{5/2};24>$	-0.0439	0.0000	-0.0068	0.0574	0.0369
$\|1f_{5/2};30>$	0.0000	0.0000	0.0111	0.0000	0.0000
$\|1f_{5/2};32>$	0.0073	0.0477	0.0202	-0.0031	-0.0287
$\|1f_{5/2};33>$	0.0048	0.0135	0.0113	-0.0048	-0.0539

Table V.V

$\|1f_{5/2};34\rangle$	0.0157	0.0000	0.0279	-0.0233	-0.0443
$\|1f_{5/2};36\rangle$	0.0000	0.0000	0.0000	-0.0540	0.0000
$\|2p_{1/2};00\rangle$	0.0000	0.5335	0.0000	0.0000	0.0000
$\|2p_{1/2};12\rangle$	-0.1591	0.0000	-0.1997	0.0000	-0.0822
$\|2p_{1/2};20\rangle$	0.0000	0.1338	0.0000	0.0000	0.0000
$\|2p_{1/2};22\rangle$	0.0590	0.0000	0.1081	0.0000	-0.1965
$\|2p_{1/2};24\rangle$	0.0000	0.0000	0.0000	-0.1270	0.0000
$\|2p_{1/2};30\rangle$	0.0000	-0.0422	0.0000	0.0000	0.0000
$\|2p_{1/2};32\rangle$	-0.0115	0.0000	-0.0197	0.0000	0.0195
$\|2p_{1/2};33\rangle$	0.0000	0.0000	0.0184	-0.0120	0.0000
$\|2p_{1/2};34\rangle$	0.0000	0.0000	0.0000	0.0409	0.0000

The following values were used in the calculations for the parameters:

$g_R = Z/A$

$g_\ell = 1$

$gs_{eff} = 2.794$

$e_{p_{eff}} = 9.606 \times 10^{-10}$ esu

$k = 40$ MeV

$R_o = 1.18 \times 10^{-13} A^{1/3}$ cm.

b) Results

Tables V.VI, V.VII, V.VIII and V.IX show the theoretical B(E2) and B(M1) values as compared with the experimentally determined ones. Two sets of values are given: one with the last odd proton having the free proton charge and spin gyromagnetic ratio, the other set with the effective charge and effective spin gyromagnetic ratio.

II. Anharmonic Core and Quasiparticle

In this modified version of the ICM, quasiparticles are considered. The results using this model are compared with the classical model to see whether any definite improvements are made.

Table V.VI Reduced Transition Probabilities in Cu^{59}

Reduced Transition Probabilities in Cu^{59}			B(E2) in e^2fm^4							B(M1) in μ_N^2							
			Anharmonic Core and Particle				Anharmonic Core and Quasiparticle		Experiment OR other Refs.	Anharmonic Core and Particle				Anharmonic Core and Quasiparticle		Experiment OR other Refs.	
			Exptl. Parameters		Best Fit					Exptl. Parameters		Best Fit					
I_i	I_f	ΔE in MeV	$e_p = e$ $g_s^* = g_s$	$e_p = 2e$ $g_s^* = 0.5g_s$	$e_p = 2e$ $g_s^* = g_s$	$e_p = 2e$ $g_s^* = 0.5g_s$	$e_p = e$ $g_s^* = g_s$	$e_p = 2e$ $g_s^* = 0.5g_s$		$e_p = e$ $g_s^* = g_s$	$e_p = 2e$ $g_s^* = 0.5g_s$	$e_p = e$ $g_s^* = g_s$	$e_p = 2e$ $g_s^* = 0.5g_s$	$e_p = e$ $g_s^* = g_s$	$e_p = 2e$ $g_s^* = 0.5g_s$		
$(1/2)_1$	$(3/2)_1$	0.4899	2.98×10^2	1.02×10^2	9.76×10^2	5.34×10^2	3.06×10	5.09×10^2	2.59×10^2	8.96×10^{-1}	1.61×10^{-2}	1.362	2.35×10^{-1}				$2.69,\ 8.59 \times 10^{-1}$
$(5/2)_1$	$(3/2)_1$	0.914	1.67×10	1.13×10^2	8.43×10	7.20×10	1.10×10	9.11×10	9.0×10	1.238×10^{-2}	1.85×10^{-3}	0.417	7.76×10^{-2}				$7.2 \times 10^{-3},\ 2.96 \times 10^{-3}$
$(7/2)_1$	$(3/2)_1$	1.322	1.24×10^2	1.12×10^2	2.154×10^2	1.97×10^2	3.47×10	3.47×10^2	2.17×10^2	0.0	0.0	0.0	0.0	0.0	0.0	0.0	0.0
$(5/2)_2$	$(3/2)_1$	1.575	2.25×10^2	2.28×10^2	3.75×10^2	3.84×10^2	6.15×10	2.68×10	8.5×10	7.92×10^{-2}	2.49×10^{-2}	7.56×10^{-2}	2.78×10^{-2}				$4.88 \times 10^{-2},\ 2.96 \times 10^{-2}$
$(7/2)_1$	$(5/2)_1$	0.408	4.44×10^{-1}	6.30×10^{-1}	3.72×10^{-2}	2.18×10^{-2}	2.95×10	2.65×10^2	6.44×10^{-4}	7.86×10^{-2}	2.18×10^{-2}	2.03×10^{-1}	5.74×10^{-1}	2.79×10^{-1}	7.39×10^{-2}		$9.9 \times 10^{-1},\ 3.36 \times 10^{-1}$
$(5/2)_2$	$(5/2)_1$	0.661	5.75	4.67	2.09 x 10	1.68 x 10	1.19×10^2	8.42×10^2	2.96 x 10	8.09×10^{-2}	2.00×10^{-3}	1.88×10^{-2}	1.01×10^{-2}	2.51×10^{-1}	6.43×10^{-2}		$1.30 \times 10^{-1},\ 2.22 \times 10^{-2}$
$(3/2)_2$	$(5/2)_1$	0.654	9.04	7.24	3.01 x 10	2.54 x 10	1.79 x 10	1.78×10^{-2}		1.20×10^{-1}	3.19×10^{-2}	1.87×10^{-1}	4.66×10^{-2}	8.76×10^{-1}	1.08×10^{-2}		
$(5/2)_1$	$(1/2)_1$	0.424	1.57×10	7.03	4.67×10	3.04×10	2.84×10^2	1.74×10^2	1.43×10^2	0.0	0.0	0.0	0.0	0.0	0.0	0.0	0.0
$(7/2)_1$	$(1/2)_1$	0.832	0.0	0.0	0.0	0.0	0.0	0.0		0.0	0.0	0.0	0.0	0.0	0.0	0.0	0.0
$(3/2)_2$	$(1/2)_1$	1.078	5.5×10^{-1}	7.69×10^{-1}	4.04	3.31	3.44×10^2	2.60×10^2	1.37	2.90×10^{-1}	8.41×10^{-2}	2.35×10^{-1}	6.69×10^{-2}	3.85×10^{-1}	1.07×10^{-1}		$4.50 \times 10^{-2},\ 5.6 \times 10^{-2}$
$(5/2)_2$	$(1/2)_1$	1.085	2.34	2.50	2.32 x 10	2.16 x 10	1.20×10^2	1.29×10^2	2.16 x 10	0.0	0.0	0.0	0.0	0.0	0.0	0.0	0.0
$(3/2)_2$	$(7/2)_1$	0.246	5.77	1.75	3.49 x 10	2.35 x 10	1.45×10^0	6.86×10	9.24 x 10	0.0	0.0	0.0	0.0	0.0	0.0	0.0	0.0
$(5/2)_2$	$(7/2)_1$	0.253	5.14	1.01×10	3.62×10	4.54×10	3.87×10	1.06×10^2		7.73×10^{-1}	2.34×10^{-1}	4.9×10^{-1}	1.15×10^{-1}	2.33×10^{-1}	7.12×10^{-2}		$1.59 \times 10^{-1},\ 9.28 \times 10^{-2}$
$(3/2)_2$	$(5/2)_2$	0.708×10^{-2}	6.71	2.94	6.98	1.23×10	1.42×10^2	1.00×10^2		1.17	3.50×10^{-1}	7.06×10^{-1}	2.24×10^{-1}	1.10×10^{-1}	5.41×10^{-2}		
$(3/2)_2$	$(3/2)_1$	1.568	1.35×10^2	1.50×10^2	1.60×10^2	1.76×10^2	1.90×10	1.90×10	6.05×10	1.78×10^{-1}	5.37×10^{-2}	2.02×10^{-1}	6.213×10^{-2}				$1.02 \times 10^{-1},\ 5.11 \times 10^{-2}$

Table V.VII Reduced Transition Probabilities in Cu^{61}

Reduced Transition Probabilities in Cu^{61}			B(E2) in e^2fm^4							B(M1) in μ_N^2						
			Anharmonic Core and Particle				Anharmonic Core and Quasiparticle		Experiment OR other Refs.	Anharmonic Core and Particle				Anharmonic Core and Quasiparticle		Experiment OR other Refs.
			Best fit Parameters		Exptl. Parameters					Best fit Parameters		Exptl. Parameters				
I_i	I_f	ΔE in MeV	$e_p = e$ $g_s^* = g_s$	$e_p = 2e$ $g_s^* = 0.5g_s$	$e_p = e$ $g_s^* = g_s$	$e_p = 2e$ $g_s^* = 0.5g_s$	$e_p = e$ $g_s^* = g_s$	$e_p = 2e$ $g_s^* = 0.5g_s$		$e_p = e$ $g_s^* = g_s$	$e_p = 2e$ $g_s^* = .5g_s$	$e_p = e$ $g_s^* = g_s$	$e_p = 2e$ $g_s^* = 0.5g_s$	$e_p = e$ $g_s^* = g_s$	$e_p = 2e$ $g_s^* = 0.5g_s$	
$(1/2)_1$	$(3/2)_1$	0.463	8.52×10^{2}	2.77×10^{1}	2.40×10^{1}	7.11×10^{1}	9.00×10^{2}	3.51×10^{2}	2.80×10^{2}	1.20×10^{-1}	3.04×10^{-2}	7.97×10^{-2}	1.90×10^{-2}			$2.75, 8.82 \times 10^{-1}$
$(5/2)_1$	$(3/2)_1$	0.959	7.84×10^{2}	6.65×10^{2}	1.74×10^{2}	1.19×10^{2}	7.26×10	2.10×10^{2}	3.17×10^{2}	4.38×10^{-2}	8.60×10^{-3}	1.45×10^{-2}	2.34×10^{-3}			
$(7/2)_1$	$(3/2)_1$	1.303	1.56×10^{2}	1.40×10^{2}	1.01×10^{3}	8.99×10^{2}	1.80×10	1.80×10	2.47×10^{2}	0.0	0.0	0.0	0.0	0.0	0.0	
$(3/2)_2$	$(3/2)_1$	1.579	2.249×10^{2}	2.48×10^{2}	1.24×10^{2}	1.39×10^{3}	1.38×10	1.38×10	7.11×10	1.52×10^{-1}	4.43×10^{-2}	1.80×10^{-1}	5.48×10^{-2}			$9.9^{7} \times 10^{-2}, 5.11 \times 10^{-2}$
$(5/2)_2$	$(3/2)_1$	1.454	3.31×10^{2}	3.41×10^{2}	2.21×10^{2}	2.25×10^{3}	8.71×10^{-1}	2.78×10	8.8×10	5.24×10^{-2}	2.02×10^{-2}	6.66×10^{-2}	2.28×10^{-2}			$4.76 \times 10^{-2}, 2.88 \times 10^{-2}$
$(5/2)_1$	$(1/2)_1$	0.497	2.78×10	1.53×10	1.28×10^{2}	5.05×10	1.32×10^{2}	5.30×10^{2}	1.58×10^{2}	0.0	0.0	0.0	0.0	0.0	0.0	
$(7/2)_1$	$(1/2)_1$	0.840	0.0	0.0	0.0	0.0	0.0	0.0	0.0	0.0	0.0	0.0	0.0	0.0	0.0	
$(3/2)_2$	$(1/2)_1$	1.117	2.214×10	3.36×10	9.95	1.33×10	1.12×10^{2}	1.34×10^{2}	1.06	1.86×10^{-1}	8.34×10^{-2}	3.18×10^{-1}	9.38×10^{-2}	2.07×10^{-2}	5.46×10^{-3}	$7.3 \times 10^{-2}, 4.2 \times 10^{-2}$
$(5/2)_2$	$(1/2)_1$	0.992	3.25×10	2.93×10	3.44×10	3.45×10	5.34×10	2.09×10^{2}	3.46×10	0.0	0.0	0.0	0.0	0.0	0.0	
$(7/2)_1$	$(5/2)_1$	0.344	1.566	1.544	6.84×10^{-1}	8.76	1.51×10	4.13×10^{2}	1.04×10^{-1}	2.20×10^{-1}	6.32×10^{-2}	9.72×10^{-2}	2.75×10^{-2}	2.94×10^{-1}	8.79×10^{-2}	$1.10 \times 10^{-1}, 3.96 \times 10^{-1}$
$(3/2)_2$	$(5/2)_1$	0.620	3.41×10	2.62×10	1.04×10^{2}	8.18×10	1.45×10^{2}	4.45×10^{2}		3.27×10^{-1}	9.83×10^{-2}	1.45×10^{-1}	3.93×10^{-2}	5.57×10^{-1}	1.65×10^{-1}	
$(5/2)_2$	$(5/2)_1$	0.495	1.701×10	1.24×10	5.92×10	4.52×10	1.11×10^{2}	3.69×10^{2}	3.65×10	2.17×10^{-1}	1.43×10^{-2}	5.76×10^{-2}	2.09×10^{-3}	3.74×10^{-1}	1.02×10^{-2}	$1.8^{7} \times 10^{-1}, 3.55 \times 10^{-2}$
$(3/2)_2$	$(7/2)_1$	0.276	2.75×10^{-1}	1.27	6.37×10	2.09×10	8.23×10^{0}	2.67×10^{4}		0.00	0.0	0.0	0.0	0.0	0.0	
$(5/2)_2$	$(7/2)_1$	0.151	5.15×10	3.63×10	2.13×10^{2}	1.31×10^{2}	4.38×10^{2}	1.18×10^{3}	1.40×10^{2}	3.51×10^{-1}	1.10×10^{-1}	6.45×10^{-1}	1.98×10^{-1}	7.41×10^{-1}	2.21×10^{-1}	$1.29 \times 10^{-1}, 8.68 \times 10^{-2}$
$(5/2)_2$	$(5/2)_2$	0.125	1.72×10	1.029	8.64×10	4.10×10	5.99×10^{2}	1.59×10^{3}		1.01	2.65×10^{-1}	1.08	2.23×10^{-1}	1.58	4.15×10^{-1}	

Table V.VIII Reduced Transition Probabilities in Cu^{63}

Reduced Transition Probabilities in Cu^{63}			B(E2) in e^2fm^4							B(M1) in μ_N^2						
			Anharmonic Core and Particle				Anharmonic Core and Quasiparticle		Experiment OR other Refs.	Anharmonic Core and Particle				Anharmonic Core and Quasiparticle		Experiment OR other Refs.
			Exptl. Parameters		Best Fit					Exptl. Parameters		Best Fit				
I_i	I_f	ΔE in MeV	$g_p = e$ $g_s^* = g_s$	$g_p = e$ $g_s^* = 0.5g_s$	$g_p = e$ $g_s^* = g_s$	$g_p = 2e$ $g_s^* = 0.5g_s$	$g_p = e$ $g_s^* = g_s$	$g_p = 2e$ $g_s^* = 0.5g_s$		$g_p = e$ $g_s^* = g_s$	$g_p = 2e$ $g_s^* = 0.5g_s$	$g_p = e$ $g_s^* = g_s$	$g_p = 2e$ $g_s^* = 0.5g_s$	$g_p = e$ $g_s^* = g_s$	$g_p = 2e$ $g_s^* = 0.5g_s$	
$(1/2)_1$	$(3/2)_1$	0.670	4.77×10^1	1.58×10^1	1.213×10^2	1.751×10^2	4.98×10^2	1.07×10^2	[1] 232 [2] 168.7 [3] 220 [6] 220 ± 8	5.06×10^{-2}	1.31×10^{-2}	8.27×10^{-1}	2.24×10^{-1}	0.0	0.0	[1] 1.24, [2] 0.66
$(5/2)_1$	$(3/2)_1$	0.969	4.04×10^1	1.59×10^2	4.334×10^2	3.516×10^2	1.00×10^2	9.72×10	[1] 232 [2] 166.0 [3] 220, 333 [1] 200 [4] 30, 42, 127, 258	6.57×10^{-3}	1.32×10^{-3}	2.878×10^{-1}	2.662×10^{-1}			0.60 [1] 0.13, [2] 0.09
$(7/2)_1$	$(3/2)_1$	1.139	4.31×10^3	3.80×10^3	5.92×10^2	5.21×10^2	1.04×10^2	1.04×10^2		0.0	0.0	0.0	0.0	0.0	0.0	
$(3/2)_2$	$(3/2)_1$	1.277	5.53×10^3	6.39×10^3	8.23×10^1	9.45×10	5.56×10	5.56×10	[4] 2, 0, 4, 12, 16	1.05×10^{-1}	3.19×10^{-2}	1.385×10^{-1}	4.21×10^{-2}			[4] 0.04, 0.094
$(5/2)_2$	$(3/2)_1$	1.277	7.04×10	7.28×10	1.00×10	1.08×10	9.12×10^0	2.92×10	[4] 1, 0, 1, 4, 9 [5] 1.61×10^2	5.12×10^{-2}	1.64×10^{-2}	3.42×10^{-2}	1.24×10^{-2}			[4] 0.033
$(5/2)_1$	$(1/2)_1$	0.300	2.58×10^2	1.83×10	2.41×10^2	4.17×10^{-1}	5.32	2.30×10^{-1}		0.0	0.0	0.0	0.0			
$(7/2)_1$	$(1/2)_1$	0.469	0.0	0.0	0.0	0.0	0.0	0.0		0.0	0.0	0.0	0.0	0.0	0.0	
$(3/2)_2$	$(1/2)_1$	0.607	1.95×10	4.80×10	3.07	5.93	1.003	2.08×10^{-2}		4.74×10^{-1}	1.44×10^{-1}	0.51	1.54×10^{-1}	2.46×10^{-1}	7.46×10^{-2}	
$(5/2)_2$	$(1/2)_1$	0.607	2.29×10	4.27×10	6.87×10	3.03×10	7.29	2.59×10		0.0	0.0	0.0	0.0	0.0	0.0	
$(7/2)_1$	$(5/2)_1$	0.169	2.38×10	1.95×10	1.27×10	5.47	1.34×10^2	2.34×10^2		7.95×10^{-2}	2.37×10^{-2}	3.25×10^{-1}	9.72×10^{-2}	7.10×10^{-1}	2.17×10^{-1}	
$(3/2)_2$	$(5/2)_1$	0.307	8.20×10	3.32×10	3.90×10	1.44×10	1.35×10^2	1.42×10		1.59×10^{-1}	4.70×10^{-2}	6.58×10^{-1}	1.96×10^{-1}	8.52×10^{-2}	2.58×10^{-1}	
$(5/2)_2$	$(5/2)_1$	0.306	7.39×10	2.54×10	5.61×10	2.30×10	8.94×10^{-1}	3.88×10^{-1}		1.05×10^{-1}	2.02×10^{-3}	3.27×10^{-1}	1.11×10^{-2}	6.10×10^{-3}	1.44×10^{-4}	
$(3/2)_2$	$(7/2)_1$	0.138	2.59×10	4.10×10	9.08	2.35×10^{-1}	7.08×10	8.41 10		0.0	0.0	0.0	0.0	0.0	0.0	
$(5/2)_2$	$(7/2)_1$	0.138	9.64×10	2.47×10	6.57×10	1.49×10	5.81×10^{-1}	1.04×10^{-1}		9.48×10^{-1}	2.89×10^{-1}	4.26×10^{-1}	1.31×10^{-1}	3.51×10^{-3}	1.06×10^{-3}	
$(3/2)_2$	$(5/2)_2$	0.216×10^{-2}	3.35×10	1.69×10	1.37×10	2.51	5.77×10^{-1}	6.14×10^{-1}		1.58	4.82×10^{-1}	8.58×10^{-1}	2.61×10^{-1}	3.98×10^{-3}	1.02×10^{-3}	

Table V.IX Reduced Transition Probabilities in Cu^{65}

Reduced Transition Probabilities in Cu^{65}			B(E2) in e^2fm^4						Experiment OR other Refs.	B(M1) in μ_N^2						Experiment OR other Refs.
			Anharmonic Core and Particle				Anharmonic Core and Quasiparticle			Anharmonic Core and Particle				Anharmonic Core and Quasiparticle		
			Exptl. Parameters		Best Fit					Exptl. Parameters		Best Fit				
I_i	I_f	ΔE in MeV	$e_p = e$ $g_s^* = g_s$	$e_p = 2e$ $g_s^* = 0.5g_s$	$e_p = e$ $g_s^* = g_s$	$e_p = 2e$ $g_s^* = 0.5g_s$	$e_p = e$ $g_s^* = g_s$	$e_p = 2e$ $g_s^* = 0.5g_s$		$e_p = e$ $g_s^* = g_s$	$e_p = 2e$ $g_s^* = 0.5g_s$	$e_p = e$ $g_s^* = g_s$	$e_p = 2e$ $g_s^* = 0.5g_s$	$e_p = e$ $g_s^* = g_s$	$e_p = 2e$ $g_s^* = 0.5g_s$	
$(1/2)_1$	$(3/2)_1$	0.766	7.40×10^1	8.28×10^1	2.43×10^2	6.43×10^2	1.27×10^2	5.81×10	[1] 184, 218 [4] 37, 292, 506, 779	5.76×10^{-3}	5.76×10^{-3}	1.31×10^{-1}	1.31×10^{-1}			0.23 [1] 1.99 [4] 3.12 [5] 0.054 [4] 0.06
$(5/2)_1$	$(3/2)_1$	1.077	4.06×10^1	1.55×10^1	1.34×10^2	1.18×10^2	7.22 x 10	5.32 x 10	[1] 193, [4] 28, 96, 203, 351	3.99×10^{-4}	3.99×10^{-4}	4.29×10^{-2}	4.29×10^{-2}			
$(7/2)_1$	$(3/2)_1$	1.483	6.115×10^2	5.48×10^2	2.08×10^2	1.91×10^2	1.22×10^2	1.22×10^2	[1] 180 [4] 32, 98, 151, 255	0.0	0.0	0.0	0.0	0.0	0.0	
$(3/2)_2$	$(3/2)_1$	1.704	7.36×10^2	8.34×10^2	2.33×10^2	2.63×10^2	1.13×10^2	1.13×10^2	[4] 3, 0, 2, 9, 22	7.44×10^{-2}	7.44×10^{-2}	1.59×10^{-2}	1.59×10^{-2}			[4] 0.10
$(5/2)_2$	$(3/2)_1$	1.644	9.25×10^2	9.48×10^2	3.35×10^2	3.45×10^2	5.72 x 10	9.31 x 10	[1] <200 [4] 4, 6, 9, 12, 15	4.77×10^{-2}	4.77×10^{-2}	1.26×10^{-2}	1.26×10^{-2}			[4] 0.01
$(5/2)_1$	$(1/2)_1$	0.311	1.98 x 10	2.05 x 10	1.23 x 10	4.67	5.51 x 10	1.10×10^2		0.0	0.0	0.0	0.0	0.0	0.0	[1] 0.0 [4] 0.0
$(7/2)_1$	$(1/2)_1$	0.717	0.0	0.0	0.0	0.0	0.0	0.0		0.0	0.0	0.0	0.0	0.0	0.0	
$(3/2)_2$	$(1/2)_1$	0.938	2.22	4.59	5.57	6.95	7.02 x 10	9.58 x 10		2.45	2.45	4.33×10^{-2}	4.33×10^{-2}	1.22×10^{-2}	3.04×10^{-2}	
$(5/2)_2$	$(1/2)_1$	0.878	1.73	3.46 x 10	1.21 x 10	1.09 x 10	2.18×10^{-1}	2.98		0.0	0.0	0.0	0.0	0.0	0.0	
$(7/2)_1$	$(5/2)_1$	0.406	2.39	2.63	3.27	2.17	4.49 x 10	6.08		3.34×10^{-2}	3.34×10^{-2}	1.57×10^{-2}	1.57×10^{-2}	3.12×10^{-2}	3.72×10^{-2}	
$(3/2)_2$	$(5/2)_1$	0.627	1.24 x 10	6.75	2.78	1.19	2.19 x 10^2	1.29 x 10^2		6.12×10^{-2}	6.12×10^{-2}	3.51×10^{-2}	3.51×10^{-2}	7.82×10^{-2}	7.82×10^{-2}	
$(5/2)_2$	$(5/2)_1$	0.566	8.90	4.56	5.08 x 10	3.99 x 10	1.10	5.23		5.77×10^{-1}	5.77×10^{-1}	1.562	1.562	1.96×10^{-1}	1.96×10^{-1}	
$(3/2)_2$	$(7/2)_1$	0.221	8.47	6.96×10^{-1}	8.36	1.47 x 10	1.11 x 10	2.78 x 10		0.0	0.0	0.0	0,0	0.0	0.0	
$(5/2)_2$	$(7/2)_1$	0.160	1.78 x 10	3.10×10^{-1}	1.69 x 10	6.89	1.84 x 10	2.01		7.03×10^{-1}	7.03×10^{-1}	3.95×10^{-2}	3.95×10^{-2}	1.55×10^{-2}	1.54×10^{-2}	
$(3/2)_2$	$(5/2)_2$	0.0602	7.30	2.27×10^{-1}	7.63×10^{-1}	3.23×10^{-3}	7.91 x 10	4.46 x 10		1.13×10^{-1}	1.13×10^{-1}	5.51×10^{-2}	5.51×10^{-2}	2.35×10^{-2}	1.57×10^{-2}	

Table V.X Quasiparticle Amplitudes and Quasihole Amplitudes used in the Anharmonic Core and Quasiparticle Model Calculations of Cu^{59}, Cu^{61}, Cu^{63} and Cu^{65}

Isotope	j	U_j	V_j
Cu^{59}	1/2	0.938	0.346
	3/2	0.854	0.520
	5/2	0.943	0.332
Cu^{61}	1/2	0.566	0.825
	3/2	0.748	0.663
	5/2	0.424	0.906
Cu^{63}	1/2	0.728	0.686
	3/2	0.812	0.583
	5/2	0.616	0.787
Cu^{65}	1/2	0.831	0.557
	3/2	0.860	0.510
	5/2	0.781	0.625

1. Energy Levels and Eigenfunctions

a) Parameter used

The single particle energy separations ε and ε' now become the single-quasiparticle energy spacings between the single quasiparticle states $2p_{3/2}$, $1f_{5/2}$ and $2p_{1/2}$. These are taken to be 1.3 Mev and 1.1 MeV respectively[81].

The quasiparticle and quasihole amplitudes U_j and V_j in state j used in this part of the calculations were obtained from recent experimental results.[79] Table X lists these amplitudes for j = 1/2, 3/2 and 5/2 for each Cu isotope.

In this model, the parameters $\hbar\omega$, ε, ε', η_0, η_2 and η_4 are not varied. These are extracted from experimental information of the core nuclei. ξ is varied and the chosen values of ξ together with other parametric values are shown in Table V.XI.

The experimental results, i.e. the transition rates and quadrupole moments of the core nuclei used to calculate the matrix elements of (see eqs. (III.113) and (III.114)) are taken from ref. 2. The matrix elements $\langle N'R'||\alpha||NR\rangle$ for each isotope are listed in Table V.XII. The plausible assumptions that for the second phonon states $\alpha(2^{*}+) = -\alpha(2+)$ and $\alpha(4+) = \alpha(2+)$ are made here.

b) Results

The same procedure of diagonalization of the total Hamiltonian

Table V.XI Parameters used in the extended ICM

(Anharmonic Core and Quasiparticles)

Isotope	Core	$\hbar\omega$ (Mev)	ε ($\hbar\omega$)	ε' ($\hbar\omega$)	ζ	η_o	η_2	η_4
Cu^{59}	Ni^{58}	1.452	0.895	0.758	1.0	-0.307	-0.092	-0.004
Cu^{61}	Ni^{60}	1.3325	0.975	0.826	0.9	-0.2814	-0.3805	-0.1195
Cu^{63}	Ni^{62}	1.172	1.109	0.939	2.9	-0.2534	-0.035	-0.0034
Cu^{65}	Ni^{64}	1.340	0.970	0.821	1.8	-0.306	-0.1567	-0.0522

Table V.XII Matrix Elements <N'R'||α||NR> used in the Extended ICM

<N'R'||α||NR>	Cu^{59}	Cu^{61}	Cu^{63}	Cu^{65}
<12||α||00>	2.2361	2.2361	2.2361	2.2361
<12||α||12>	-2.3490	-3.2854	-1.7664	1.5675
<20||α||12>	1.4050	0.3482	0.7071	0.8022
<20||α||22>	5.2505	5.2882	4.2286	2.2126
<22||α||00>	0.1150	0.1076	0.1999	0.3098
<22||α||12>	6.0632	2.1667	2.6242	2.6479
<22||α||22>	3.0374	3.2854	1.7664	-1.5675
<24||α||12>	7.8594	10.869	1.0763	0.3080
<24||α||24>	-3.0374	-3.2854	-1.7664	1.5675

is followed here as in the anharmonic core and particle model. Figures V.14 and V.15 show the dependence of ξ on the energy levels in each isotope. The best fit values of ξ of Cu^{59}, Cu^{61}, Cu^{63} and Cu^{65} are chosen to be 1.0, 0.9, 2.9 and 1.8 respectively.

Figs. V.10, V.11, V.12 and V.13 are the energy spectra of Cu^{59-63} using the values of the parameters giving the best fit to the experimental levels, as well as the original values taken from measurements on the core nuclei. These are compared in the same diagrams with the energy spectra obtained using the classical model of anharmonic core and particles.

2. Electromagnetic Transition Rates

Eqs. (III.91) and (III.108) are used to calculate the B(E2) and B(M1) values.

a) Parameters

Tables V.XIII, V.XIV, V.XV and V.XVI list the expansion coefficients of the first six levels obtained in the calculation of the energy levels above. These are used in computing the reduced transition rates.

The same set of values for e_p, g_R, g_ℓ, gs_{eff}, κ and R_o is used as in the classical model of anharmonic core and particles.

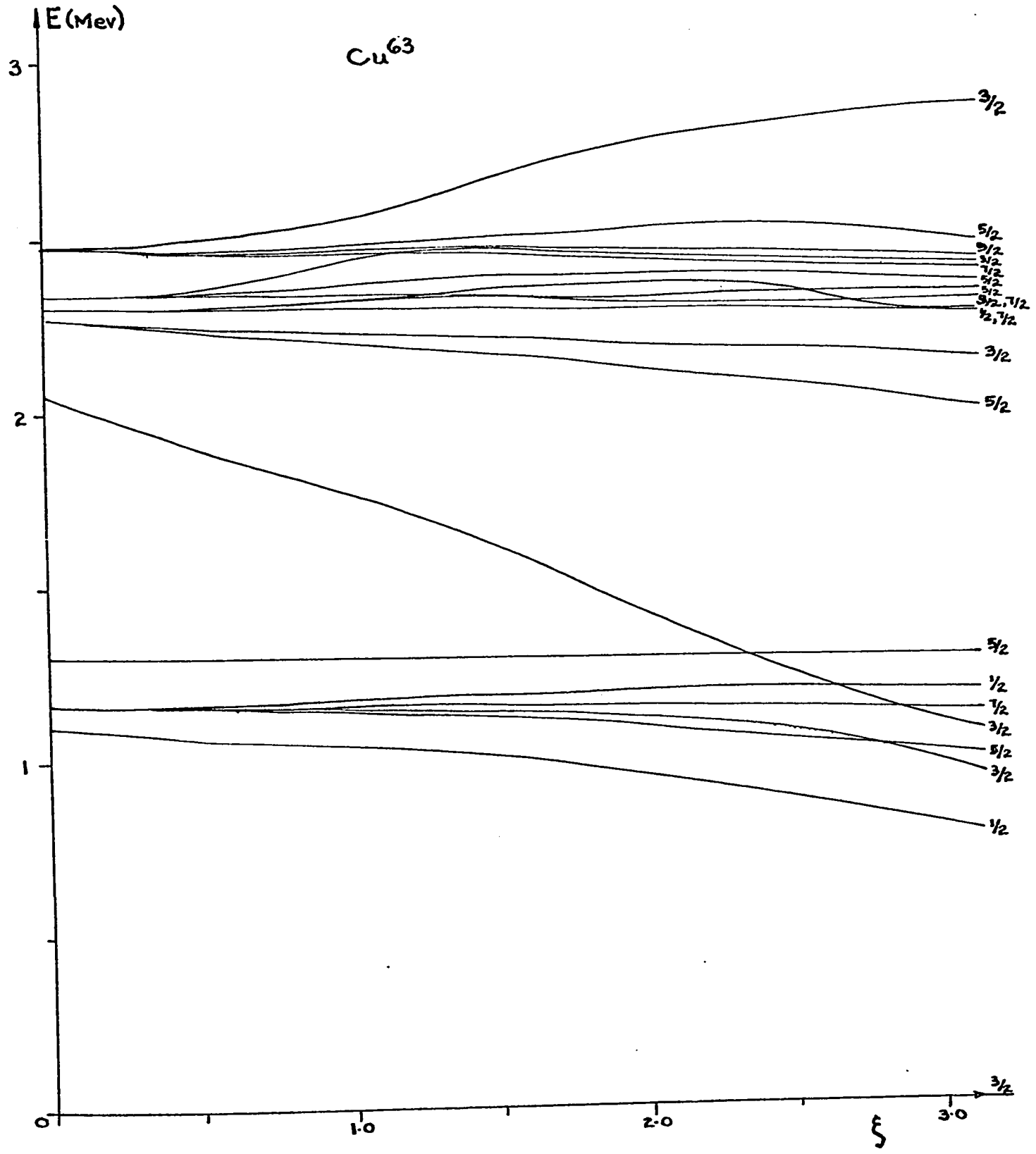

Fig. V.14

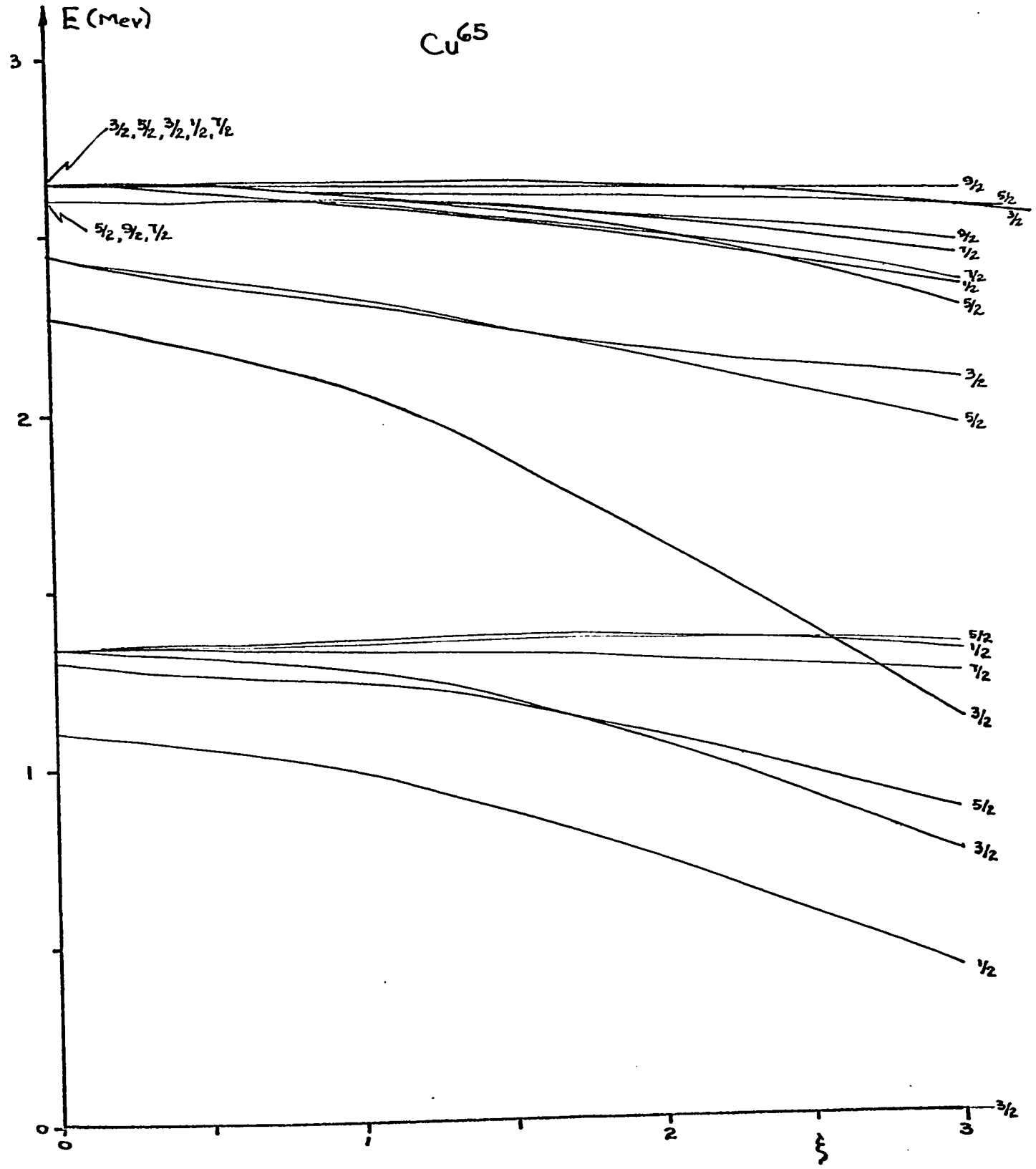
E (Mev)
Cu65
3
2
1
0
0
1
2
3
ξ
3/2, 5/2, 3/2, 1/2, 7/2
5/2, 9/2, 7/2
9/2
5/2
3/2
9/2
7/2
7/2
1/2
5/2
3/2
5/2
5/2
1/2
7/2
3/2
5/2
3/2
1/2
3/2

Fig. V.15

b) Results

The B(E2) and B(M1) values are displayed in Tables V.VI, V.VII, V.VIII and V.IX, next to those values obtained from the classical model. In this revised model, again, two sets of results are shown, one with the last odd proton having the free proton charge and spin gyromagnetic ratio, the other set with the effective charge and effective spin gyromagnetic ratio.

3. Spectroscopic Factors

Spectroscopic factors for single-particle transfer in Cu isotopes are calculated here, using eq. (III.122) in section IV.3, Chapter III.

a) Parameters used

From Tables V.XIII, V.XIV, V.XV, and V.XVI, the expansion coefficients $A(jNRI|E)$ for $j = I$, required for calculating the spectroscopic factors are extracted for each isotope and tabulated in Table V.XVII. In the same table, the values of U_j concerned are also indicated.

To show a comparison with the classical model, the expansion coefficients $A(jOOI|E)$ for $j = I$ are also tabulated for two sets of parameters from the anharmonic core and particle model in Table V.XVII. The spectroscopic factors corresponding to this model are then estimated.

b) Results

The calculated spectroscopic factors $S(I_\alpha)$ of Cu^{59-65} for

Table V.XIII Expansion Coefficients Corresponding to States $|E(Mev):I^-\rangle$ of Cu^{59} in the Extended ICM

Basic States $\|\ell_j;NR\rangle$	$\|0;3/2^-\rangle$	$\|0.528;1/2^-\rangle$	$\|0.807;5/2^-\rangle$	$\|1.355;7/2^-\rangle$
$\|2p_{3/2};00\rangle$	1.0000	0.0000	0.0000	0.0000
$\|2p_{3/2};12\rangle$	0.0000	0.6142	0.5921	0.9720
$\|2p_{3/2};20\rangle$	0.0000	0.0000	0.0000	0.0000
$\|2p_{3/2};22\rangle$	0.0000	-0.2497	0.0151	-0.1738
$\|2p_{3/2};24\rangle$	0.0000	0.0000	-0.2677	0.0228
$\|2p_{3/2};30\rangle$	0.0000	0.0000	0.0000	0.0000
$\|2p_{3/2};32\rangle$	0.0000	0.0169	0.0041	0.0013
$\|2p_{3/2};33\rangle$	0.0000	0.0000	0.0082	0.0022
$\|2p_{3/2};34\rangle$	0.0000	0.0000	0.0197	-0.0019
$\|1f_{5/2};00\rangle$	0.0000	0.0000	-0.1324	0.0000
$\|1f_{5/2};12\rangle$	0.0000	0.3867	0.3530	-0.1336
$\|1f_{5/2};20\rangle$	0.0000	0.0000	0.0591	0.0000
$\|1f_{5/2};22\rangle$	0.0000	-0.2072	-0.1877	0.0812
$\|1f_{5/2};24\rangle$	0.0000	0.0000	-0.1457	0.0009
$\|1f_{5/2};30\rangle$	0.0000	0.0000	0.0000	0.0000
$\|1f_{5/2};32\rangle$	0.0000	0.0163	0.0088	0.0000
$\|1f_{5/2};33\rangle$	0.0000	0.0000	0.0147	0.0000
$\|1f_{5/2};34\rangle$	0.0000	0.0000	0.0094	0.0002

Table V.XIII. (cont.)

$\|1f_{5/2};36\rangle$	0.0000	0.0000	0.0000	0.0004
$\|2p_{1/2};00\rangle$	0.0000	0.5837	0.0000	0.0000
$\|2p_{1/2};12\rangle$	0.0000	0.0000	-0.5581	0.0000
$\|2p_{1/2};20\rangle$	0.0000	0.1635	0.0000	0.0000
$\|2p_{1/2};22\rangle$	0.0000	0.0000	0.2514	0.0000
$\|2p_{1/2};24\rangle$	0.0000	0.0000	0.0000	0.0040
$\|2p_{1/2};30\rangle$	0.0000	0.0000	0.0000	0.0000
$\|2p_{1/2};32\rangle$	0.0000	0.0000	0.0000	0.0000
$\|2p_{1/2};33\rangle$	0.0000	0.0000	0.0000	0.0000
$\|2p_{1/2};34\rangle$	0.0000	0.0000	0.0000	0.0000

Table V.XIV Expansion Coefficients Corresponding to States $|E(MeV);I>$ of Cu^{61} in the Extended ICM

Basic States $\|\ell_j;NR>$	$\|0;3/2^->$	$\|1.057;1/2^->$	$\|1.270;5/2^->$	$\|1.326;7/2^->$
$\|2p_{3/2};00>$	1.0000	0.0000	0.0000	0.0000
$\|2p_{3/2};12>$	0.0000	-0.1326	0.5861	0.9971
$\|2p_{3/2};20>$	0.0000	0.0000	0.0000	0.0000
$\|2p_{3/2};22>$	0.0000	-0.0034	0.0300	-0.0212
$\|2p_{3/2};24>$	0.0000	0.0000	-0.0056	0.0105
$\|2p_{3/2};30>$	0.0000	0.0000	0.0000	0.0000
$\|2p_{3/2};32>$	0.0000	-0.0003	0.0004	0.0002
$\|2p_{3/2};33>$	0.0000	0.0000	0.0000	0.0003
$\|2p_{3/2};34>$	0.0000	0.0000	0.0002	-0.0003
$\|1f_{5/2};00>$	0.0000	0.0000	0.8088	0.0000
$\|1f_{5/2};12>$	0.0000	-0.1473	-0.0084	0.0657
$\|1f_{5/2};20>$	0.0000	0.0000	0.0148	0.0000
$\|1f_{5/2};22>$	0.0000	-0.0292	0.0155	-0.0296
$\|1f_{5/2};24>$	0.0000	0.0000	-0.0078	-0.0004
$\|1f_{5/2};30>$	0.0000	0.0000	0.0000	0.0000
$\|1f_{5/2};32>$	0.0000	-0.0004	0.0004	0.0000
$\|1f_{5/2};33>>$	0.0000	0.0000	0.0007	0.0000

$\|1f_{5/2};34\rangle$	0.0000	0.0000	0.0004	0.0000
$\|1f_{5/2};36\rangle$	0.0000	0.0000	0.0000	0.0000
$\|2p_{1/2};00\rangle$	0.0000	0.9800	0.0000	0.0000
$\|2p_{1/2};12\rangle$	0.0000	0.0000	0.0239	0.0000
$\|2p_{1/2};20\rangle$	0.0000	0.0062	0.0000	0.0000
$\|2p_{1/2};22\rangle$	0.0000	0.0000	-0.0177	0.0000
$\|2p_{1/2};24\rangle$	0.0000	0.0000	0.0000	-0.0004
$\|2p_{1/2};30\rangle$	0.0000	0.0000	0.0000	0.0000
$\|2p_{1/2};32\rangle$	0.0000	0.0000	0.0000	0.0000
$\|2p_{1/2};33\rangle$	0.0000	0.0000	0.0000	0.0000
$\|2p_{1/2};34\rangle$	0.0000	0.0000	0.0000	0.0000

Table V.XV Expansion Coefficients corresponding to States $|E(Mev);I>$ of Cu^{63} in the Extended ICM

Basic States $\|\ell_j;NR>$	$\|0;3/2^->$	$\|0.823;1/2^->$	$\|1.016;5/2^->$	$\|1.152;7/2^->$
$\|2p_{3/2};00>$	1.000	0.0000	0.0000	0.0000
$\|2p_{3/2};12>$	0.0000	0.7720	0.9503	0.9911
$\|2p_{3/2};20>$	0.0000	0.0000	0.0000	0.0000
$\|2p_{3/2};22>$	0.0000	-0.2707	0.2873	-0.1315
$\|2p_{3/2};24>$	0.0000	0.0000	-0.0046	0.0001
$\|2p_{3/2};30>$	0.0000	0.0000	0.0000	0.0000
$\|2p_{3/2};32>$	0.0000	0.0046	0.0019	0.0000
$\|2p_{3/2};33>$	0.0000	0.0000	0.0047	0.0001
$\|2p_{3/2};34>$	0.0000	0.0000	0.0052	-0.0000
$\|1f_{5/2};00>$	0.0000	0.0000	-0.0621	0.0000
$\|1f_{5/2};12>$	0.0000	-0.0362	-0.0105	-0.0178
$\|1f_{5/2};20>$	0.0000	0.0000	-0.0201	0.0000
$\|1f_{5/2};22>$	0.0000	-0.0133	-0.0128	0.0114
$\|1f_{5/2};24>$	0.0000	0.0000	0.0007	0.0000
$\|1f_{5/2};30>$	0.0000	0.0000	0.0000	0.0000
$\|1f_{5/2};32>$	0.0000	-0.0018	-0.0011	0.0000
$\|1f_{5/2};33>$	0.0000	0.0000	-0.0018	0.0000

Table V.XV (con't)

$\|1f_{5/2};34\rangle$	0.0000	0.0000	-0.0012	-0.0000
$\|1f_{5/2};36\rangle$	0.0000	0.0000	0.0000	0.0000
$\|2p_{1/2};00\rangle$	0.0000	0.5716	0.0000	0.0000
$\|2p_{1/2};12\rangle$	0.0000	0.0000	-0.0476	0.0000
$\|2p_{1/2};20\rangle$	0.0000	0.0503	0.0000	0.0000
$\|2p_{1/2};22\rangle$	0.0000	0.0000	0.0870	0.0000
$\|2p_{1/2};24\rangle$	0.0000	0.0000	0.0000	0.0000
$\|2p_{1/2};30\rangle$	0.0000	0.0000	0.0000	0.0000
$\|2p_{1/2};32\rangle$	0.0000	0.0000	0.0000	0.0000
$\|2p_{1/2};33\rangle$	0.0000	0.0000	0.0000	0.0000
$\|2p_{1/2};34\rangle$	0.0000	0.0000	0.0000	0.0000

Table V.XVI Expansion Coefficients corresponding to States $|E(MeV);I>$ of Cu^{65} in the Extended ICM

Basic States $\|\ell_j;NR>$	$\|0;3/2^->$	$\|0.786;1/2^->$	$\|1.122;5/2^->$	$\|1.308;7/2^->$
$\|2p_{3/2};00>$	1.0000	0.0000	0.0000	0.0000
$\|2p_{3/2};12>$	0.0000	0.6385	0.8288	0.9910
$\|2p_{3/2};20>$	0.0000	0.0000	0.0000	0.0000
$\|2p_{3/2};22>$	0.0000	-0.1671	0.2121	-0.0998
$\|2p_{3/2};24>$	0.0000	0.0000	0.0056	-0.0007
$\|2p_{3/2};30>$	0.0000	0.0000	0.0000	0.0000
$\|2p_{3/2};32>$	0.0000	0.0097	0.0023	0.0010
$\|2p_{3/2};33>$	0.0000	0.0000	0.0049	0.0017
$\|2p_{3/2};34>$	0.0000	0.0000	0.0056	-0.0012
$\|1f_{5/2};00>$	0.0000	0.0000	-0.4924	0.0000
$\|1f_{5/2};12>$	0.0000	0.1100	-0.0009	0.0650
$\|1f_{5/2};20>$	0.0000	0.0000	-0.0095	0.0000
$\|1f_{5/2};22>$	0.0000	-0.0334	-0.0058	0.0607
$\|1f_{5/2};24>$	0.0000	0.0000	0.0011	0.0001
$\|1f_{5/2};30>$	0.0000	0.0000	0.0000	0.0000
$\|1f_{5/2};32>$	0.0000	0.0056	0.0018	0.0000
$\|1f_{5/2};33>$	0.0000	0.0000	0.0030	0.0000
$\|1f_{5/2};34>$	0.0000	0.0000	0.0019	0.0001
$\|1f_{5/2};36>$	0.0000	0.0000	0.0000	0.0000

Table V.XVI. (continued)

Basic States $\|\ell_j;NR\rangle$	$\|0;3/2^-\rangle$	$\|0.786;1/2^-\rangle$	$\|1.122;5/2^-\rangle$	$\|1.308;7/2^-\rangle$
$\|2p_{1/2};00\rangle$	0.0000	0.7384	0.0000	0.0000
$\|2p_{1/2};12\rangle$	0.0000	0.0000	0.1442	0.0000
$\|2p_{1/2};20\rangle$	0.0000	0.0769	0.0000	0.0000
$\|2p_{1/2};22\rangle$	0.0000	0.0000	0.0679	0.0000
$\|2p_{1/2};24\rangle$	0.0000	0.0000	0.0000	0.0002
$\|2p_{1/2};30\rangle$	0.0000	0.0000	0.0000	0.0000
$\|2p_{1/2};32\rangle$	0.0000	0.0000	0.0000	0.0000
$\|2p_{1/2};33\rangle$	0.0000	0.0000	0.0000	0.0000
$\|2p_{1/2};34\rangle$	0.0000	0.0000	0.0000	0.0000

Table V.XVII Expansion Coefficients corresponding to N = R = 0 and j = I i.e. A(j00I E) used in calculating Spectroscopic Factors.

	Isotope	A(½ 00 ½)	A(3/2 00 3/2)	A(5/2 00 5/2)
Classical ICM using Experimental Parameters	Cu^{59}	0.7351	0.9273	0.8608
	Cu^{61}	0.7066	0.9277	0.8468
	Cu^{63}	0.7281	0.9651	0.9095
	Cu^{65}	0.7756	0.9637	0.9215
Classical ICM using Best-fitting Parameters	Cu^{59}	0.6459	0.8906	0.8609
	Cu^{61}	0.6891	0.9060	-0.7078
	Cu^{63}	0.6771	0.9522	-0.7049
	Cu^{65}	0.5335	0.9637	0.9215
Extended ICM using Experimental Parameters	Cu^{59}	0.5837	1.0000	-0.1324
	Cu^{61}	0.9797	1.0000	0.8088
	Cu^{63}	0.5716	1.0000	-0.0621
	Cu^{65}	0.7384	1.0000	-0.4924

both models are shown in Table V.XVIII, together with experimental estimates and other references.

III. ANALYSIS OF RESULTS

1. Energy Levels

The calculated energy levels are shown in figs. V.10, V.11, V.12 and V.13 for Cu^{59}, Cu^{61}, Cu^{63}, and Cu^{65} respectively. In each diagram, column 1 and 2 shows the experimental spectrum. Columns 3 and 4 show the spectra from the classical model of anharmonic core and particles. Column 5 shows the spectrum from a modified version of anharmonic core and quasiparticles. The other columns show the levels from other recent theoretical investigations.

The theoretical investigations used for comparisons here are the results from:

R. P. Singh, R. Raj, M. L. Rustgi and H. W. Kung (June 1970)

Jose M. G. Gomez (March 1971)

D. Larner (February 1970)

V. K. Thankappan and William W. True (October 1964)

and S. S. M. Wong (August 1970)

Each theoretical reference will be introduced briefly here. R. P. Singh et al. carried out a shell-model calculated on Cu^{59}, assuming an inert Ni^{56}

Table V.XVIII Spectroscopic Factors S_j

Isotope	j	Anharmonic Core and Particle Best Fit S_j	Anharmonic Core and Particle Exptl. Parameters S_j	Anharmonic Core and Quasiparticle S_j	Experiment or Other Refs. S_j	References
Cu^{59}	1/2	0.37	0.48	0.30	[1] 1.25, [2] 1.05, [4] 1.02, 1.49, 0.98, [10] 0.22, [10] 0.26	[1] V. V. Okorokov et al. Yadenaya Fizika, vol.8 #4 p.668-77 (Oct. '68)
	3/2	0.68	0.63	0.73	[1] 1.19, [2] 0.9, [4] 1.02, 1.40	[2] A. G. Blair Phys. Rev. 140 B648 (1965)
	5/2	0.45	0.66	0.16	[1] 1.73, [4] 1.34, [10] 0.37 [10] 0.61, 0.37	[3] D.D. Armstrong et al. Phys. Rev. 155, 1254 (1967)
Cu^{61}	1/2	0.32	0.34	0.65	[2] 1.00, [3] 1.24, 1.23, [4] 0.95 0.80, [5] 1.00, [7] 0.80, [8] 1.24, [9] 0.75, [6] 0.31	[4] V. V. Okorokov et al. Yadernaya Fizika (USSR) vol. 9, #4 p.710-14 (April 1969)
	3/2	0.36	0.38	0.44	0.36, [2] 0.90, [3] 0.74, 1.24, [4] 0.93, 0.78, [5] 0.90, [6] 0.30, [7] 0.89	[5] Blair, A. G. Phys. Rev., 140 B648 (1965).
	5/2	0.41	0.59	0.64	[8] 0.74, [9] 0.85, 0.25, [2] 1.04, [3] 1.08, [4] 0.73, [5] 1.04, [6] 0.21 [8] 1.08, [9] 0.38	[6] Pullen and Rosner Phys. Rev. 170 (1968) p. 1034
						[7] Reanalysis from 6).

Table V. XVIII. Spectroscopic Factors S_j (continued)

Cu^{63}	1/2	0.22	0.25	0.15	$^{10)}0.12$, $^{10)}0.37$, 0.53, $^{11)}0.85$, $^{11)}0.65$, $^{2)}0.82$ $^{3)}0.89$	$^{8)}$D. D. Armstrong Phys. Rev. 155 (1967) 1254
	3/2	0.31	0.32	0.34	0.10, 0.26, 0.24, $^{11)}0.70$ $^{11)}0.94$, $^{2)}0.77$, $^{3)}0.65$	$^{9)}$Thankappan and True Phys. Rev. 137 (1965) B793 - Theory.
	5/2	0.31	0.51	0.0024	$^{11)}0.43$, $^{11)}0.43$, $^{2)}0.53$ $^{3)}0.79$	$^{10)}$J. C. Browne et al. Nucl. Phys. A153, (1970) p. 481-501
Cu^{65}	1/2	0.09	0.19	0.17	$^{11)}0.84$, $^{11)}0.76$, $^{2)}1.43$, $^{3)}0.84$, $^{10)}0.21$, $^{10)}0.62$	$^{11)}$S. S. M. Wong Nucl. Phys. A159 (1970) p. 235-248
	3/2	0.22	0.24	0.26	$^{11)}0.89$, $^{11)}0.95$, $^{2)}0.80$ $^{3)}0.80$	Nucl Data B2-3('68) B2-6 ('69)
	5/2	0.21	0.33	0.10	$^{11)}0.29$, $^{11)}0.09$, $^{2)}1.18$ $^{3)}0.75$.	

core with three extra core particles to occupy the $1p_{3/2}$, $0f_{5/2}$ and $1p_{1/2}$ orbitals. The effect of including the $0g_{9/2}$ orbital was included. The renormalized reaction matrix elements as derived by Kuo and Brown for this mass region were used.

The intermediate coupling model was used in the calculation of Gomez who describes the low-lying levels of the odd-mass copper isotopes as a proton in the $2p_{3/2}$, $1f_{5/2}$ and $2p_{1/2}$ orbits coupled to a quadrupole vibrator.

Larner used the intermediate-coupling model with quasi-vibrational core, as developed by True and Thankappan. A pattern search routine is used to fit the five parameters to the levels and stripping strengths. Calculations on $Cu^{61,63,65}$ are included in his study of N = 29 and N = 29 Nuclei.

Properties of the low-lying Cu^{63} levels were calculated by Thankappan and True, using a core-to-particle interaction of the form

$$H_{INT.} = -\zeta(J_c^{(1)} \cdot j_p^{(1)}) - \eta(Q_c^{(2)} \cdot Q_p^{(2)})$$

where $J_c^{(1)}$ and $Q_c^{(2)}$ are respectively, the angular momentum operator and the mass quadrupole operator of the core, while $j_p^{(1)}$ and $Q_p^{(2)}$ play a similar role for the particle. The same interaction was used in Larner's investigation.

S. S. M. Wong's study is a shell-model study of Cu^{65} and Cu^{63}. Their low-lying states are studied in the frame work of the ($1f_{5/2}$, $2p_{3/2}$ $2p_{1/2}$) shell model with realistic effective interaction. The weak-coupling scheme of coupling a proton to the quadrupole vibrations of Nickel is

found to be valid provided admixtures of $2p_{1/2}$ and $1f_{5/2}$ proton states are allowed in addition to the usual $2p_{3/2}$ state.

It should be mentioned here that our computer programmes used in the classical intermediate coupling model calculations in this study were tested by using the given parameters of other authors and producing the same results as theirs. This was tested on Chaudhury's [87] study on Cs^{131}, Rustgi's [88] calculation of I^{127} and Bailey's [64] investigation of Mg^{27}. The same programme was used to test the results of Gomez but failed to reproduce their results.

In fig. V.10, we can see that the results from both models are in very close fit to the experimental spectrum of Cu^{59}. Correct ordering is predicted in both. The anharmonic core and particle model with the best-fit parameters show excellent agreement in the lower levels, especially the first three. The fourth level which is lower than the experimental energy, is improved by the anharmonic core and quasiparticle model. From the overall picture, it can be said that the anharmonic core and particle model with the best-fit parameters gives the best agreement while the anharmonic core and quasiparticle model gives a better fit than the classical model with the experimental parameters. Our best results show a closer fit than the spectrum from Gomez. All of our energy spectra display a superiority over the shell-model calculation of Singh et al.

In fig. V.11, again, we can see very good agreement between the calculated levels of Cu^{61} and the experimental ones. The anharmonic

core and particle model with best-fit parameters gives an excellent fit for the lower levels, while the higher levels are improved by the modified model with quasiparticles. The first 7/2 and first 5/2 levels are lower than the observed ones. As in Cu^{59}, the anharmonic core and quasiparticles model still give levels with closer fit than the classical model with experimental parameters. Column 4 shows a slight improvement over Larner's levels, and much better agreement than Gomez's spectrum.

Fig. V.12 gives the energy spectra of Cu^{63}. Good agreement with experiment in both models is achieved in the ordering as well aa the energies of the levels. The fourth and fifth levels are lower than the experimental estimates in general. The modified model improves these levels somewhat. Column 5 shows the second level (1/2) being too high, but it is still in closer fit to the experimental levels than Column 4. Column 3, representing the classical model with best-fit parameters, gives the best agreement, superior to Gomez's spectrum. Except for the fourth and fifth levels, it also shows closer fit than Larner's results. Columns 3, 4 and 5 show a better fit than Thankappan and True for the lower levels. They are all in much closer agreement than Wong's levels.

Fig. V.13 shows the energy levels of Cu^{65}. All 3 columns, 3, 4, and 5 show very good agreement with experiment. Column 5 shows an improved third level, but its fourth and fifth levels are low. It displays better higher levels than the other two columns though. Column 4 shows improved agreement over Gomez's levels, whereas column 5

gives better prediction of level spins than Gomez. The above conclusion is also true compared to Larner's and Wong's levels, except for the first 5/2 level which is too low. It is useful to draw general trends for each lower energy level. Here, we shall discuss the first three excited levels, i.e. the 1/2, 5/2 and 7/2 levels, which are well established in all experimental observations.

The classical model with best-fitting parameters give excellent first excited levels, $(1/2^-)$ giving identical values as the observed ones, except for Cu^{61} (0.463 as compared to 0.475). The classical model with experimental parameters and the extended model give level values higher than the best-fitting case and hence, higher than the experimental levels. The only exception is in Cu^{65}, where the classical model with experimental parameters shows a first excited level lower than the experimental level.

The closest agreement between the theoretical second excited levels $(5/2^-)$ and the experimental ones are found in the classical model with best-fitting parameters. This is the case for all three isotopes, $Cu^{59,61,63}$. Cu^{65} differs because the anharmonic core and quasiparticle model has the closest fit here. The classical model with experimentally extracted parameters gives second levels to much lower than observed values. The extended model gives these levels higher than experiment with the exception of Cu^{59}.

For the third excited levels $(7/2^-)$, the closest agreements to observation are found in Cu^{59} and Cu^{63}, given by the extended model

of quasiparticles, in Cu^{61} and Cu^{65} given by the best-fitting classical model. Except for Cu^{65}, all third levels in the best-fitting case are lower than the observed levels. The classical model with experimental parameters has third levels too low, whereas the extended model gives levels about the same as the best-fitting case.

From the individual analysis of each isotope of each lower excited level, certain definite conclusions can be drawn in general.

Both of the models; classical and revised produce energy levels in better agreement with the experimentally observed levels than recent theoretical investigations. Excellent predictions in level spins, and good agreement in energies are offered by them. The theoretically calculated levels higher than those observed by experiments can then be assumed to be good predictions.

The extended model usually predicts a high second level. This is the case in Cu^{59}, Cu^{61} and Cu^{63}. It gives improved higher levels over the classical model with best-fitting parameters in Cu^{61} and Cu^{65}.

The classical model with best-fitting parameters predicts levels in better agreement than the extended model in general although their spectra are quite close to each other. In all cases, the classical model with experimental parameters give energy levels inferior to those from the extended model.

The level structure depends on the quadrupole moment of the 2+ state of the core. In order to obtain a best fit from the extended model, the quadrupole moment $Q_{NR}(2+)$ should be varied[34] to find the

value which gives the best agreement between the calculated levels and the experimental levels. Also, the other parameters are not varied to give the best-fitting spectrum in the extended model. So one cannot conclude that the extended model is not superior to the classical model in the medium mass region explored here. It can be established though that when using sets of unvaried parameters taken from experimental data of the core nucleus, it is superior to the classical model. When the classical model uses best-fitting parameters and the extended model uses unvaried parameters, the latter model is as good as the former one.

2. Electromagnetic Transition Rates

Tables V.VI, V.VII, V.VIII and V.IX are examined here. There are no experimental transition data for Cu^{59} and Cu^{61} available at present, so a comparison of the theoretical reduced transition rates B(E2) and B(M1) with experiment is not possible at this time. However, theoretical values have been calculated since it is expected that experimental results will soon be available. In Tables V.VI and V.VII, the calculated values of B(E2) and B(M1) and using both models are compared to the theoretical results of Gomez. Close agreement is reached within an order of 10 in most cases.

In Table V.VIII, the reduced transition rates of Cu^{63} are shown. Experimental values are only available for the transitions of the first three levels to the ground state. The B(E2) results will be

discussed first. For B(E2:(1/2)→Ground state) columns I and II show values less than the experimental values by a factor of 10. Columns III, IV, V, and VI give values with the same order of magnitude as the experimental values. The best agreement is given by column IV (175.1) as compared to reference 2 (168.7). For B(E2 :(5/2) → Ground state) all results have the same order of magnitude as the experimental values, except for columns I and VI, which have values less by a factor of 3 or 4. Best agreements are between column II (195) and reference 2 (166.0), and between column IV (351.6) and reference 3 (333.). For B(E2:(7/2) → Ground state , columns I and II show values larger than the experimental values by a factor of 15 to 20. The other theoretical values have the correct orders of magnitude. Best agreement with the experimental value of 200 (ref. 1) is offered by the extended model (104).

Again, experimental B(M1) values are only available for the transitions of the first three levels to the ground state. Columns I and II for the first two transitions show B(M1) values which are too small. The classical model with best-fitting parameters give values in close agreement with the experimental values. B(M1) values for all first three transitions to ground state are zero in the extended model. This is because the expansion coefficients for the ground state (3/2-) are all zero, except for the eigenstate $|jNR\rangle = |\ 3/2\ 00\rangle$, when $A(3/2\ 00\ 3/2|0)$ is 1.

In Table V.IX, B(E2) and B(M1) values for Cu^{65} are tabulated. As one can see, experimental values of B(E2) are available for only four

transitions. For B(E2 : (1/2) → Ground state), columns I, II and VI show values smaller than the experimental value by approximately half. The best value, is that in column V, 127 is compared to the experimental value of 184. For B(E2 : (5/2) → Ground state), all values are within an order of 10, in comparison to experiment. The best value of 134 is in column III. The experimental B(E2) value here is 193. For B(E2 : $(7/2)_1$ → Ground state), close agreement, within an order of 10 is obtained between the theoretical values and the experimental value of 180. Best agreement is the value of 191 in column IV, whereas both values from the extended model are consistent at 122. For B(E2:$(5/2)_2$ → Ground state), experiment gives an estimate of being less than 200. This is in agreement with the values of the extended model only.

Excellent agreement is displayed between the B(M1) values in the classical model with best-fitting parameters and the experimental values. The zero values for the transitions to the ground state are again explained by the same reason discussed for Cu^{63} in Table V.VIII.

It can be concluded that the general trend is that the classical model with best-fitting parameters and with the effective charge as well as effective gyromagnetic ratio give electromagnetic transition rates in best agreement with experimental values, as compared to the other calculated ones. In most transitions, the anharmonic core and quasiparticle model gives better values of B(E2) and B(M1) than the classical model with the unvaried experimental parameters, thus confirming the conclusions drawn in section 1 of this analysis.

3. Spectroscopic Factors

The spectroscopic factors for all four isotopes are shown in Table V.XVIII. The $S(I_\alpha)$ values for Cu^{59} are small compared to the references quoted, especially S(1/2) and S(5/2). The S(3/2) value in the modified model is in better agreement with the references than the others.

All the spectroscopic factors of Cu^{61} are within the range of the values given by the references. The modified model of anharmonic core and quasiparticles has S(1/2) and S(5/2) values in better agreement with the averaged value of the references. The S(3/2) values in all cases are too low.

All the S(I) values of Cu^{63} are within the range of the quoted references, except for the S(5/2) value in the modified model, which is much too small and in poor agreement with the references. The value of S(1/2) and S(3/2) for both models are all lower than the average of the reference values.

All of the S(1/2) and S(3/2) values of Cu^{65} are too low and out of the range of the quoted values, except for the S(5/2) values.

From these data, we can say that definite and sound comparisons with the quoted references cannot be made because of their wide range in general. All of the spectroscopic factors of $Cu^{59,61,63}$ are within this range, except for a poor S(5/2) of Cu^{63} mentioned above. The spectroscopic factors of Cu^{65} are mostly low as compared to the quoted values.

One explanation of the theoretical spectroscopic factors not being in good agreement with the references quoted is that in the model used here Ni^{56} with 28 protons and 28 neutrons is assumed to be a closed core. The spectroscopic factors are sensitive to the wave functions and are therefore sensitive to any assumptions concerning the closed core. Perhaps this closed core assumption on which our calculations are based is not a complete one.

There is still the general trend that the spectroscopic factors calculated using anharmonic core and quasiparticles are in better fit to the average value of the references than the classical model. This is expected because the validity of using eq. (III.122) to calculate the spectroscopic factors in the classical model using quasiparticle amplitudes is not clearly established.

CHAPTER VI RESULTS AND ANALYSIS OF Cu ISOTOPES APPLYING THE HARTREE-FOCK METHOD

Hartree-Fock theory described in Chapter III is applied to the Cu isotopes in the 2p-1f shell. Each nucleus is considered to have a Ni^{56} core, with (A-56) nucleons in the $2p_{1/2}$, $1f_{5/2}$ and $2p_{3/2}$ states. Hence Cu^{59} has one proton and two neutrons outside the reference core, while Cu^{61} has one proton, four neutrons, Cu^{63} has one proton, six neutrons and Cu^{65} has 1 proton and eight neutrons outside Ni^{56}. In the present study, the HF theory is applied to Cu^{59} and Cu^{61} only.

I. Computation and Parameters

A modified form of the Hamiltonian of eq. (IV.7) in Chapter IV which introduces pairing effects is used. The actual computation becomes:

$$H'' = H' - \lambda_1 \frac{1}{\sqrt{24}} \sum_{m,m'} (-)^{3/2-m}(1)^{5/2-m'} a^{\dagger}_{5/2m'} a^{\dagger}_{5/2-m'} a_{3/2m} a_{3/2-m}$$

$$- \lambda_2 \frac{1}{\sqrt{8}} \sum_{m,m'} (-)^{3/2-m} (-)^{1/2-m'} a^{\dagger}_{1/2m'} a^{\dagger}_{1/2-m'} a_{3/2m} a_{3/2-m}$$

$$- \lambda_3 \frac{1}{\sqrt{12}} \sum_{m,m'} (-)^{5/2-m} (-)^{1/2-m'} a^{\dagger}_{1/2m} a^{\dagger}_{1/2-m} a_{5/2m} a_{5/2-m} \qquad \text{(IV.1)}$$

making use of the following orbitals:

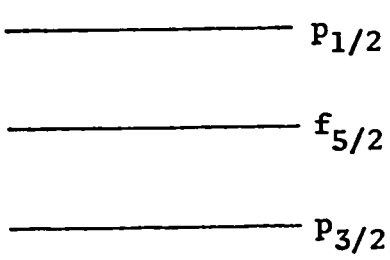

H' is defined by equation (IV.72) in Chapter IV. The single-particle energies in this Hamiltonian are taken to be:

$$\varepsilon(2p_{1/2}) = 1.08 \text{ MeV}$$
$$\varepsilon(1f_{5/2}) = 0.78 \text{ MeV}$$
$$\varepsilon(2p_{3/2}) = 0.00 \text{ MeV}$$

In this calculation, the effective interaction matrix elements $<|V|>$ of Kuo and Brown are used.

We are fortunate to have available Dr. Castels' computer programme for these HF calculations. The IBM 360/65 computer is used again for this part of the study. Five parameters are involved here, i.e., λ_2^o, λ_4^o, λ_1, λ_2 and λ_3. The first two parameters are the Lagrange multipliers in eq. (VI.1). Each parameter is varied until separate minimum is located for each angular momentum state, i.e., 3/2, 5/2, 7/2 and 9/2 states in the k = 1/2 and k = 3/2 band. Finally, the set of parameters giving the lowest minima of each state is found for each k band.

II Results

The calculated properties of Cu^{59} for fixed values of λ_2^o, λ_4^o, λ_1, λ_2 and λ_3 for both k = 1/2 and k = 3/2 bands are shown in Table (VI.1). Each column represents a HF solution. DN and DP are the total number of neutrons and protons, respectively.

Table (VI.2) shows the calculated energies and populations of neutrons and protons of Cu^{61}, at fixed values of λ_2^o, λ_4^o, λ_1, λ_2 and λ_3. Again, results for both k = 1/2 and k = 3/2 bands are represented. Figs. (VI.1) and (VI.2) show how λ_2^o and λ_4^o respectively, vary with energy in the case of Cu^{59} (k = 3/2).

Fig. (VI.3) gives the energy spectra of Cu^{59} and Cu^{61}. In both nuclei, the spectrum from the Projected Hartree-Fock method is compared to the experimental spectrum.

III. Analysis of Results

In Fig. (VI.1), the separate minimum for each angular momentum state in the k = 3/2 band of Cu^{59} is located. These minima all occur at $\lambda_2^o = 0.4$, which then becomes the fixed value for λ_4^o Similarly, in Fig. (VI.2), the minima are located at the point $\lambda_4^o = 0.05$.

Table VI.I Calculated Properties of Cu^{59} in the Hartree-Fock Model

	k = 1/2 band	k = 3/2 band
λ_2^o	0.40	0.40
λ_4^o	0.00	0.05
λ_1	2.0	2.0
λ_2	-1.0	-1.0
λ_3	1.0	0.0
$E(1/2^-)$	-4.0044	---
$E(3/2^-)$	-4.0976	-4.0348
$E(5/2^-)$	-3.4654	-3.8524
$E(7/2^-)$	-2.8363	-2.8601
$E(9/2^-)$	-2.1699	-2.4483
$E(1/2^-)$	---	-1.1876
$DP(f_{5/2})$ j = 1/2	0.2685	---
j = 3/2	0.1400	0.2265
j = 5/2	0.4651	0.2498
j = 7/2	0.0268	0.3757
j = 9/2	0.7348	0.1033
j = 11/2	---	1.1269

Table VI.I (continued)

$DP(p_{3/2})$	j = 1/2	0.4648	---
	j = 3/2	0.7269	0.5504
	j = 5/2	0.3503	0.6226
	j = 7/2	0.8425	0.4297
	j = 9/2	0.0277	0.7646
	j = 11/2	---	-0.3086
$DP(p_{1/2})$	j = 1/2	0.2667	---
	j = 3/2	0.1331	0.2231
	j = 5/2	0.1846	0.1276
	j = 7/2	0.1307	0.1946
	j = 9/2	0.2375	0.1322
	j = 11/2	---	0.1818
$DP(f_{5/2})$	j = 1/2	0.5177	---
	j = 3/2	0.5514	0.5287
	j = 5/2	0.6884	0.6154
	j = 7/2	0.6957	0.7424
	j = 9/2	0.7864	0.7037
	j = 11/2	---	1.1283

Table VI.I (continued)

$DN(p_{3/2})$	j = 1/2	0.2964	---
	j = 3/2	0.2846	1.1114
	j = 5/2	0.2531	1.1358
	j = 7/2	0.3482	0.9502
	j = 9/2	0.2705	0.9542
	j = 11/2	---	0.8945
$DN(p_{1/2})$	j = 1/2	1.0858	---
	j = 3/2	1.1641	0.3599
	j = 5/2	1.0585	0.2488
	j = 7/2	0.9561	0.3074
	j = 9/2	0.9431	0.3421
	j = 11/2	---	-0.0228

Table VI.II Calculated Properties of Cu^{61} in the Hartree-Fock Model

		k = 1/2 band	k = 3/2 band
	λ_2^o	-0.10	-0.05
	λ_4^o	0.00	-0.65
	λ_1	2.0	2.0
	λ_2	1.0	1.0
	λ_3	1.0	1.0
	$E(1/2^-)$	-5.5646	---
	$E(3/2^-)$	-5.7746	-5.6627
	$E(5/2^-)$	-4.4606	-5.6035
	$E(7/2^-)$	-4.1101	5.5650
	$E(9/2^-)$	-3.0618	-4.9588
	$E(11/2^-)$	---	-6.2788
$DP(f_{5/2})$	j = 1/2	0.0427	---
	j = 3/2	0.0076	0.0322
	j = 5/2	0.3393	0.0601
	j = 7/2	0.0097	1.3993
	j = 9/2	0.5845	-0.0622
	j = 11/2	0.5845	-0.3617

Table VI.II (continued)

$DP(p_{3/2})$	j = 1/2	0.4005	---
	j = 3/2	0.9288	0.6167
	j = 5/2	0.3471	0.9164
	j = 7/2	0.9474	-1.9587
	j = 9/2	0.1037	1.1409
	j = 11/2	---	1.6146
$DP(p_{1/2})$	j = 1/2	0.5568	---
	j = 3/2	0.0637	0.3511
	j = 5/2	0.3135	0.0235
	j = 7/2	0.0430	1.5595
	j = 9/2	0.3118	-0.0787
	j = 11/2	---	-0.2529
$DN(f_{5/2})$	j = 1/2	0.2161	---
	j = 3/2	0.1349	0.2029
	j = 5/2	0.4208	0.1853
	j = 7/2	0.4853	2.6568
	j = 9/2	0.6950	0.3222
	j = 11/2	---	-0.0327

Table VI.II (continued)

$DN(p_{3/2})$	j = 1/2	0.3933	---
	j = 3/2	0.2399	0.3293
	j = 5/2	0.4770	0.2568
	j = 7/2	0.6869	2.7486
	j = 9/2	0.5059	0.4378
	j = 11/2	---	0.4738
$DN(p_{1/2})$	j = 1/2	3.3905	---
	j = 3/2	3.6253	3.4678
	j = 5/2	3.1021	3.5578
	j = 7/2	2.8278	-1.4054
	j = 9/2	2.7991	3.2399
	j = 11/2	---	3.5589

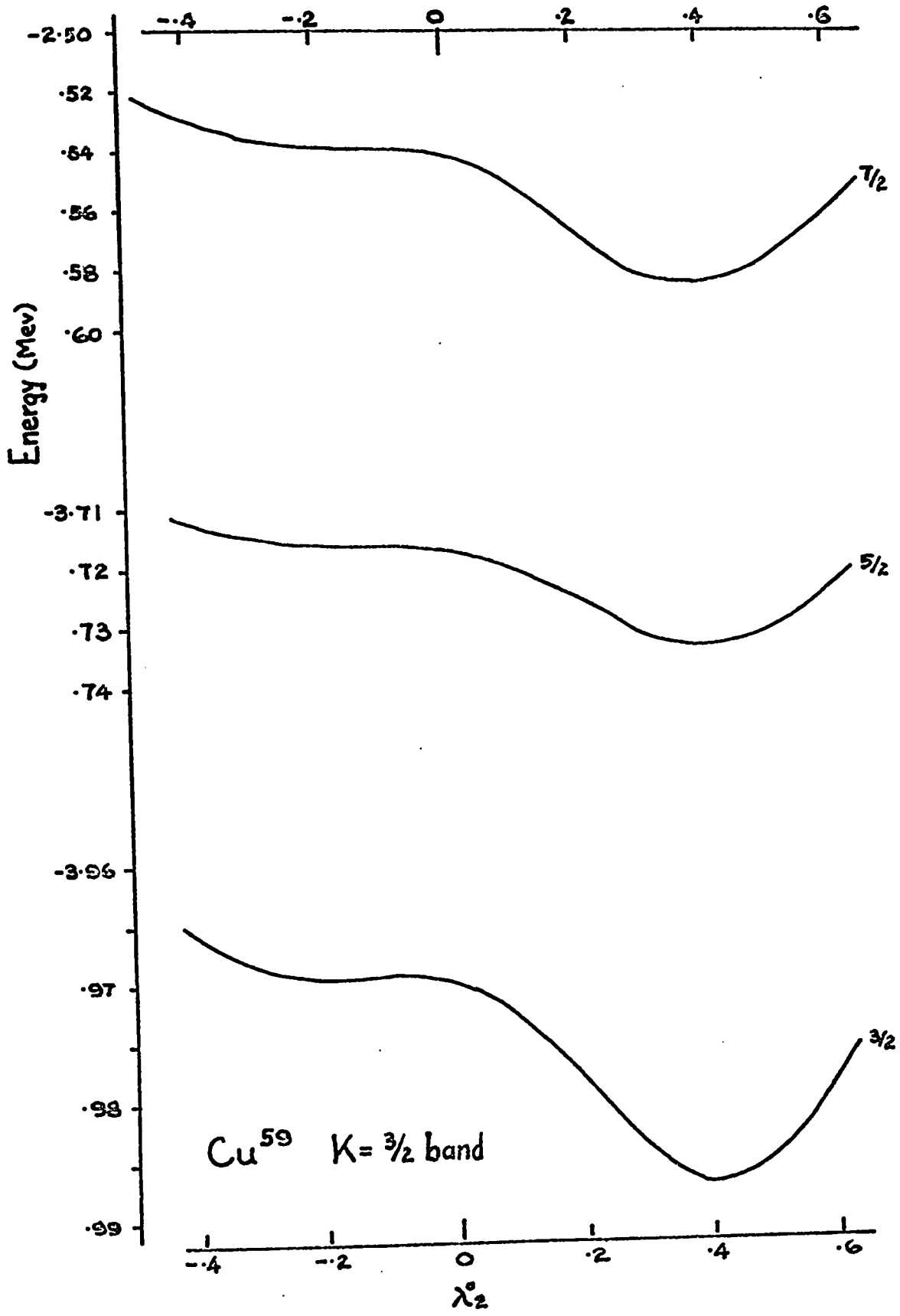
-.4
-.2
0
.2
.4
.6
-2.50
.52
.54
.56
.58
.60
Energy (Mev)
7/2
-3.71
.72
.73
.74
5/2
-3.96
.97
.98
.99
3/2
Cu59 K= 3/2 band
-.4
-.2
0
.2
.4
.6
λ2

Fig. VI.1

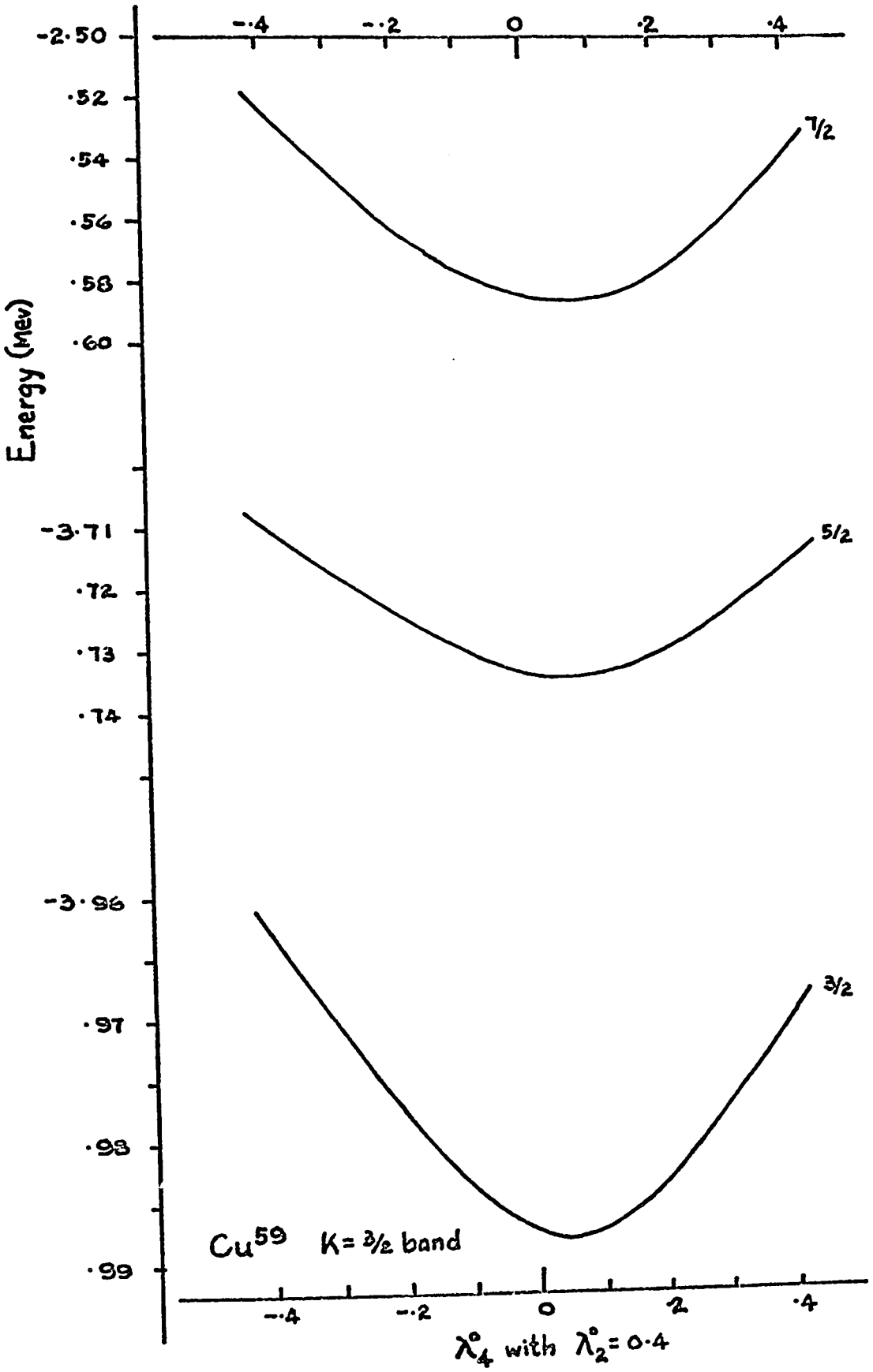
-2·50
·52
·54
·56
·58
·60
-3·71
·72
·73
·74
-3·96
·97
·98
·99
Energy (Mev)
-·4
-·2
0
·2
·4
7/2
5/2
3/2
Cu59 K= 3/2 band
λ°4 with λ°2= 0·4

Fig. VI.2

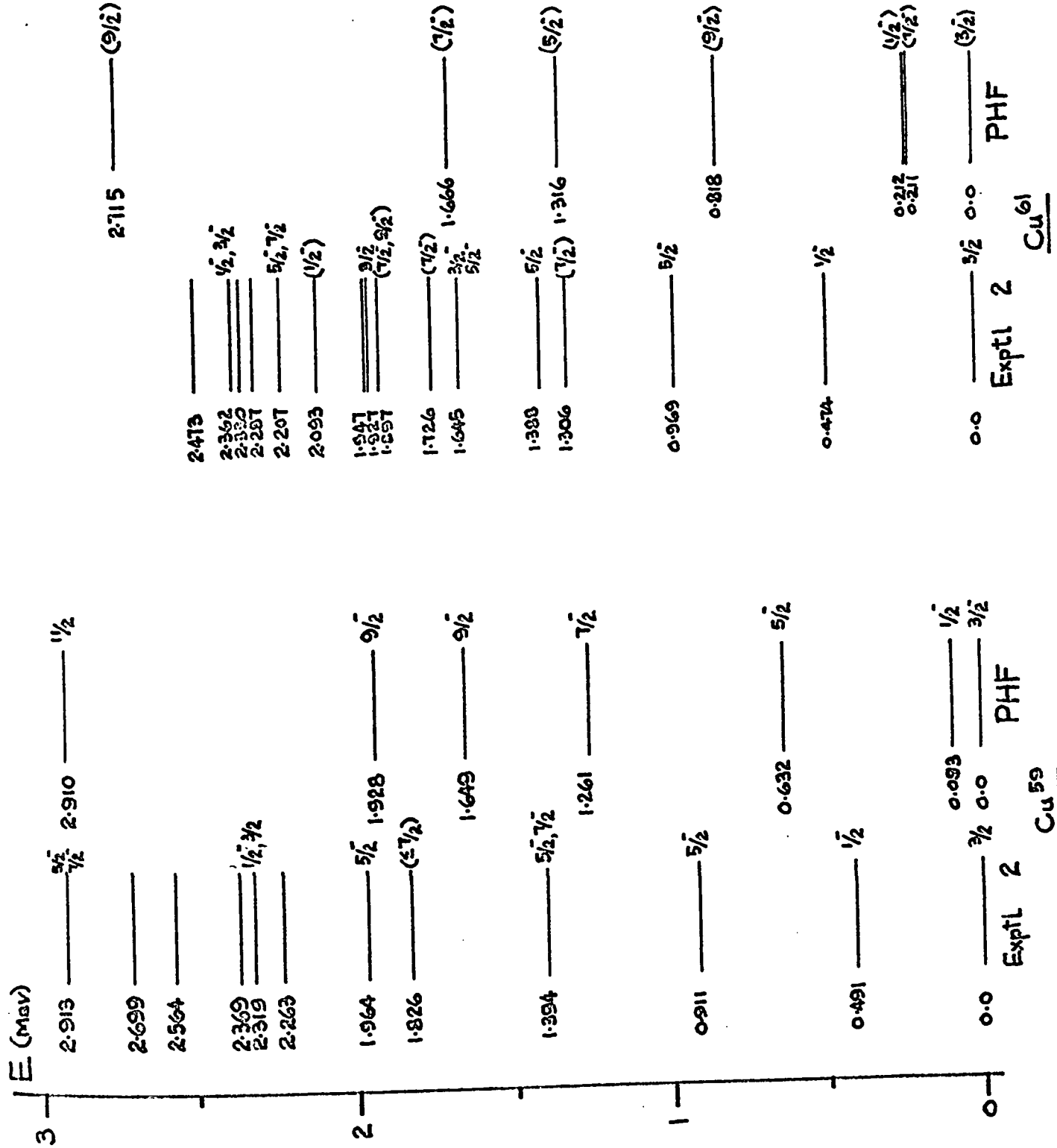
E (MeV)
3
2
1
0
2.913
2.910
2.699
2.564
2.369
2.319
2.263
1.964
1.928
1.826
1.649
1.394
1.261
0.911
0.632
0.491
0.093
0.0
Expt'l
PHF
Cu59
2.115
2.413
2.362
2.330
2.297
2.207
2.093
1.947
1.927
1.897
1.726
1.645
1.666
1.383
1.316
1.306
0.969
0.818
0.474
0.212
0.211
0.0
Expt'l
PHF
Cu61

Fig. VI.3

This is an example showing how values for the parameters λ_2^o and λ_4^o are chosen.

In Table (VI.1), the $3/2^-$ level at -4.0976 of k = 1/2 band of Cu^{59} is chosen to be the ground state, being the lowest in energy, so that other levels are adjusted relative to this level. Similarly, for Cu^{61}, the $3/2^-$ level at -5.7764 of the k = 1/2 band becomes the ground state. The adjusted energy spectra of Cu^{59} and Cu^{61} are displayed in Fig. (VI.3).

The spectrum of Cu^{59} is first examined. As one can see, the first $1/2^-$ level is much too low, being at 0.0932. This is much too drastic a comparison with the experimental level at 0.491. The other levels are much improved, but all are lower than the observed levels, i.e., 0.632 compared to 0.911, 1.238 compared to 1.394, 1.649 compared to 1.826 and 1.928 compared to 1.964. The spin of the 1.649 level is predicted to be $9/2^-$, but the experimental level has its spin less than or equal to $7/2^-$. Also, the 1.928 level, spin $9/2^-$ is different from the observed $5/2^-$ spin for this equivalent experimental level at 1.964.

The spectrum of Cu^{61} shows incorrect spin predictions for the first two excited states. The levels are much too low. For example, the $1/2^-$ state is at 0.212 MeV as compared to the observed 0.474 level. Again, the other levels, except for the highest one shown, at 2.715 ($9/2^-$) are all lower than the corresponding observed levels. The third excited state, 0.818 also has its spin incorrectly

predicted to be $9/2^-$. It is apparent that the lower three levels are in poor agreement with experiment, but the higher levels improve in their fit.

In general, both spectra do not show very good agreement with experimental levels, especially for the lower levels. The first excited states are much too low, especially that of Cu^{59}. All the other levels are lower than the experimental levels, with higher levels improving in their agreement with observed levels. Cu^{59} has its spectrum at a better fit than Cu^{61} judging from the predicted spins as well as the energies.

It becomes obvious from the results that certain inaccuracies are involved in the calculations. It is discovered that the wave functions used here are very complicated, and may not have been the c correct wave functions required for this specific mass region. There are several minima (more than six) corresponding to several solutions to the HF equation. These are very sensitive to the wave functions chosen, and so any inaccuracies in the choice of the wave functions would mean inaccurate location of the exact minima. This point is further strengthened by the proton and neutron populations in Table (VI.2). The k = 3/2 band of Cu^{59} displays negative proton and neutron populations, i.e. $DP(p_{3/2})$ and $DN(p_{1/2})$ of the 11/2 state. This symptom is more common in the k = 3/2 band of Cu^{61}. There are negative populations in

the $7/2^-$ state, i.e. $DP(p_{3/2})$ and $DN(p_{1/2})$, in the 9/2 state, i.e. $DP(f_{5/2})$ and $DP(p_{1/2})$, as well as in the 11/2 state, i.e. $DP(f_{5/2})$, $DP(p_{1/2})$ and $DN(f_{5/2})$. The populations are plotted against λ_2^o and λ_4^o in Figs. 4 to 7 to show how they vary with these parameters. In Fiv. VI.1, the minima in energy of each state is located at $\lambda_o^2 = 0.4$. In Fig. VI.4, we can see that the proton populations of the $f_{5/2}$ orbit of i.e. $DP(f_{5/2})$ of all 4 states: 3/2, 5/2, 7/2 and 9/2 have maxima at $\lambda_2^o = 0.4$. For $DP(p_{1/2})$, the 5/2 and 9/2 state have maximum population at this point, where the 3/2 and 7/2 states show minima. For $DP(p_{3/2})$, all states have lowest population at this point, except for the 7/2 state which has a maximum. Fig. VI.6 shows exactly the same trend for the point $\lambda_4^o = 0.05$ when λ_2^o is fixed at λ_4^o. This is again where the energy minima are located.

In Fig. VI.5, all 4 states have maximum neutron populations in the $f_{5/2}$ orbit at $\lambda_2^o = 0.4$. Three states i.e. 3/2, 5/2, and 9/2 have maximum $DN(p_{1/2})$ at this point while the 7/2 state shows a minimum here. All states have minimum neutron populations in the $p_{3/2}$ orbit, i.e. $DN(p_{3/2})$ when $\lambda_2^o = 0.4$. Again, exactly the same pattern is exhibited in Fig. VI.7 at $\lambda_4^o = 0.05$.

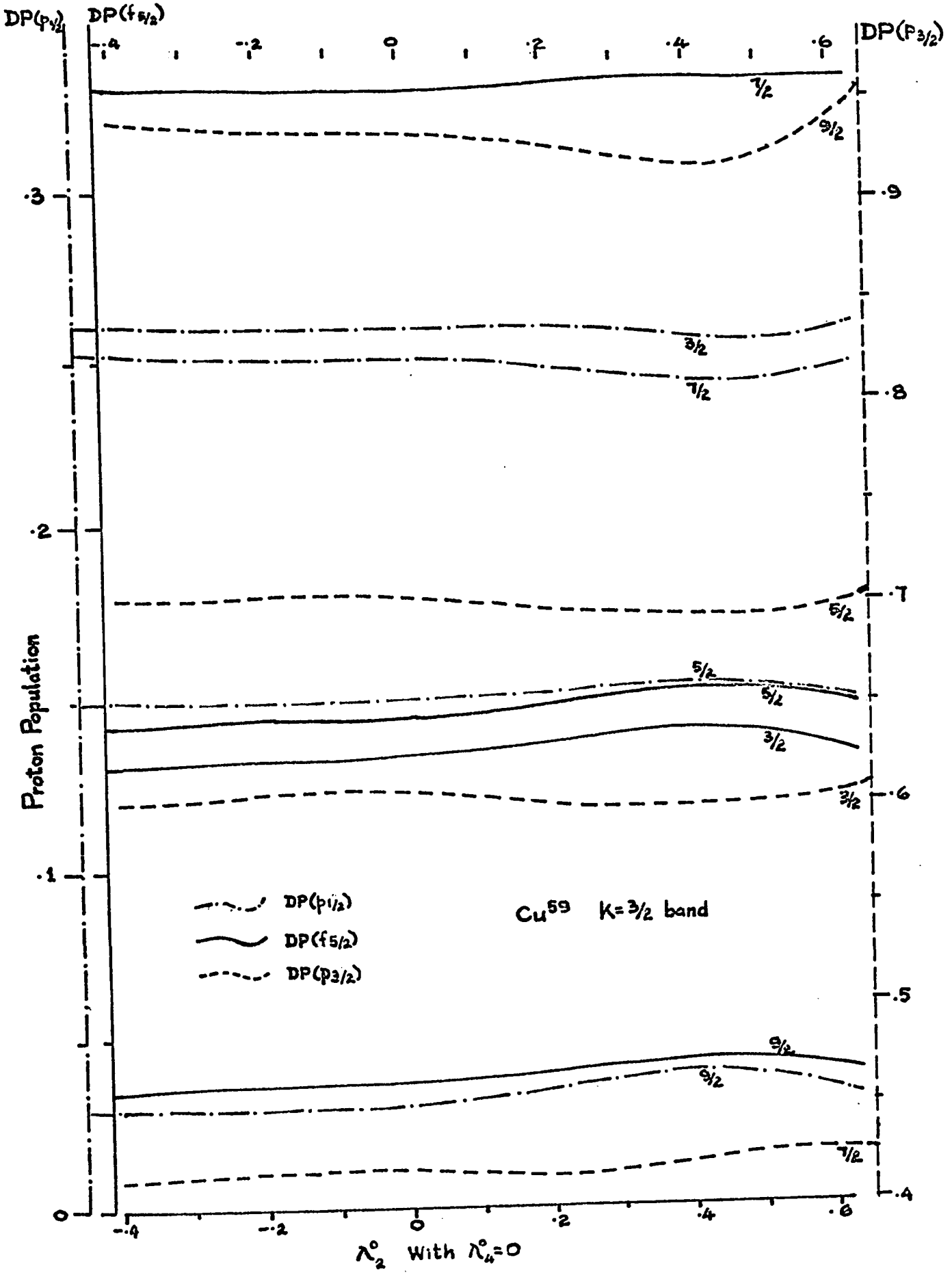
DP(p1/2)
DP(f5/2)
DP(p3/2)
Proton Population
Cu59 K=3/2 band
DP(p1/2)
DP(f5/2)
DP(p3/2)
λ°2 With λ°4=0
7/2
9/2
3/2
7/2
5/2
5/2
5/2
3/2
3/2
9/2
9/2
7/2

Fig. VI.4

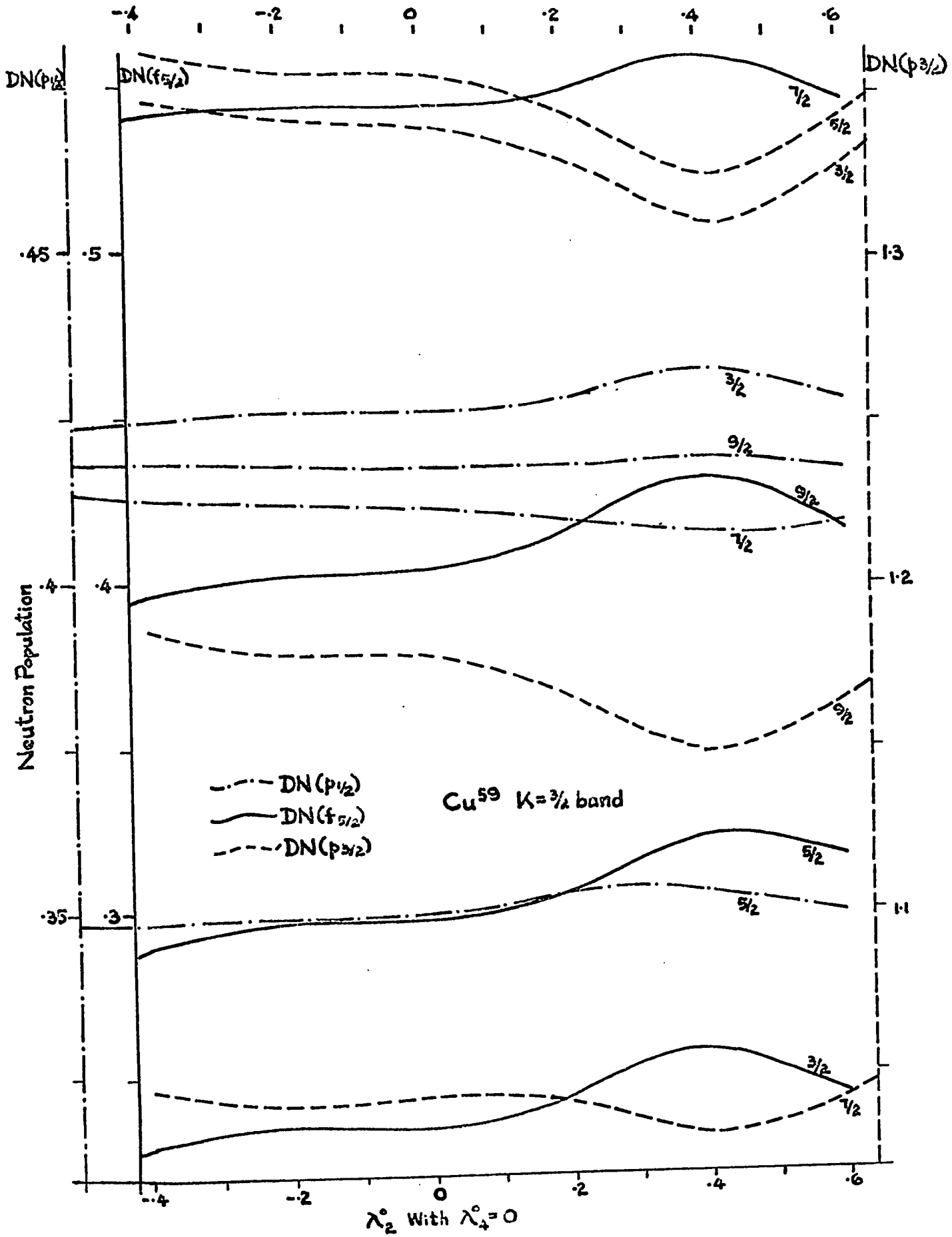
-.4
-.2
0
.2
.4
.6
DN(p1/2)
DN(f5/2)
DN(p3/2)
7/2
5/2
3/2
.45
.5
1.3
3/2
9/2
9/2
7/2
.4
.4
1.2
Neutron Population
9/2
DN(p1/2)
DN(f5/2)
DN(p3/2)
Cu59 K=3/2 band
5/2
5/2
.35
.3
1.1
3/2
7/2
-.4
-.2
0
.2
.4
.6
λ°2 With λ°4=0

Fig. VI.5

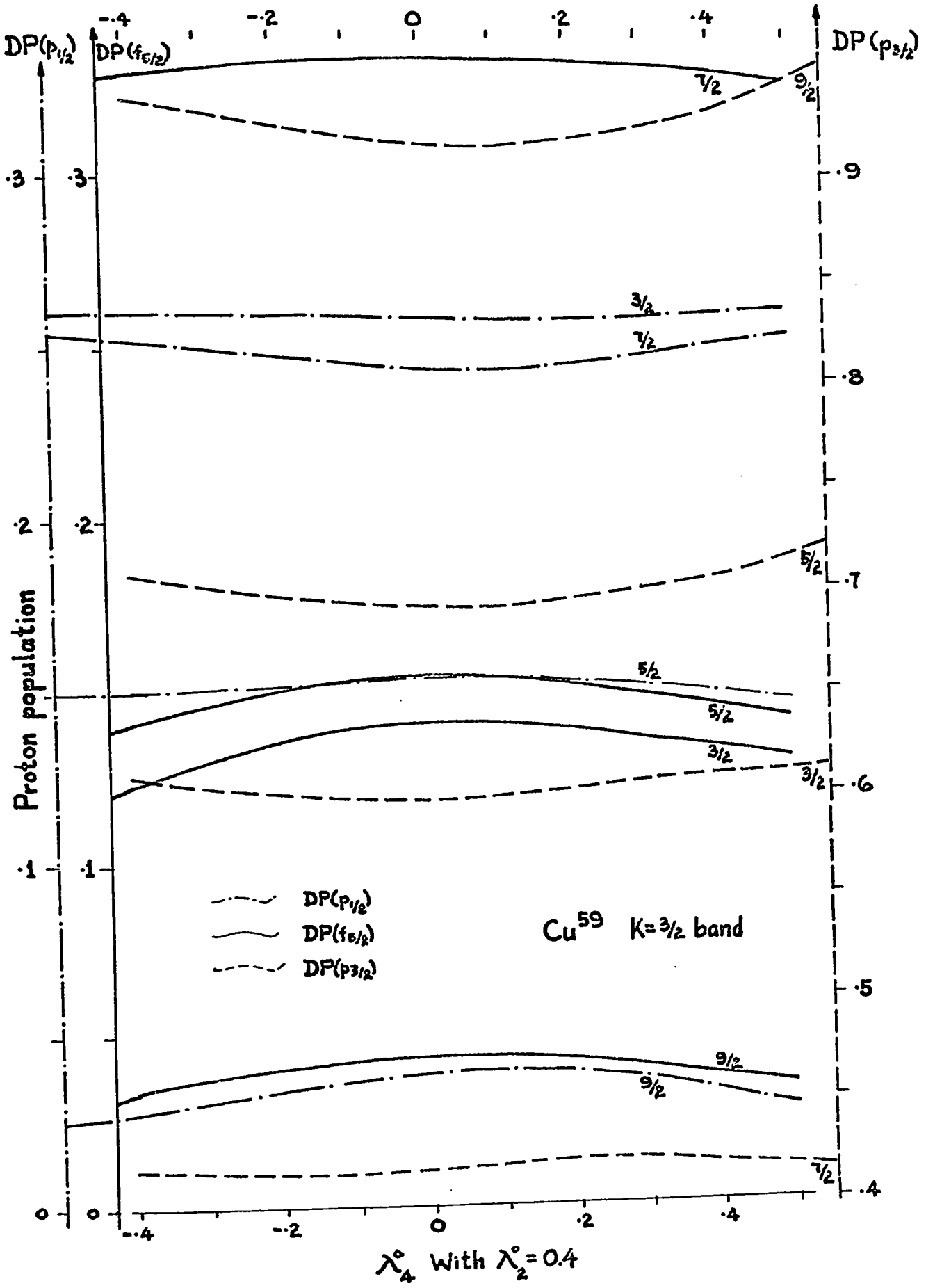
DP(p1/2)
DP(f5/2)
DP(p3/2)
Proton population
λ°4 With λ°2 = 0.4
DP(p1/2)
DP(f5/2)
DP(p3/2)
Cu59 K=3/2 band
7/2
9/2
3/2
7/2
5/2
5/2
5/2
3/2
3/2
9/2
9/2
7/2

Fig. VI.6

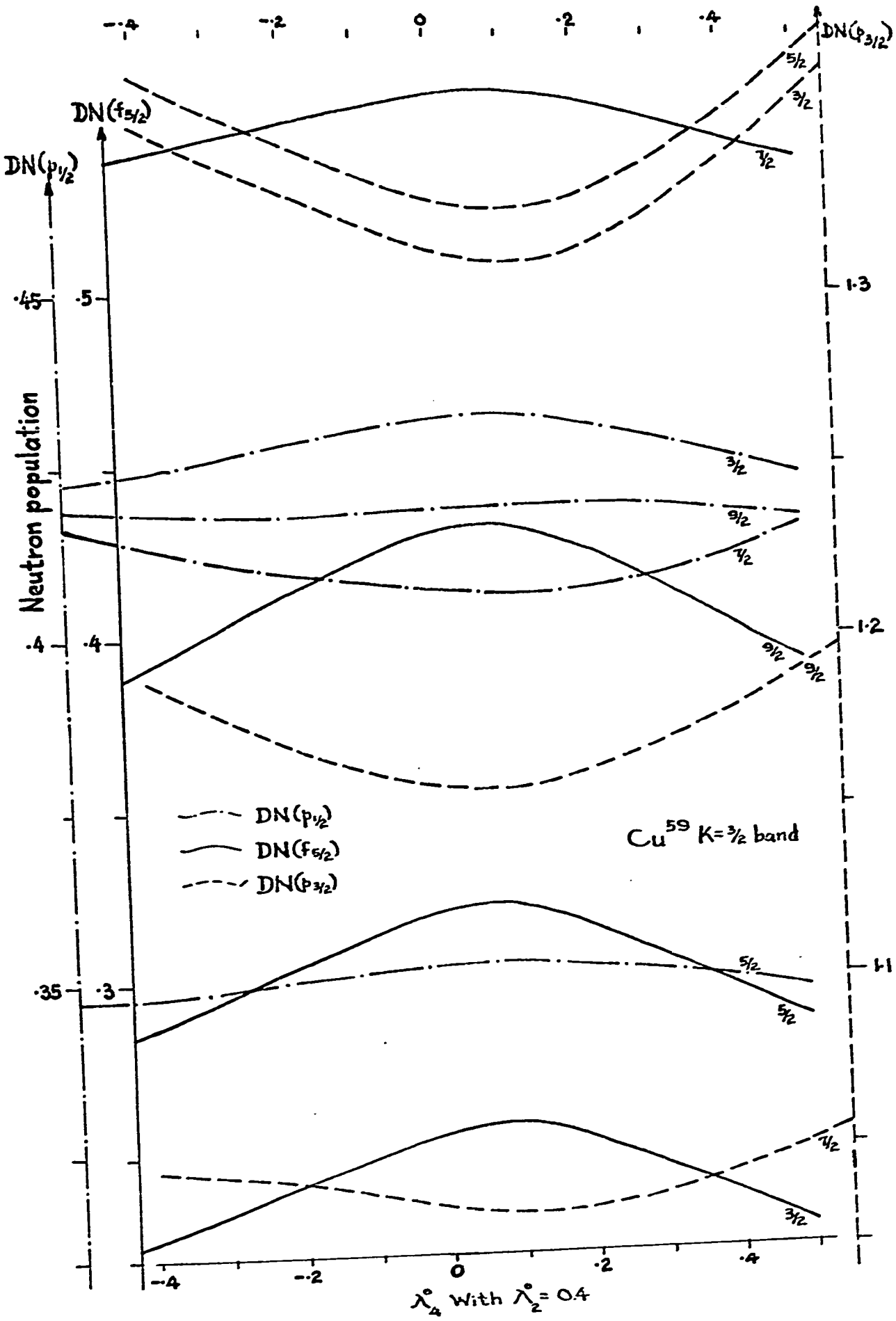
DN(p3/2)
DN(f5/2)
DN(p1/2)
Neutron population
Cu59 K=3/2 band
DN(p1/2)
DN(f5/2)
DN(p3/2)
λ4 With λ2 = 0.4

Fig. VI.7

CHAPTER VII DISCUSSION AND CONCLUSIONS

From the first part of the study conducted, it is evident that the intermediate coupling approach in the Unified Model gives a very valid description of the low-energy properties of the odd-mass Copper isotopes. The energies, spins and parities of the low-lying levels are in excellent agreement with the experimental results. The classical and extended intermediate coupling models both produce levels in better agreement to the observed levels than other recent theoretical investigations.

In the classical intermediate coupling approach, two sets of parameters were used; one set extracted from experimental data of the neighbouring even nuclei and one set adjusted to give the best fit. In the extended model, only the unvaried set using experimentally extracted values was used. It was found that the classical model with best fitting parameters usually gave best agreement with experiments, even though the spectra obtained were usually quite close to those from the extended model with experimental parameters. In all cases, the classical model with experimental parameters gave inferior results as compared to those calculated in the other two approaches. So using the same set of parametric values, the extended version is superior to the classical approach. One suggestion for further investigation can be made here and that is to adjust the parameters of

the extended model until a best fit is obtained. Then the best-fitting levels of the extended model can be compared on equal basis with those of the classical model. Then perhaps it can be proved that the extended version is definitely superior to the classical model in this mass region, of A = 59 to 65.

Of all four isotopes, the Cu^{65} shows best agreement with experiment in both approaches. There are a few discrepancies noted between theory and experiment. For example, the 1.964 MeV level of Cu^{59} was reported to have a spin of 5/2 whereas the theoretical value obtained in the extended approach was 3/2. In the case of Cu^{61}, experimental observations show a level at 1.7326 MeV with a spin of 7/2. This level was assigned to have a spin of 3/2 in the classical model and 5/2 in the extended version. In Cu^{63}, experiments show a 3/2 level at 1.547 MeV, but there is not corresponding level in the extended model. Except for these few discrepancies, the agreement between theory and experiment is excellent.

The reduced electromagnetic transition rates for electric quadrupole and magnetic dipole radiation were calculated using energy eigenfunctions obtained by diagonalization of the total nuclear Hamiltonian. The agreement here with experiment is not spectacular, but quite good, particularly considering the fact that these results are strongly dependent on the amount of mixing and the values chosen for the parameters.

In these calculations, an effective charge and an effective

spin gyromagnetic ratio were assigned to the last odd nucleon to account for polarization in a phenomenological way as has been done by others. It was found that the general trend in the reduced transition rates was that the classical model with best-fitting parameters and with the effective charge as well as effective gyromagnetic ratio gave the best agreement with experiment. This seems to indicate that core polarization effects cannot be ignored in these nuclei. In most transitions, the anharmonic core and quasiparticle model (extended model) gave better B(E2) and B(M1) values than the classical model with the unvaried experimental parameters. Thus the same conclusion concerning energy levels can be drawn here.

The reduced electromagnetic transition rates are calculated in this investigation for $e_{p_{eff}} = e_p$ and $0.5\ e_p$ with $g_{s_{eff}} = g_s$ and $0.5\ g_s$ These values are chosen because they are most commonly used in theoretical studies. Some authors use other values, for example, B. Castel found that the effective g-factor $g_{s_{eff}} = 0.6\ g_s$ gave the best fit to the observed magnetic moment of ground state. It is therefore very possible to improve our B(M1) and B(E2) values by choosing different values of $e_{p_{eff}}$ and $g_{s_{eff}}$. The proper procedure would be to vary these values so that effects on the reduced transition rates due to their adjustments can be studied. The values to be adopted will be those which can give a best fit to the observed electric and magnetic moments of the ground state.

Finally, spectroscopic factors were calculated. The difficulty in comparison with experiments here is the wide range of the experimentally determined and other theoretically investigated values. In most cases, the spectroscopic factors calculated are too low. The extended model gave S(I) values in closer agreement to the averaged values of the references than the classical model. But of course, the validity of using the same equation for calculating spectroscopic factors in both models is not completely established. An explanation was offered for the discrepancy between theory and experiment here in Chapter IV.

In the calculation of the energy eigenvalues and the expansion coefficients of the basis states of the nuclear wave functions, only collective states involving up to three phonons have been included. The validity of this assumption can be tested by examining the amplitude of the basis states corresponding to the highest phonon states considered. The sum of the squares of the amplitudes for these states should be very small compared to unity. It was found that this condition was satisfied for the classical intermediate coupling model so that this approximation is valid. This is not exactly true for the anharmonic core and quasiparticle model. Certain states are 100 percent pure in that the one expansion coefficient in each of these states can be unity with all the other expansion coefficients in the same state being zero. For example, the ground state of all four isotopes have 100 percent of $p_{3/2}$ admixtures. Perhaps in the extended

model, it is not sufficient to consider collective states involving up to three phonons and the N = 3 states should also be included. The approximation which is valid in the classical model seems to break down in the extended model. It is also worth noting that the mixing of states has little effect on the energy spectra, but that the electromagnetic transition rates are extremely sensitive to mixing. This then explains why the B(M1) values for all transitions from the first three excited states to the ground states are zero in the extended model. The spectroscopic factors of the ground state ($I=3/2^-$) are also zero.

Since the low-lying levels show good agreement with experiments in the present study, the theoretically predicted higher levels should be good estimates of the experimental results. But more experimental data are required before any further conclusions are drawn. This is especially true for the electromagnetic transition rates where not much experimental information is available.

In the second part of this investigation, the Projected Hartree-Fock model was applied to Cu^{59} and Cu^{61}. Energies and spins were calculated and compared to experiments. The agreement here is not good with all the theoretical levels being too low. It was concluded that the wave functions used in this calculation were not entirely correct and a closer examination should reveal where the inaccuracy lied. It is still evident that the Hartree-Fock model does not give as good agreement between the calculated energy levels and the experimental levels as the intermediate coupling model does

in this mass region. A more detailed study is required since a rather inconclusive stage is reached here. Perhaps this can serve as a basis for further investigations.

In conclusion, it is believed that the present analysis aids in understanding the features of the experimental results of the properties of low-lying levels in the odd-mass Copper isotopes. It is hoped that it can help in stimulating new experiments.

APPENDIX A

VALUES OF THE REDUCED MATRIX ELEMENTS OF THE SPIN TWO BOSON CREATION OPERATORS .

N = 1:

$$\langle 1R' \| b^* \| 0R \rangle = \begin{cases} I & \text{if } R = 0 \text{ and } R' = 2 \\ 0 & \text{otherwise} \end{cases}$$

N = 2:

$$\langle 2R' \| b^* \| 1R \rangle = \begin{cases} \sqrt{2} & \text{if } R = 2 \text{ and } R' = 0, 2, \text{ or } 4 \\ 0 & \text{otherwise} \end{cases}$$

N = 3: The reduced matrix elements are zero unless R = 0, 2, or 4 and R' = 0, 2, 3, 4, or 6. The values of the reduced matrix elements for the allowed values of R and R' are listed in the table show below.

$$\langle 3R' \| b^* \| 2R \rangle =$$

R \ R'	0	2	3	4	6
0	0	$\sqrt{7/15}$	0	0	0
2	$\sqrt{3}$	$\sqrt{4/7}$	$\sqrt{15/7}$	$\sqrt{11/7}$	0
4	0	$\sqrt{36/35}$	$-\sqrt{6/7}$	$\sqrt{10/7}$	$\sqrt{3}$

APPENDIX B

MATRIX ELEMENTS OF TENSOR OPERATOR T^k_g.

Using the strong coupling wave functions given by Eq. (IV.52), i.e.,

$$|\psi^J_k> = \sqrt{\frac{2J+1}{16\pi^2}} \{ D^J_{Mk}(\Omega)|\phi_k> + (-)^{J+k} D^{J*}_{M-k}(\Omega)|\phi_{-k}>\} ,$$

the matrix elements of a tensor operator are given by:

$$<\psi^{J_1}_{M_1 k_1}| T^k_g|\psi^{J_2}_{M_2 k_2}> = \sqrt{\frac{2J_2+1}{2J_1+1}} \begin{bmatrix} J_2 & k & J_1 \\ M_2 & g & M_1 \end{bmatrix}$$

$$\times \sum_\nu \{ \begin{bmatrix} J_2 & \nu & J_1 \\ k_2 & \nu & k_2 \end{bmatrix} <\phi_{k_1}| T^k_\nu|\phi_{k_2}> + (-)^{J_1+k_2} \begin{bmatrix} J_2 & \kappa & J_1 \\ k_2 & \nu & -k_1 \end{bmatrix}$$

$$\times <\phi_{-k_1}|T^k_\nu|\phi_{k_2}>\} \qquad \text{(A-1)}$$

The above matrix elements imply the well-known k selection rule.

$$|k_1 - k_2| \leq k \qquad \text{(A-2)}$$

in addition to the selection rules given by the Clebsch-Gordan coefficient.

Using the projected wave functions given by eq. (IV.54), i.e.

$$|\psi^{J}_{Mk}> = \frac{2J+1}{8\pi^2 N^{\frac{1}{2}}_{Jk}} \int d\Omega D^{J*}_{Mk}(\Omega) R(\Omega) |\phi_k>$$

the matrix element of an operator T^k_g is given by:

$$<\psi^{J_1}_{M_1k_1}|T^k_g|\psi^{J_2}_{M_2k_2}> = \frac{(2J_1+1)(2J_2+1)}{(8\pi^2)^2 N^{\frac{1}{2}}_{J_1k_1} N^{\frac{1}{2}}_{J_2k_2}}$$

$$\times \int d\Omega_1 d\Omega_2 D^{J_1}_{M_1k_1}(\Omega_1) D^{J_2^*}_{M_2k_2}(\Omega_2) \quad x \quad <\phi_{k_1}|R^{-1}(\Omega_1) T^k_g R(\Omega_2)|\phi_{k_2}> \qquad \text{(A-3)}$$

Eq. (A-3) is reduced to a single integral by using the commutation rule between the tensor operator T^k_g and the rotation operator $R(\Omega_2)$, i.e.

$$T^k_g R(\Omega_2) = \sum_\nu D^{k*}_{g\nu}(\Omega_2) R(\Omega_2) T^k \qquad \text{(A-4)}$$

Since rotations form a group, the rotation $R(\Omega_1)$ may be written as

$$R(\Omega_1) = R(\Omega_2) R^{-1}(\Omega_3) \qquad \text{(A-5)}$$

Taking the matrix element of eq. (A-5), between states $|J_1 M_1\rangle$ and $|J_1 k_1\rangle$, we get

$$D^{J_1}_{M_1 k_1}(\Omega_1) = \sum_{\mu} D^{J_1}_{m_1 \mu}(\Omega_2) D^{J_1 *}_{k_1 \mu}(\Omega_3) \qquad \text{(A-6)}$$

Equations (A-4), (A-5) and (A-6) give the desired matrix element,

$$\langle \psi^{J_1}_{M_1 k_1} | T^k_g | \psi^{J_2}_{M_2 k_2} \rangle = \frac{2J_2 + 1}{8\pi^2 N^{\frac{1}{2}}_{J_1 k_1} N^{\frac{1}{2}}_{J_2 k_2}} \begin{bmatrix} J_2 & k & J_1 \\ M_2 & g & M_1 \end{bmatrix}$$

$$\sum_{\mu\nu} \begin{bmatrix} J_2 & k & J_1 \\ k_2 & \nu & \mu \end{bmatrix} \times \int d\Omega D^{*J_1}_{k_1 \mu}(\Omega) \langle \phi_{k_1} | R(\Omega) T^k_{\nu} | \phi_{k_2} \rangle$$

(A-7)

This becomes eq. (IV.60) in Chapter IV.

BIBLIOGRAPHY

1. D. C. Chaudhury, Mat. Fys. Medd. Dan. Vid. Selsk. 28, No. 4 (1954).
2. A. Bohr, Mat. Fys. Medd. Dan, Vid. Selsk. 26, No. 14 (1952).
3. A. Bohr and B. R. Mottelson, Mat. Fys. Medd. Dan. Vid. Selsk. 27 No. 16 (1953).
4. A. Bohr and B. R. Mottelson, Beta and Gamma Ray Spectroscopy, Ed. by K. Siegbahn, North-Holland Publ. Co., Amsterdam (1955), pp. 468-493.
5. N. Bohr, Nature 137, (1936) 344, 351.
6. N. Bohr and F. Kalckar, Mat. Fys. Medd. Dan. Vid. Selsk. 14, No. 10 (1937).
7. J. Frenkel, J. Phys. (U.S.S.R.) 1, 125 (1939).
8. J. Frenkel, Phys. REv. 55, 987 (1939).
9. J. M. Blatt and V. F. Weisskopf, Theoretical Nuclear Physics (J. Wiley & Sons, New York) (1952).
10. M. G. Mayer, Phys. Rev. 75, 1969 (1949).
11. O. Haxel, J. H. D. Jensen, and H. E. Suess, Phys. Rev. 75, 1766 (1949).
12. G. Z. Gamow, Physik, 89, 592 (1934).
13. W. J. Elsasser, J. Phys. Rad. 5, 635 (1934).
14. R. R. Roy and B. P. Nigam, Nuclear Physics: Theory and Experiment (John Wiley & Sons) (1967) pp. 227.

15. R. D. Woods and D. S. Saxon, Phys. Rev. 95, 577 (1954).

16. O. Haxel, J. H. D. Jensen and H. E. Suees, Z. Physik 128, 295 (1950).

17. M. G. Mayer, Phys. Rev. 78, 16 (1950).

18. K. A. Brueckner, C. A. Levinson and H. M. Mahmoud, Phys. Rev. 95, 217 (1954).

19. L. C. Gomes, J. D. Walecka and V. F. Weisskopf, Ann. Phys. (N.Y.) 3, 241 (1958).

20. S. G. Nilsson, Dan. Mat. Fys. Medd. 29, No. 16 (1955).

21. B. R. Mottelson and S. G. Nilsson, Mat. Fys. Medd. Dan. Vid. Selsk. 1, No. 8 (1959).

22. M. Goldhaber and A. W. Sunyar, Phys. Rev. 83, 906 (1951).

23. H. B. G. Casimir, On the Interaction between Atomic Nuclei and Electrons, Teyler's Tweede Genootschap, Haarlem (I;V) (1936).

24. J. Rainwater, Phys. Rev. 79, 432 (1950).

25. I. Tamm, J. Phys. (U.S.R.) 9, 449 (1945); and S. M. Dancoff, Phys. Rev. 78, 382 (1950).

26. V. K. Thankappan and S. P. Pandya, Nucl. Phys. 19 303 (1960); Nucl. Phys. 39 394 (1962).

27. D. C. Choudhury and T. F. O'Dwyer, Nucl. Phys. A93, 300 (1967).

28. F. G. Bailey and D. C. Choudhury, Bull. Am. Phys- Soc. 12 1034 (1967).

29. B. Castel, K. W. C. Stewart and M. Harvey, Can. J. Phys. 47, 1490 (1970).

30. L. N. Cooper, Phys. Rev. 104, 1189 (1956).

31. J. Bardeen, L. N. Cooper and J. R. Schrieffer, Phys. Rev. 108, 1175 (1957).

32. S. T. Belyaev, Mat. Fys. Medd. Dan. Vid. Selsk. 31, No. 11 (1959).

33. J. G. Valatin, Nuovo Cimento 7, 843 (1958).

34. B. Castel, K. W. C. Stewart and M. Harvey, Nucl. Phys. A162, 273 (1971).

35. G. Ripka, Advances in Nuclear Physics, edited by E. Vogt et al. Plenum Press, Inc., N.Y. (1968).

36. D. Rowe, Nuclear Collective Motion - Models and Theory, Methuen and Co. Ltd., (1970).

37. G. Brown, Unified Theory of Nuclear Models, North-Holland Publ. Co., Amsterdam, (1964).

38. C. S. Warke and M. R. Gunye, Phys. Rev. 155, No. 4 (1966).

39. M. R. Gunye and C. S. Warke, Phys. Rev. 156, 1087 (1967).

40. R. Muthukrishnan and M. Baranger, Phys. Lett. 18, 160 (1965), K. Davies, S. Krieger and M. Baranger, Nucl. Phys. 84, 545 (1966), A. Kerman, J. Svenne and F. Villars, Phys. Rev. 147, 716 (1966).

41. R. E. Peierls and J. Yoccoz, Proc. Phys. Soc. A70, 381 (1957).

42. M. Redlich, Phys. Rev. 110, 468 (1958).

43. D. Picman, Nuc-. Phys. 10, 313 (1959).

44. G. Ripka, Phys. Lett. 15, 980 (1965).

45. M. Baranger, 1962 Cargese Lectures in Theoretical Physics, W. A. Benjamin, N.Y. (1963).

46. F. Villars, Proc. Int. School of Phys. Enrico Fermi Course 23, Ed. by V. F. Weisskopf, Academic Press, N.Y. (1963).

47. J. Bar-Tow and I. Kelson, Phys. Rev. 138, B1035 (1966).

48. W. H. Bassichis, A. K. Kerman and J. P. Svenne, Phys. Rev. 160, 746 (1967).

49. M. Bouten and P. van Leuven, Physica 34, 461 (1967).

50. M. Bouten, P. van Leuven, H. Depuydt and L. Schotsmans, Nucl. Phys. A100, 90 (1967).

51. C. S. Warke and M. R. Gunye, Phys. Rev. 155, 1084 (1967).

52. M. R. Gunye and C. S. Warke, Phys. Rev. 159, No. 4, 885.

53. H. J. Kiplin, N. Meshkov and A. J. Glick, Nucl. Phys.

54. B. Castel and J. P. Svenne, Nucl. Phys. A127, 141 (1969).

55. B. Castel and J. C. Parikh, Phys. Rev. C vol. 1 No. 3, 990 (1966).

56. R. Dreizler, P. Federman, B. Giraud and E. Omnes, Nucl. Phys. A113, 145 (1968).

57. W. H. Bassichis, B. Giraud and G. Ripka, Phys. Rev. Lett. 15 90 (1965).

58. S. Das Gupta and M. Harvey, Nucl. Phys. A94, 602 (1967).

59. D. J. Rowe, Phys. Rev. 175, 1283 (1968).

60. E. N. Condon and G. H. Shortley, The Theory of Atomic Spectra, Cambridge University Press, Cambridge (1935).

61. L. Rosenfeld, from Nuclear Binding Energies. unpublished.

62. K. T. Hect, 'Collective Models' in Selected Topics in Nuclear Spectroscopy, edited by B. J. Verhaer, North-Holland Publ. Co., Amsterdam, (1964).

63. F. J. Milford, Phys. Rev. 93, 1297 (1954).

64. F. G. Bailey, Ph.D. Thesis, 'Theoretical Investigation of the Properties of the Odd A Nuclei', University Microfilms Ltd., (1969).

65. M. A. Preston, Physics of the Nucleus, Addison-Wesley Publ. Co., Reading, Mass. (1962).

66. A. de-Shalit and I. Talmi, Nuclear Shell Theory, Academic Press, New York (1963).

67. L. S. Kisslinger and R. A. Sorenson, Rev. Mod. Phys. 35, 853 (1963).

68. K. Heyde and P. J. Brussaard, Nucl. Phys. A104, 81 (1967).

69. S. A. Moszkowski, Phys. Rev. 89, 474 (1953).

70. N. N. Bogolyubov, J.E.T.P., U.S.S.R. 34, 58 & 73 (1958).

71. N. N. Bogolyubov, Nuovo Cimento 7, 794 (1958).

72. N. Macdonald and A. C. Douglas, unpublished.

73. K. Kumar, to be published

74. S. Yosida, Phys. Rev. 123, 2122 (1961).

75. D. L. Hill and J. A. Wheeler, Phys. Rev. 108, 311 (1957).

76. B. J. Verhaar, Nucl. Phys. 41, 53 (1963); 45, 129 (1963); 54, 641 (1964).

77. J. C. Parikh and D. J. Rowe, Phys. Rev. 175, 1293 (1968).

78. N. Ullah and D. J. Rowe, Univ. of Toronto Report, Phys. Rev. 188, 1640 (1969).

79. N. Auerbach, Phys. Rev. 163, 1203 (1967).

80. A. G. Blair and D. D. Armstrong, Phys. Lett. 16, 57 (1965).

81. K. W. C. Stewart, B. Castel and B. P. Singh, Phys. Rev. C vol. 4 No. 6, 2131 (1971).

82. R. P. Singh, R. Raj, M. L. Rustgi and H. W. Kung, Phys. Rev. C. vol. 2 No. 5, 1715 (1970).

83. Jose M. Gomez, Nucl. Phys. A173, 537 (1971).

84. D. Larner, Phys. Rev. C. vol. 2, No. 2, 522 (1970).

85. V. K. Thankappan and William W. True, Phys. Rev. vol. 137, no. 4B, 793 (1965).

86. S. S. M. Wong, Nucl. Phys. A159, 235 (1970).

87. D. C. Choudbury and J. N. Friedman, Phys. Rev. C. vol. 3, 1619 (1971).

88. M. L. Rustgi, J. G. Lucus and S. N. Mukherjea, Nucl. Phys. A117, 321 (1968).

CHAPTER VIII EXPERIMENTAL TECHNIQUE

I. Introduction

Since the odd-mass Cu isotopes have been the object of the present theoretical study, an attempt was made to conduct experiments on Cu^{59} in order to obtain some comparison with our theoretical calculations. Certain experimental data[1] e.g. partial widths, branching ratios, Q-values, has already been available at the time, so only extended work was conducted. Our intention was to study the angular distributions for the resonances levels. Unfortunately, this experimental study was interrupted. Data on the angular distributions for the 1.424 MeV and 1.844 MeV resonances was still accumulated and presented here.

In this chapter, an attempt was made to demonstrate the small amount of experimental technique and experience studied here. A comparison between the experimental and theoretical estimates of the angular distribution of the two resonances was also presented. Hopefully, this can be of some use to future experimental investigations.

II. Theoretical Background

Angular distribution measurements of gamma rays from nuclear reactions provide the main method of determining the spins and parities of nuclear states as well as a number of associated nuclear parameters. This is a consequence of the intimate connection which the concepts of spin and parity have with the rotation and reflection of the co-ordinate system. The general theory of these processes is based on the invariance properties of the system, making use of Fano's and Racah's works on statistical tensors (1959).

The simplest angular distribution is the angular distribution of an outgoing gamma radiation with respect to a bombarding beam. In a nuclear reaction, a proton capture in this case, a nuclear alignment is produced by means of particle absorption. The initial state is aligned but not polarized. Due to this alignment the probability of emission of a gamma ray is angularly dependent and the empirical dependence can be written as:

$$W(\theta) = \sum_{K} a_K Q_K P_K(\cos\theta) \qquad \text{(VIII.1)}$$

where $W(\theta)$ is the intensity of the reaction observed at the angle θ relative to the incident beam, a_K are dependent on quantities which characterize the nuclear transition and on quantities describing the alignment of the initial nuclear state.

The attenuation coefficients Q_K depend on the geometry of

the experimental set-up and on the gamma ray absorption coefficient for the detector. $P_\kappa(\cos\theta)$ are Legendre Polynomials. The summation $\sum_\kappa$ is over even values of κ if the initial state formed has definite parity. Neglecting terms for $\kappa > 4$, we have

$$W(\theta) = a_o + a_2Q_2P_2(\cos\theta) + a_4Q_4+_4(\cos\theta) \qquad \text{(VIII.2)}$$

The anisotropy of the gamma rays can be decreased by choosing an angle such that the generally predominant angular dependent term $a_2Q_2P_2(\cos\theta)$ vanishes. $P_2(\cos\theta)$ is zero for $\theta = 125^o$.

From the above expression, one can see that in order to obtain the relative strength of given gamma rays one should average the intensity of each peak over several angles. If gamma rays are observed at 125^o, the anisotropy is reduced and the relative strength of each gamma ray is given without the need to average out over several angles.

In this experiment, the second term $a_2Q_2P_2(\cos\theta)$ is assumed to dominate and the small anisotropy of the third term $a_4Q_4P_4(\cos\theta)$ is neglected.

III. Experimental Set-Up

1. Target Preparation and Target Chamber Set-Up

The target backing consisted of a copper disc 1/8 inch thick and 2¼ inches in diameter. To obtain a high yield and for low back-

ground conditions 1/1000 of an inch of gold was electroplated on the disc. A piece of gold foil was used for this purpose. This thickness should be sufficient to stop all protons up to 2 MeV in energy. Ni^{58} was in turn electroplated on to the central one inch diameter of the gold layer. Nickel oxide solution was used because this compound was available from the Atomic Energy Research Establishment, Harwell, England. The procedures for preparing the nickel oxide solution and for plating were described in detail by Butler and Gossett[1]. The isotopic abundance of Ni^{58} was 99.76% with 0.11% of Ni^{60} and 0.12% of Ni^{62}. Fig.(VIII.1) shows the position of the target on the target mount.

The target and target chamber set-up are shown in Fig. (VIII.2). To prevent the target from deteriorating due to over-heating, direct water cooling was used. Water tubes were connected to the target chamber. To eliminate target contamination due to oil vapours, ion pumps were used instead of diffusion pumps on the beam line. A cylindrical cold finger was used before the target chamber to condense any contaminating vapour so that condensation on the target could be reduced.

In this experiment, a suppressor bias voltage was set up between the target and the target chamber. The bias circuit is shown in Fig. (VIII.3).

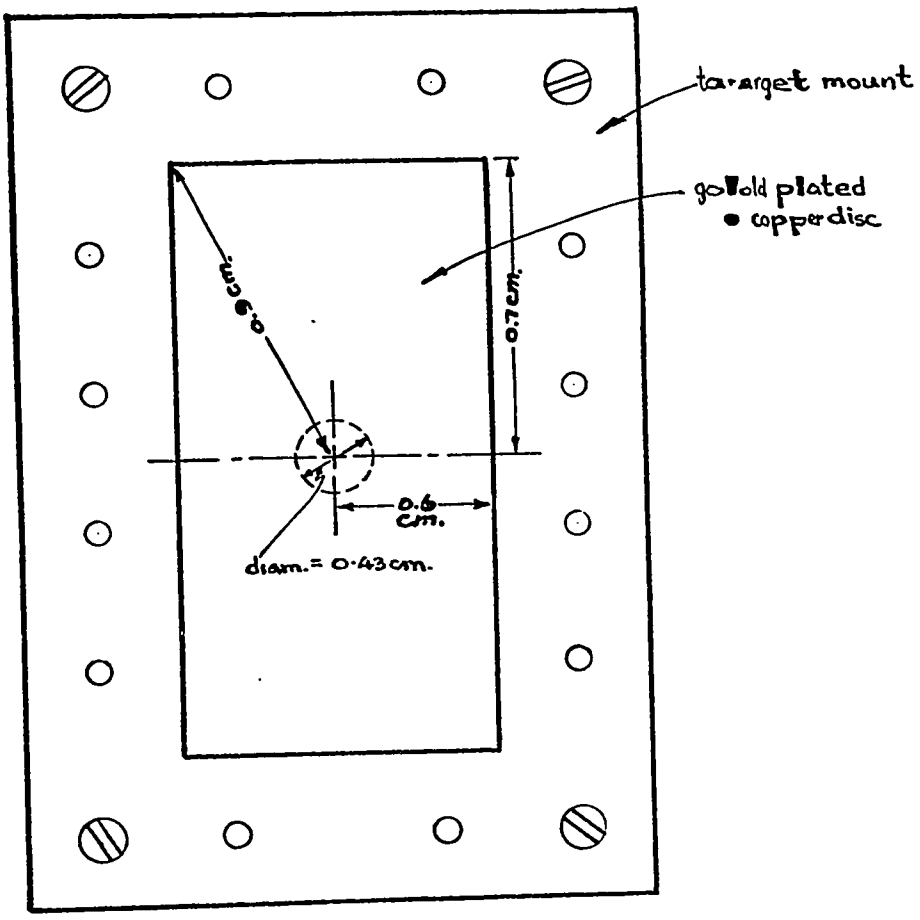

Position of target
on
target mount

Fig. VIII. 1

TARGET CHAMBER

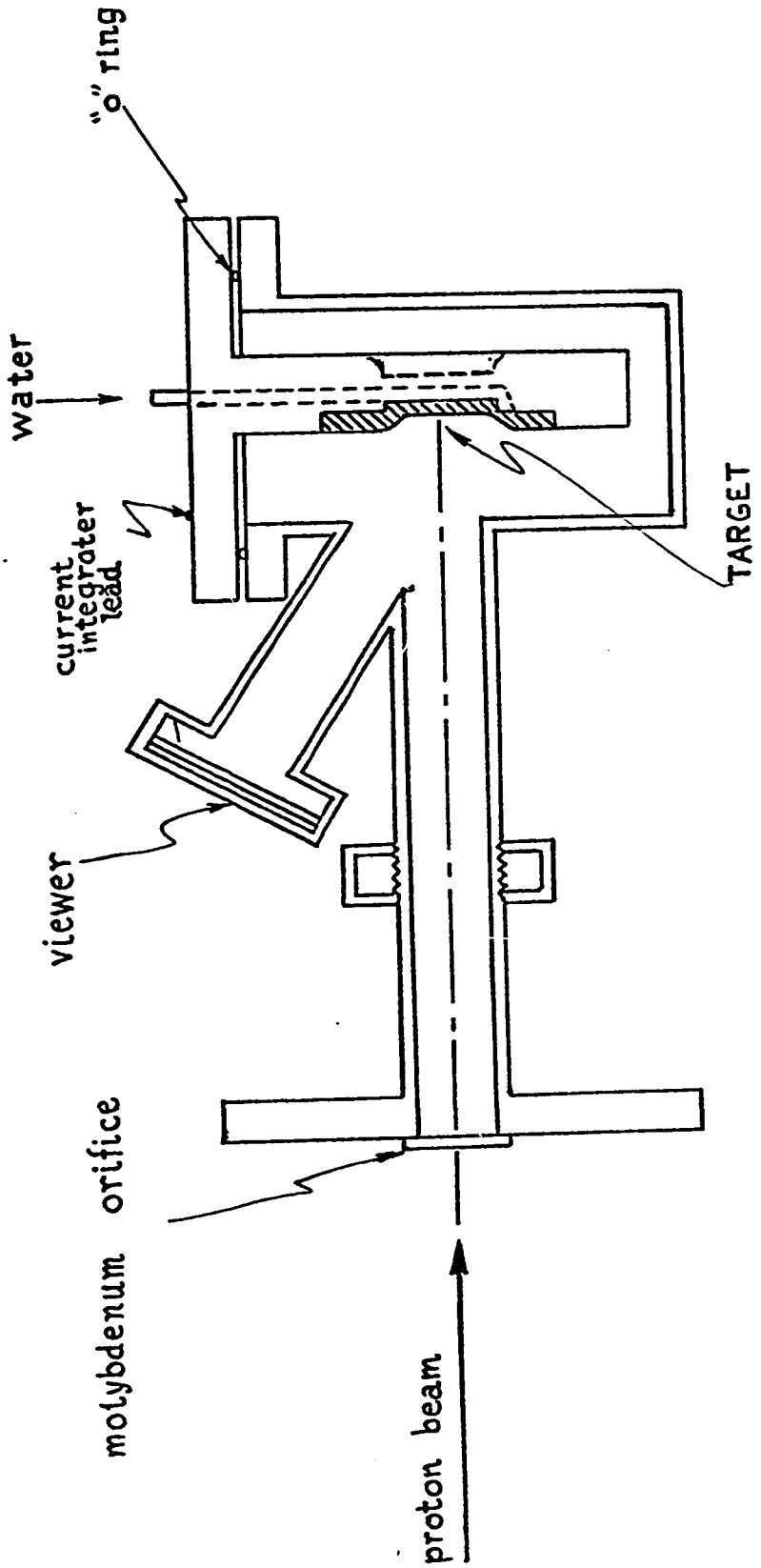

Fig. VIII.2

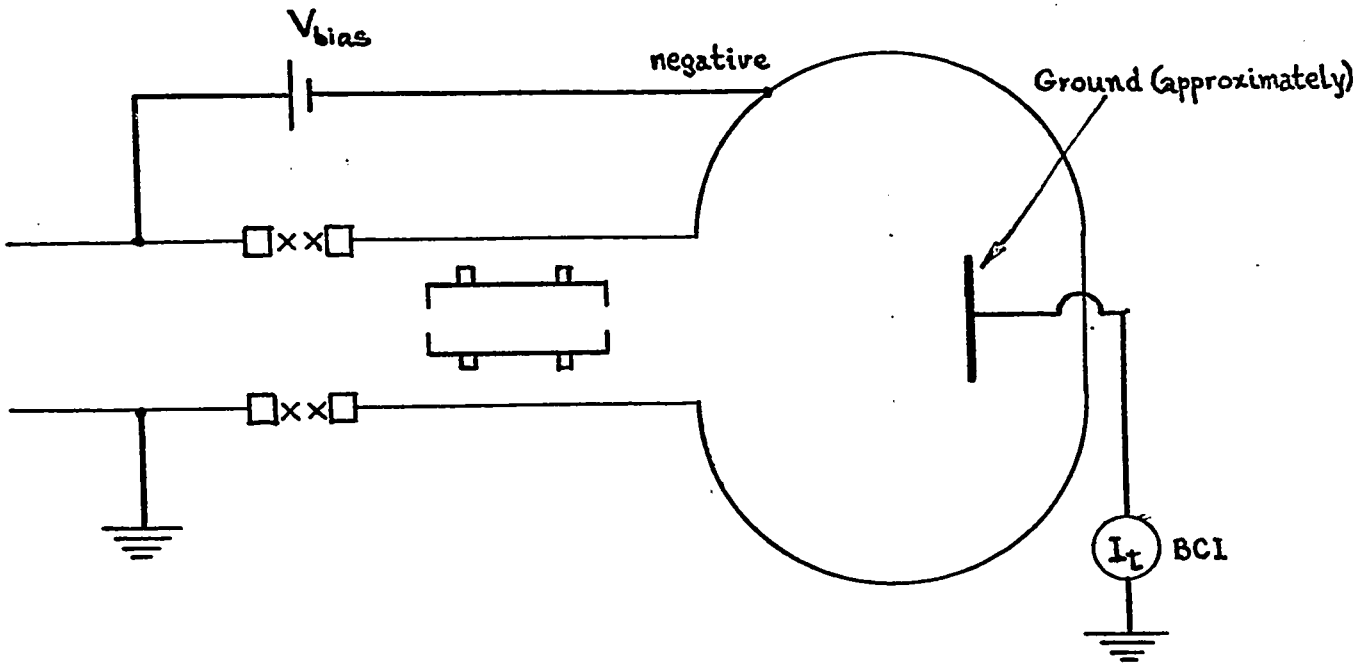

Fig. (VII.3) BIAS SET-UP

With a voltmeter and an ammeter, the target current was varied with the bias voltage. A plot of the target current against the bias voltage is shown in Fig. (VIII.4).

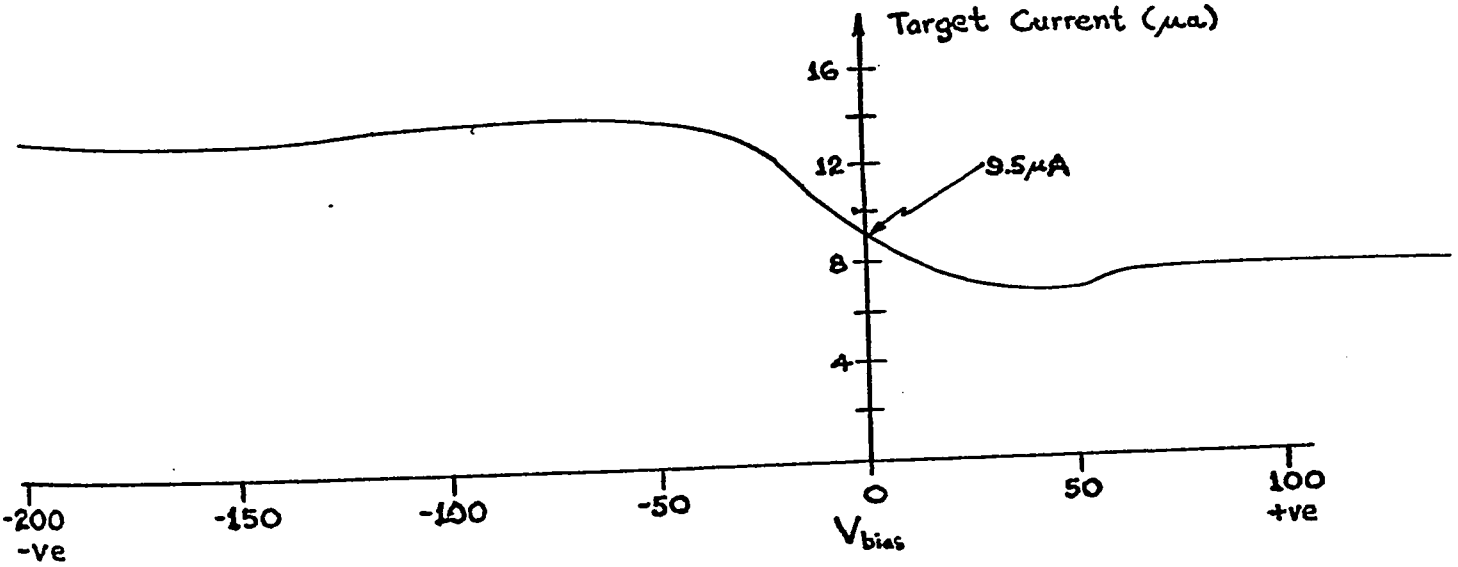

Fig. (VIII.4)

As one can see from Fig. (VIII.4), zero bias voltage occured at a target current of 9.5μA. At V_{bias} = 25 volts, the target current remained steady at 7.5μA.

The bias was set up so as to render the target chamber negative with respect to the target. The bias voltage was set at about 25 volts so that there would not be any fluctuations in target current, hence reducing the effect of secondary emission. The excitation curves of gamma rays were obtained using a 3" x 3" NaI(Tl) detector which was placed at approximately 90^{o} with respect to the direction of the proton beam and at a distance of about twelve inches from the target. In this experiment, a target thickness of about 12 keV for 1 MeV protons was found to be suitable. Background resonances can be identified by means of a table[2] of well known radiative capture reaction resonances for many different target isotopes. The main background arose from proton resonances for $(p,\alpha\gamma)$ reactions on F^{19} and N^{15} targets.

2. Detectors

Two gamma-ray detectors were used as counters in this angular distribution experiment. One was the NaI(Tl) detector which acted as a monitor counter. The other one was a Ge(Li) detector which could be rotated through any angle θ around the target chamber and was therefore the rotating counter.

The Ge(Li) detector was obtained from Ortec and was of the open-ended coaxial type with an active volume of 28.3 cm^3. An actual scale diagram is shown in Fig. (VIII.5). The applications and optimization of the Ge(Li) detector system was described in detail[3]. The optinum energy resolution was 2.6 keV for the Co^{60} 1333 keV gamma ray. The resolving power of the Ge(Li) detector was at least 10 to 20 times higher than that of the NaI(Tl) detector.

3. Gamma-Ray Detection System

The system consisted of the Ge(Li) detector and its associated electrons. The system is schematically represented in Fig. (VIII.6).

All the linear stages of the electronics, except the pre-amplifier which was thermally insulated by itself, were kept in a thermally insulated rack. The spectrum stabilizer was used to stabilize against any residual gain or zero level drifts in the electronic system. The temperature of the electronics was kept constant independent of fluctuations in room temperature. This system for precision gamma ray energy measurements was developed by Dr. A. L. Carter of Carleton University. A detailed description of the performance of this system can be found in Reference (1) and shall not be discussed here.

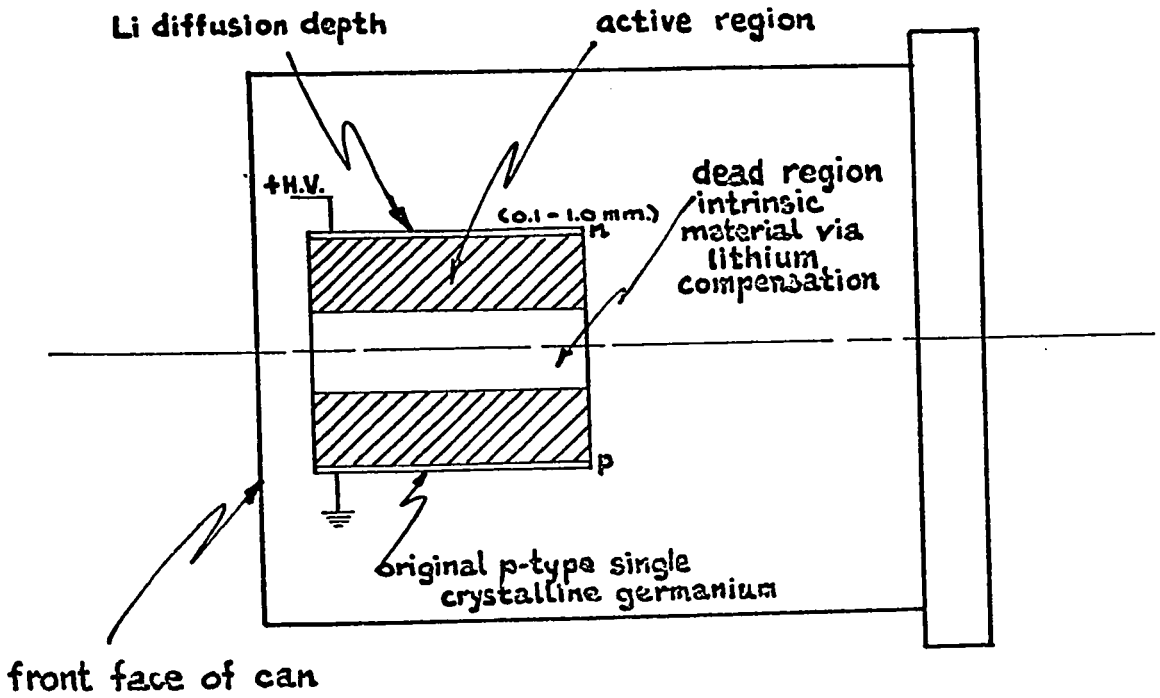

TO-SCALE DRAWING OF OPEN-ENDED COAXIAL Ge(Li) DETECTOR

Fig. VIII.5

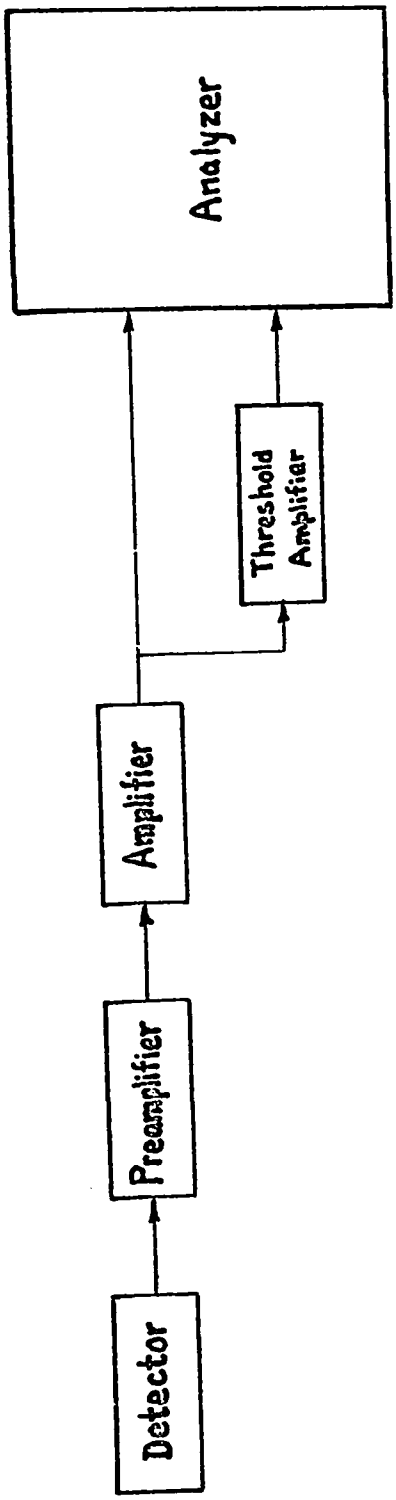

Block diagram of the Components in a typical Ge(Li) detector system

Fig. VIII.6

4. Symmetry of Geometry

The Ge(Li) detector was mounted on a turntable rotating about a vertical axis going through the centre of the beam spot on the target (see Fig. VIII.8). The distance between the target and the front face of the detector was chosen to be 7.0 cm by means of the plots of Q_2 and Q_4 values against energy[4]. Q_2 and Q_4 values are geometrical correction factors for angular correlation measurements with Ge(Li) detectors. These geometrical correction factors are constant for distances of 7.0 cm, 10.0 cm, or 14.0 cm and for the energy range desired.

The test of these Q_2 and Q_4 coefficients was made by carefully arranging the Co^{60} standardized source to have about the same size and position as the target used. The gamma rays should be isotropic from Co^{60} since there is no reference direction in space. Therefore any anisotropy measured would be due to the correction terms Q_2 and Q_4 alone. With the Co^{60} source, the Ge(Li) detector was rotated through angles of 90^{o}, -90^{o}, 45^{o} and -45^{o}. Counts at each angle was recorded for five minutes for two Co^{60} peaks. The results are shown in Table (VIII.1).

The counts are inversely proportional to the square of the distance between the target and the detector, i.e.

$$C \propto \frac{I}{r^2}$$

Table VIII.1 Counts at the rotating detector from Co^{60} source.

Angle	Counts in 5 mins	Random error	% Random error	Counts/min.
90^{o}	10610	± 10610 = ± 100.30	± 0.95%	2122
-90^{o}	9357	± 9357 = ± 96.73	± 1.03%	1871
45^{o}	11651	± 11651 = ± 107.93	± 0.93%	2330
-45^{o}	10465	± 10465 = ± 102.32	± 0.98%	2093

Table VIII.2 Cr^2 at different angles.

Angle	d in cm.	r in cm.	Cr^2 in counts cm^2/min	% deviation from mean value of Cr^2
90^{o}	2.515 ± .001	6.295 ± .011	84101	-6.86%
-90^{o}	2.924 ± .001	6.704 ± .011	84082	-6.88%
45^{o}	2.691 ± .001	6.471 ± .011	97566	+8.24%
-45^{o}	2.972 ± .001	6.752 ± .011	95432	±5.69%

mean = 90295

where C is the counting rate, I the intensity and r the distance between target and detector. It can be concluded that $Cr^2 \propto I$, or that Cr^2 should be a constant. The distance r was measured for each of the following angles, i.e. 90^o, -90^o, 45^0 and -45^o. The outside radius of the target chamber was measured to be 3.78 cm., so if d was the distance between the front face of the detector and the outer surface of the target chamber, the distance r became (d + 3.78) cm. The d values were recorded and shown in Table (VIII.2).

The C values in column four were taken from Table (VIII.1). It was suspected that the deviations in the values of Cr^2 were due to shifts in the distances r. On further examinations, it was discovered that the target was 2 mm. off the centre of the target chamber, thus causing a shift in r for each angle. This shift, Δr, was measured for each of four angles by drawing to scale an arc of radius r. Then, the shifted arc due to the 2 mm. deviation from the original centre was also drawn. The difference in these two arcs gave a measure of Δr. One example for the angle of 90^o is shown in Fig. (VIII.7).

Table (VIII.3) displays the measured shifts Δr for the corresponding distances r. Considering errors, we have :

$$\frac{\Delta I}{I} \sim \frac{\Delta C}{C} + \frac{2\Delta r}{r}$$

Doubling the entries in the last column of Table (VIII.3) we have ±6.36%, ±9.86%, ±6.18%, ±7.40% corresponding to 90^o, -90^o, 45^0 and -45^0,

Table VIII.3 Measured shifts Δr.

Angle	r in cm	Δr in cm	$\Delta r/r$ in %ages
90^{o}	6.295 ± .011	±0.20	±3.18%
-90^{o}	6.704 ± .011	±0.30	±4.48%
45^{o}	6.471 ± .011	±0.30	±3.09%
-45^{o}	6.752 ± .011	±0.25	±3.70%

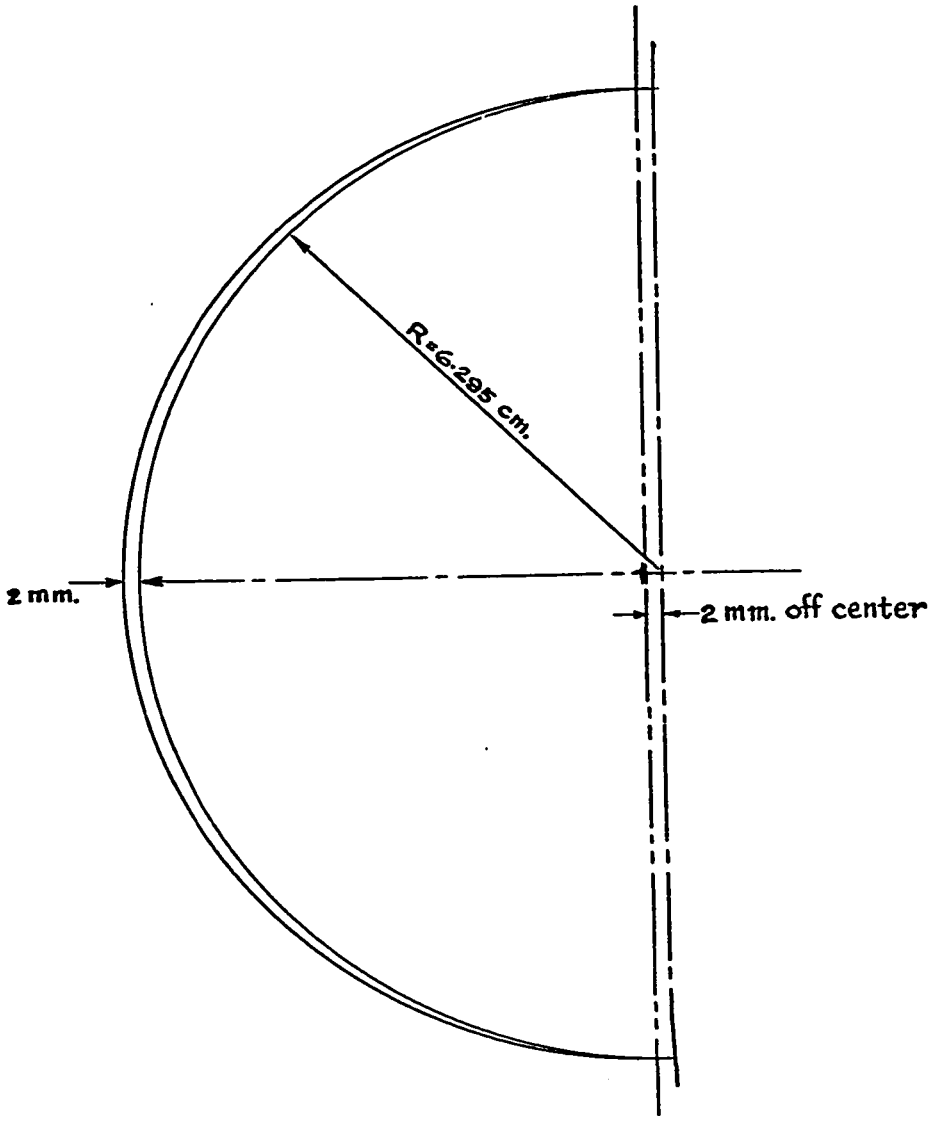

Fig. VIII.7

respectively. Adding the percentages of random errors in counting rates, i.e. ± 0.95%, ± 1.03%, ± 0.93 and ± 0.98% onto the above values, we obtain the following percentages:

± 7.31%, ± 9.99%, ± 7.11%, ± 8.38%.

Comparing these to the percentages due to deviations from the mean value of Cr^2 (last column in Table (VIII.2)), i.e.:

- 6.86%, - 6.88%, + 8.24%, + 5.69%.

We can see that the latter values are counted for by the former set, hence any deviations in geometric symmetry was caused by the target being 2 mm. off the centre of the target chamber. This was then taken into consideration for each counting rate measured.

5. Final Set-Up

The monitor, i.e., the NaI(Tl) detector, was mounted on a high stand, facing the target chamber at a fixed angle and at a fixed distance. It was connected to the multichannel analyzer. The rotating detector, i.e. Ge(Li) detector, was placed on the rotating table as shown in Fig. (VIII.8). The voltage pulses from this detector were uncoded by 4096 channel analog to digital converter. The spectrum was stored in the memory of an on-line PDP 9 computer. The stored

information could be punched out on paper tape, stored on magnetic tape, plotted out and displayed on the screen of an oscilloscope. A pulse height analysis program developed by Dr. A. L. Carter was used to analyze the spectra. Centroids, integrated counts and width at half maximum height of peaks could be determined by this program. The monitoring detector was connected to a teletype whereby voltage pulses, and hence exact counts could be recorded.

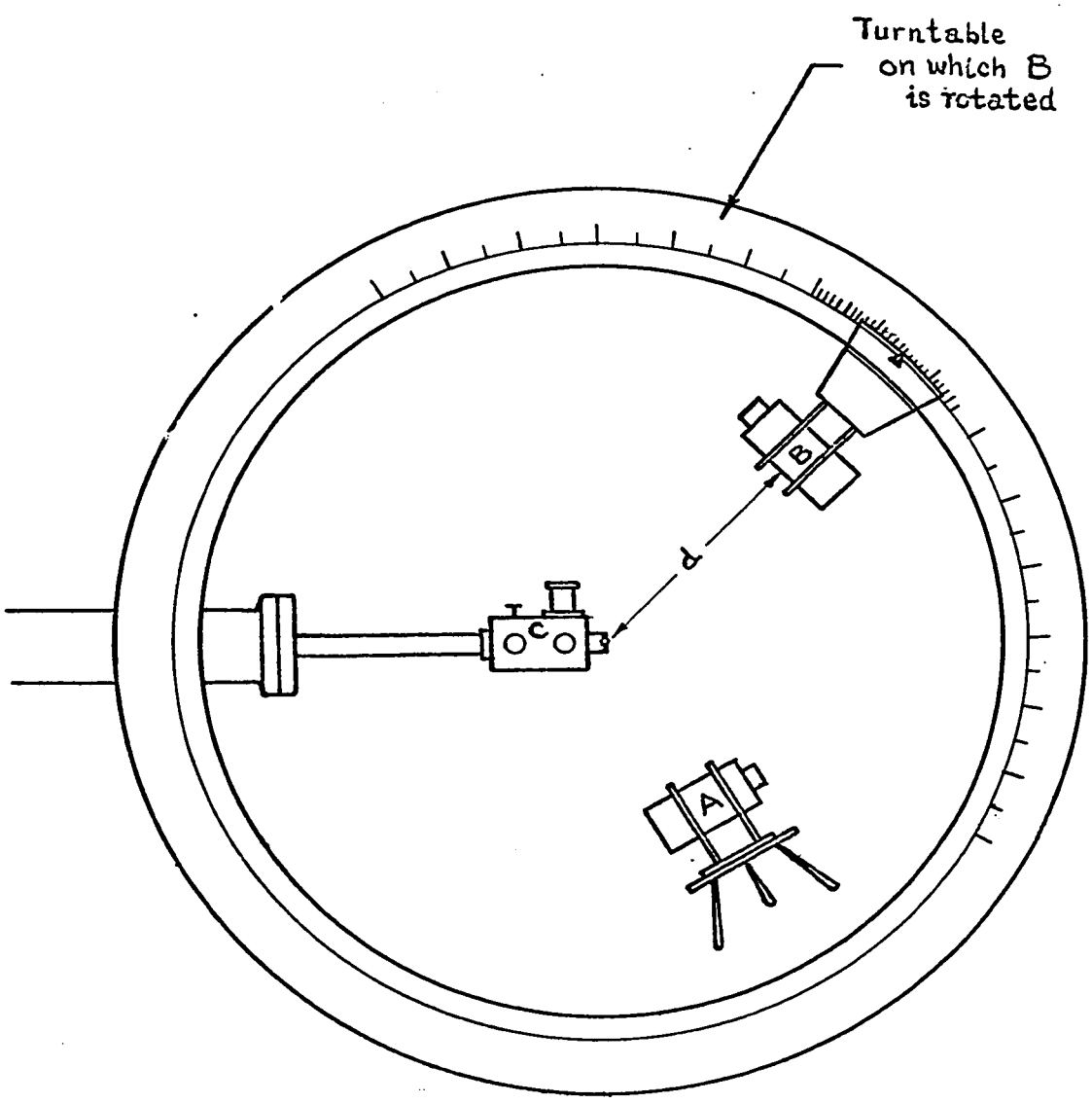

A – monitor detector

B – rotating detector

C – target chamber

Fig. VIII.8

6. Efficiency Calibration

The absolute efficiency is defined as:

$$\epsilon = \frac{\text{no. of gamma rays detected}}{\text{no. of disintegrations}}$$

It can be determined by means of a set of standardized gamma sources of known intensity. These sources can be obtained from the International Atomic Energy Agency and calibrated to within 1% typically. The sources were placed on the backing where the beam hits the target. The Ge(Li) detector was placed at an angle of 125^{o} with respect to the proton beam direction. The distance between the detector and the target should be 7 cm., thus using the same experimental arrangement for the $Ni^{58}(p, \gamma)Cu^{59}$ measurements. The efficiency was calibrated by Raymond Gauthier of Reference (1) and his results were used in this experiment. A few examples of the calibration sources for full energy peak efficiency were extracted and recorded in Table (VIII.4).

7. Gate Setting

The linear gate was first set for the rotating detector. The calibration sources Y^{88}, Th, and Co^{60} were used for this purpose. Each source was placed in the target chamber and the channel number corresponding to each E_{γ} was located by means of a pulser. These

readings are shown in Table (VIII.5). A straight line graph of channel number against energy E_γ is plotted as in Fig. (VIII.9) From this straight line graph, the following points are found, i.e.:

E_γ	Channel number
4320	347
3000	235
3500	280
4000	323
4500	368

so that for the range of E_γ from 3.0 to 3.5 MeV, the channel number range is 235 to 280, and for the range of 3.5 to 4.0 MeV the corresponding channel number of 280 to 368. The gate was set for the range of 3.5 to 4.5 MeV.

The gate for the monitor detector was set in a similar way. Table (VIII.6) gives the channel numbers for corresponding E_γ's. From the straight line graph of Fig. (VIII.10), the following points are found:

E_γ (keV)	Channel #
4320	292
4820	327

Table VIII.4 Full energy peak efficiency of calibration sources

Element	E_γ (keV)	ε
Co^{57}	122	$(7.13 \pm 0.53) \times 10^{-4}$
Y^{88}	898	$(8.00 \pm 0.50) \times 10^{-4}$
Co^{60}	1173	$(6.00 \pm 0.25) \times 10^{-4}$
Co^{60}	1333	$(4.81 \pm 0.10) \times 10^{-4}$
Y^{88}	1836	$(3.51 \pm 0.20) \times 10^{-4}$

Table VIII.5 Channel number corresponding to E_γ of Y^{88}, Co^{60} and Th - rotating detector.

Element	E_γ (keV)	Channel Number
Y^{88}	898	40
	1836	129
Co^{60}	1173	75
	1332	85
Th	2614	200

Table VIII.6 Channel number corresponding to E_γ of Y^{88}, Co^{60} and Th-rotating detector.

Element	E (keV)	Channel Number
Y^{88}	898	57
Co^{60}	1173	75
	1332	85
Th	2614	175

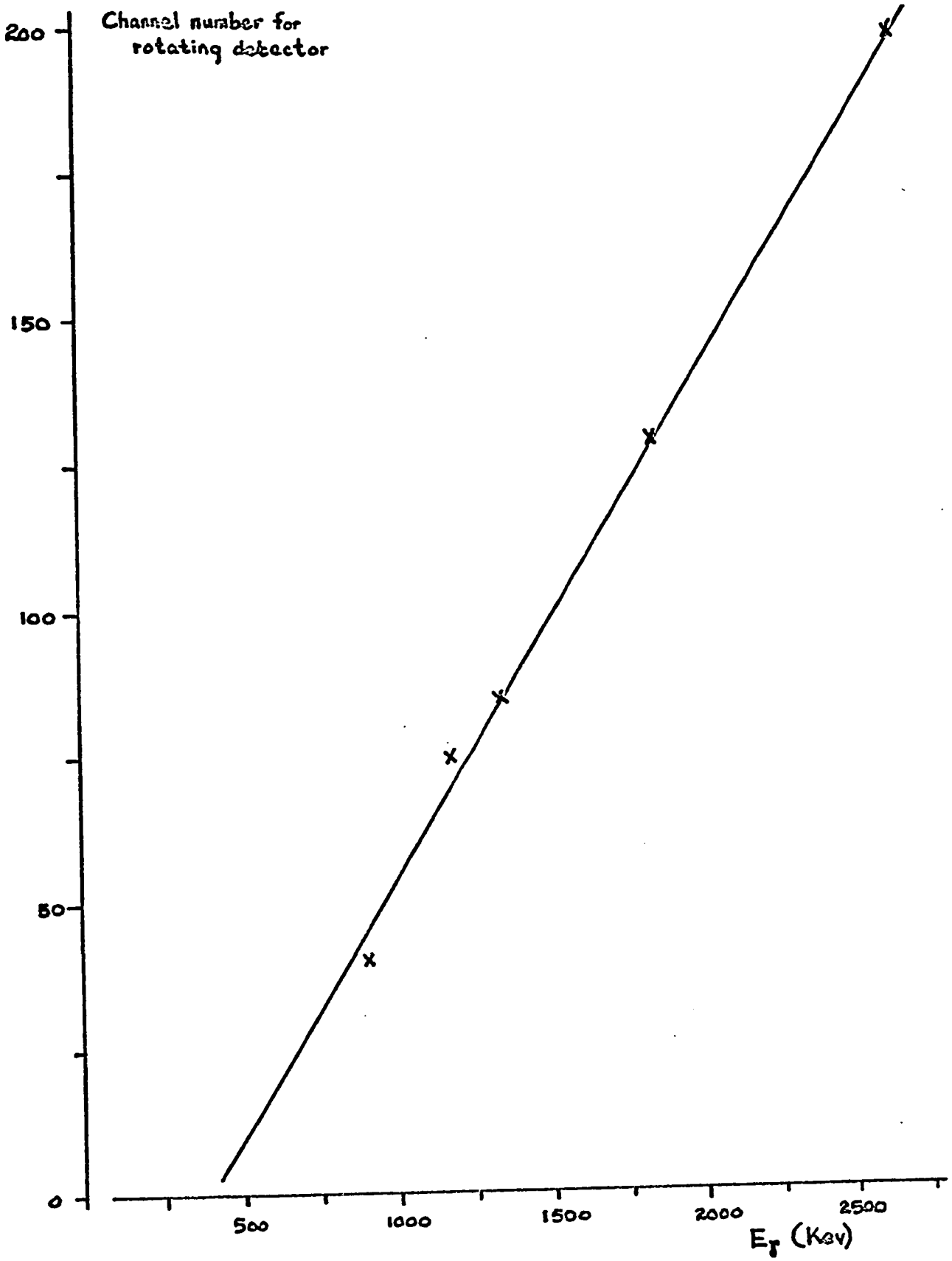
Channel number for
rotating detector
200
150
100
50
0
500
1000
1500
2000
2500
E_γ (Kev)

Fig. VIII.9

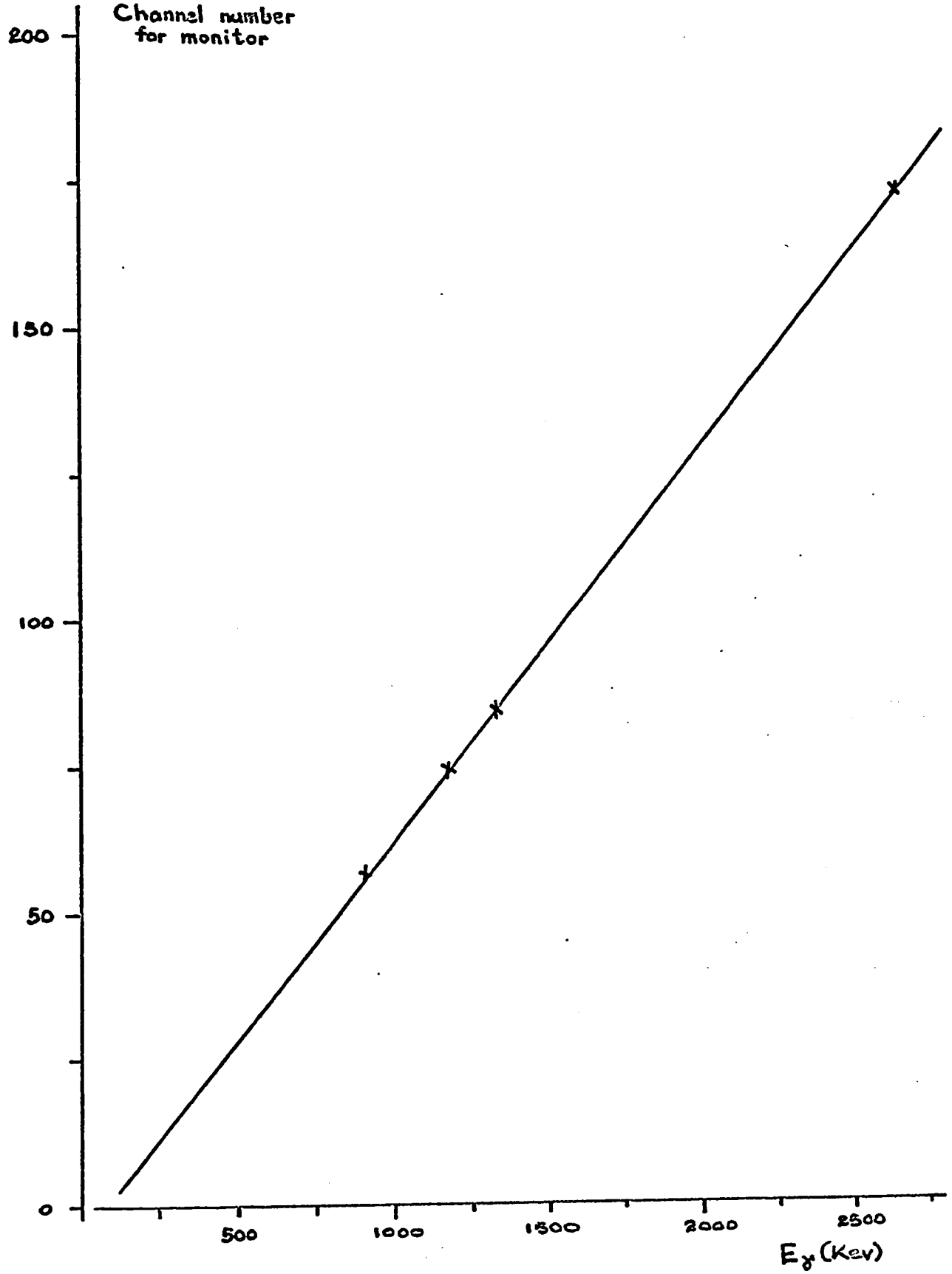
Channel number
for monitor
200
150
100
50
0
500
1000
1500
2000
2500
E_γ (Kev)

Fig. VIII.10

The energy range was set at 4.3 MeV with the corresponding channel range of 292. The gate was set using the bias amplifier instead of a single-channel analyzer so that background and actual peaks could be distinguished.

The experimental set-up was not completed and data accumulation was started at this stage.

IV. Experimental Results and Analysis

1. Data Accumulation

For the 1424 resonance, the rotating detector was positioned at $= 0^{o}$, 15^{o}, 30^{o}, 60^{o}, 75^{o}, 90^{o}, 105^{o}, 125^{o} and -45^{o}. For each angle the following procedure was used. The resonance was first located, and the counts were accumulated with the peak remaining at this resonance point. The counts were generally accumulated for 2 hrs. on the average to obtain reasonable statistics. Then the integrated counts and centroids were recorded for the double escape peaks at 4320 keV and 4820 keV for both detectors. A beam current of 14.5 microamperes to 15.5 microamperes was maintained each time.

Similar procedure was repeated for the 1844 resonance. However, results for only three angle, 0^{o}, 60^{o} and 125^{o}, were recorded.

The angular distribution results for the 1424 and 1844

resonances are shown in Tables (VIII.7) and (VIII.8), respectively.

Fig. (VIII.11) shows plottings of data of the 1424 resonance obtained from the monitor counter. The area under each peak gives the counts for each angle. These monitor counts are recorded in Table (VIII.7). The two experimental distributions $W_1(\theta)$ and $W_2(\theta)$ have been normalised by using the 878 and 1303 keV γ-rays in the spectrum of the moving Ge(Li) detector as internal monitors of the number of capture reactions occurring. This can be done because these γ-rays occur in the nucleus ^{59}Ni formed following β^+ decay of the ground state of ^{59}Cu, and may therefore be taken to be emitted isotropically.

2. Analysis of Results

a. Theoretical Angular Distributions

Theoretically, the Legendre Polynomial, $P_2(\cos\theta)$ is given by:

$$P_2(\cos\theta) = \tfrac{1}{2}(3\cos^2\theta - 1)$$
$$= \tfrac{1}{4}(3\cos 2\theta - 1) \qquad \text{(VIII.3)}$$

Table (VIII.9) gives the calculated $P_2(\cos\theta)$ for each angle θ.

If the spin of the resonance state is $J_i = 3/2$ and if the transitions are <u>pure</u> without any admixtures, then the angular distributions for transitions to final states of J_f are given by:

J_f	$W(\theta)$
3/2	$1 + 0.40\ P_2(\cos\theta)$
1/2	$1 - 0.50\ P_2(\cos\theta)$
5/2	$1 - 0.10\ P_2(\cos\theta)$
7/2	$1 + 0.14\ P_2(\cos\theta)$

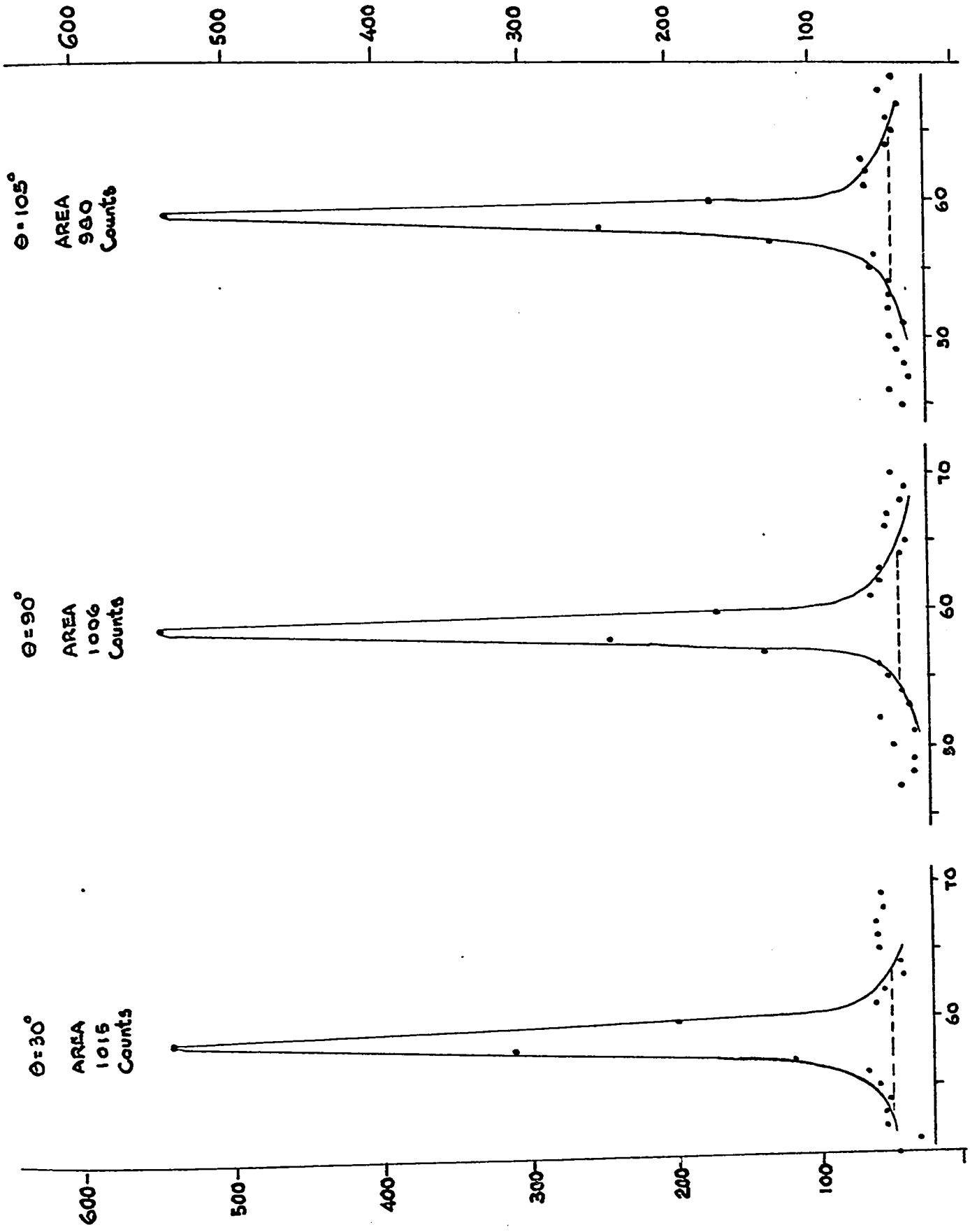
θ=30°
AREA
1015
Counts
θ=90°
AREA
1006
Counts
θ=105°
AREA
980
Counts
Monitor Counts Ep = 1424 Kev.

Fig. VIII.11

Table VIII.7 Experimental Angular Distributions of the 1424 Resonance

E_p = 1424 keV

	4320 DEP (PDP 9 and ORTEC Ge)	878 DEP (PDP 9 and ORTEC Ge)	1303 DEP (PDP 9 and ORTEC Ge)	A $\frac{4320}{878}$	B $\frac{4320}{1303}$	C $\frac{878}{1303}$	D 4320 DEP (Monitor)	E $\frac{4320}{4320}$ (Monitor)	F $\frac{878}{4320}$ (Monitor)	$W_1(\theta)$ $\frac{A(\theta)}{A(0)}$	$W_2(\theta)$ $\frac{B(\theta)}{B(0)}$	$W_3(\theta)$ $\frac{E(\theta)}{E(0)}$
0^o	1552	2005	1565	0.78	0.99	1.29	959	1.62	2.10	1.0	1.0	1.0
15^o	1511	1822	1524	0.83	0.99	1.20	986	1.54	1.85	1.07	1.0	0.95
30^o	1835	1522	1398	1.21	1.32	1.10	1015	1.8	1.50	1.55	1.33	1.12
60^o	2008	956	1128	2.10	1.78	0.85	771	2.60	1.24	2.69	1.78	1.61
70^o	1996	912	833	2.18	2.40	1.10	858	2.32	1.12	2.80	2.42	1.44
90^o	2834	1903	1525	1.49	1.86	1.25	1006	2.84	1.90	1.91	1.88	1.76
105^o	3199	2033	1590	1.58	2.05	1.28	980	3.27	2.09	2.02	2.07	2.02
125^o	3347	2242	1857	1.49	1.80	1.21	1047	3.20	2.12	1.91	1.82	1.98
-45^o	1946	1647	1459	1.18	1.33	1.13	876	2.22	1.88	1.51	1.34	1.37

Table VIII.8 Experimental Angular Distributions of the 1844 Resonance

E_p = 1844 keV.

θ	5233 DEP (PDP9 and Ortec GE)	878 DEP	1303 DEP	A $\frac{5233}{878}$	B $\frac{5233}{1303}$	C $\frac{878}{1303}$	D 5233 monitor	E $\frac{5233}{5233}$ monitor	$W_1(\theta)$ $\frac{A(\theta)}{A(0)}$	$W_2(\theta)$ $\frac{B(\theta)}{B(0)}$	$W_3(\theta)$ $\frac{E(\theta)}{B(0)}$
0^o	4168	1738	1366	2.40	3.05	1.27	1462	2.85	1.00	1.00	1.00
60^o	5223	1669	1369	3.13	3.82	1.22	2161	2.42	1.30	1.25	0.85
125^o	2344	857	701	2.74	3.34	1.23	1348	1.74	1.14	1.10	0.61

Table VIII.9 Calculated $P_2(\cos\theta)$

θ	0^o	15^o	30^o	45^o	60^o	75^o
$P_2(\cos\theta)$	+1.00	+0.90	+0.625	+0.250	-0.125	-0.40

90^o	105^o	125^o	-45^o
-0.5	-0.40	0	+0.250

The theoretically calculated angular distributions for each angle and each J_f are shown in Table (VIII.7)

b. Comparison between Theoretical and Experimental Angular Distributions.

The experimental angular distributions $W(\theta)$ normalized to $\theta = 0^o$ are plotted against cos θ in Fig. (VIII.12). The corresponding theoretical $W(\theta)$ curves are also plotted as a comparison in Fig. (VIII.12).

As shown in Fig. VIII.12, the experimental angular distributions show a minima at about $\theta = 90^o$. Their maxima are located at $\theta \simeq 105^o$ and $\theta \simeq 75^o$. The theoretical curve $J_f = 1/2$ gives a maximum at $\theta = 90^o$, while the other, $J_f = 3/2$ gives a minimum at this angle. The agreement with theory is not good here but we cannot be conclusive because the experiment itself was in a preliminary stage. The resulting inconsistency of the $W_1(\theta)$, $W_2(\theta)$ and $W_3(\theta)$ results is not completely understood.

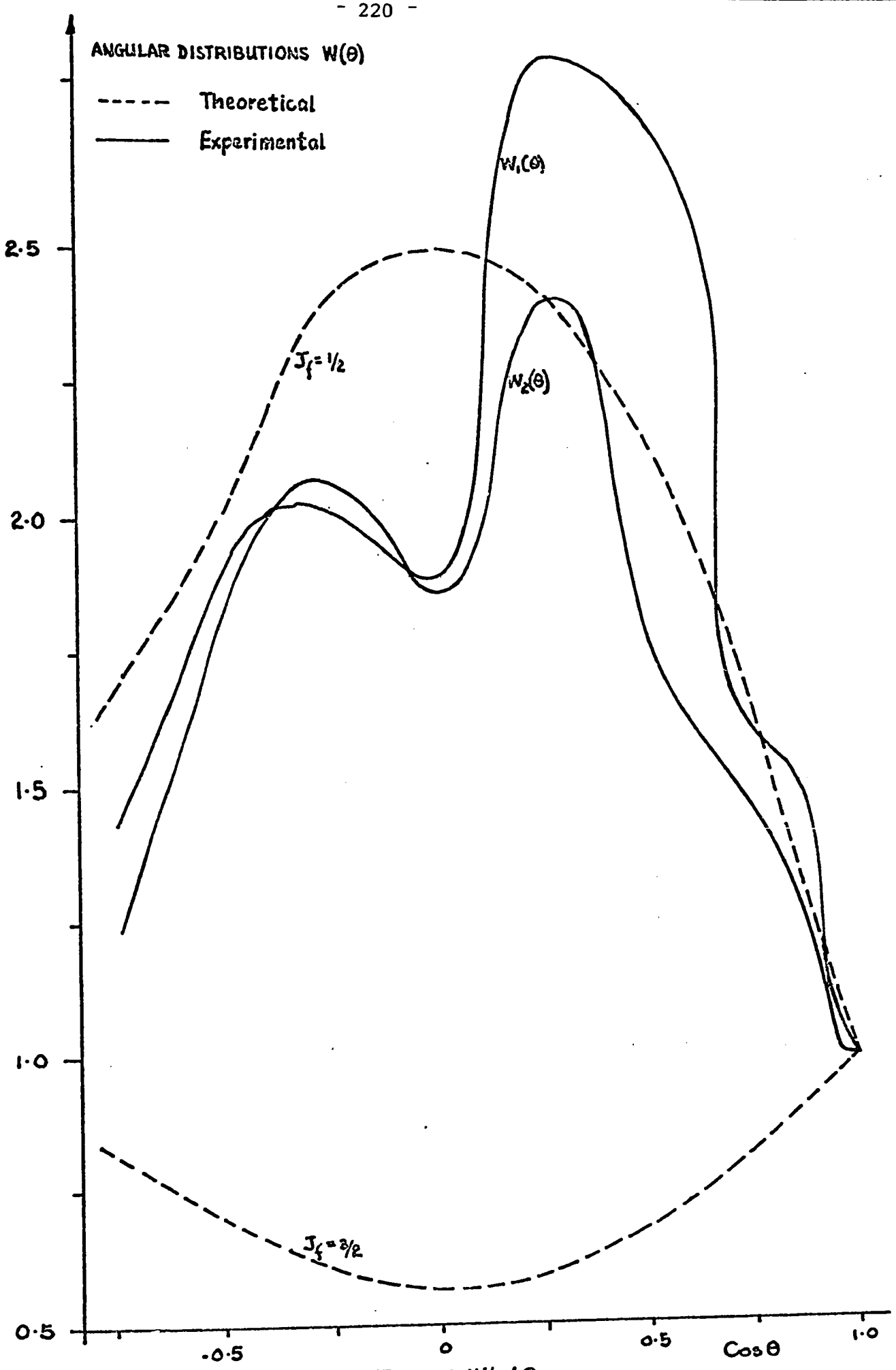
ANGULAR DISTRIBUTIONS W(θ)
Theoretical
Experimental
W1(θ)
W2(θ)
Jf = 1/2
Jf = 3/2
2·5
2·0
1·5
1·0
0·5
-0·5
0
0·5
1·0
Cos θ

Fig. VIII.12

BIBLIOGRAPHY

1. Raymond Gauthier, M.Sc. Thesis, "Relative Proton Capture Study of Cu^{59}" (1970) Department of Physics, University of Ottawa, Ottawa, Canada.
2. J. W. Butler and C. R. Gossett, Phys. Rev. 108, 1473 (1957).
3. J. W. Butler, "Table of (p, γ) Resonances, N.R.L. Report 5282" U. S. Naval Research Laboratory, Washington, D.C.
4. David C. Camp, UCRL-50156, Lawrence Radiation Laboratory, University of California, Livermore.
5. J. Barrette, G. Lamoureux and S. Monaro, "Geometrical Correction Factors for Angular Correlation Measurements with Ge(Li) Detectors", LPN-UM-53, Laboratoire de Physique Nucléaire, Département de Physique, Universite de Montréal, Montréal, Canada, (1970).